Superoxide and Nitric Oxide in Mechanisms for the Sustained Elimination of Hyper Radiosensitivity

An ESR Spin Trapping Study

Kathinka Elinor Pitman

Thesis for the Degree of Master of Science
Department of Physics

UNIVERSITY OF OSLO

June 2013

2013

Superoxide and Nitric Oxide in Mechanisms for the Sustained Elimination of Hyper Radiosensitivity - An ESR Spin Trapping Study

Kathinka Elinor Pitman

http://www.duo.uio.no/

Trykk: Reprosentralen, Universitetet i Oslo

Summary

One of the main purposes of this thesis was to establish and develop methods used for ESR spin trapping of superoxide and nitric oxide in our lab. The methods utilised were based upon protocols used by Reger (unpublished data) at the German Heart Center in Munich in order to investigate mechanisms proposed by Edin (unpublished work) for the sustained elimination of hyper radiosensitivity (HRS) in cultured cells. The measurements by Reger using a table top ESR spectrometer yielded inconclusive results and it was desirable to repeat these measurements using a larger, more involved ESR spectrometer which allows for more sensitive acquisition.

Two main groups of ESR spin trapping experiments were conducted; superoxide/ROS in cells was measured with cyclic hydroxylamine spin probe 1-hydroxy-3-methoxycarbonyl-2,2,5,5-tetramethylpyrrolidine (CMH) at ambient temperature, with measurements on both cell suspension and supernatant. Nitric oxide measurements were made with colloidal iron-dithiocarbamate spin trap $Fe(II)(DETC)_2$ at 77 K.

The ESR signal originating from the oxidised cyclic hydroxylamine spin probe $CM^{\bullet}$ was detected in both cell suspensions and supernatant from cells incubated with CMH. The oxidising species was not decidedly identified. Molecular oxygen in the air was seen to give rise to a high background oxidation.

No significant difference between ROS levels as measured in primed and unprimed T-47D and T98G cells was found.

A series of experiments examining the level of oxidation of the spin probe with reoxygenation time after hypoxia were carried out using the supernatant protocol. A reproducible trend in which the ESR signal detected was seen to increase after 1 – 2 minutes to a plateau at around 5 – 8 minutes followed by a more or less clear decline. These results were taken to reflect the increase in ROS generation upon reoxygenation of cells after hypoxia.

Colloidal iron-diethyldithiocarbamate spin trap $Fe(II)(DETC)_2$ was employed to measure nitric oxide generated in cultured cells. The method was successfully applied to samples supplemented with an $NO^{\bullet}$-donor, and the characteristic spectrum for the $NO^{\bullet}$-$Fe(II)(DETC)_2$ spin adduct was observed.

Measurements of basal $NO^{\bullet}$ proved more of a challenge and the characteristic $NO^{\bullet}$-$Fe(II)(DETC)_2$ spectrum was not observed for any of the samples. The acquired spectra were largely dominated by a signal which was attributed to the $Cu(II)(DETC)_2$ complex, which arises from chelation by free DETC of intracellular copper. One proposed reason for the absence of the $NO^{\bullet}$-$Fe(II)(DETC)_2$ signal in the basal samples is that there is very little $NO^{\bullet}$ produced in these cell, or that what little there is is preferentially scavenged by superoxide in the absence of functional superoxide dismutase (SOD). Another, and possibly coexistent reason, is that inadequate control of oxygen contamination occluded the signal.

Since no conclusive signal from nitric oxide was detected in the cells, no conclusions concerning differences in nitric oxide production between primed and unprimed cells could be made on these grounds. These results contradict the results obtained by Reger, in which signals due to nitric oxide allegedly was measured.

A signal of unknown origin was observed with varying intensity for most of the basal samples. This was speculated to originate from chelation of some intracellular transition metal other than copper by DETC, or contamination with some chemical used in cell culture or preparation of samples, possibly serum or phenol red.

Acknowledgements

The work presented in this thesis was carried out at the Biophysics group at the University of Oslo.

First of all I would like to thank my main supervisor, Post Doc Nina F. J. Edin, whose expertise and contagious enthusiasm has been of invaluable help with all aspects of this thesis.

I would also like to direct my sincere thanks to my secondary supervisors Professors Erik O. Pettersen and Eli O. Hole for their support and help, and for giving valuable feedback on earlier versions of the manuscript.

I also wish to thank:

Post Doc Andre Krivokapic who kindly introduced me to the ESR spectrometer and assisted with the first measurements.

Professor Einar Sagstuen for all assistance with ESR-related matters.

Efim Brondtz for all his inventive solutions to my problems.

Joe A. Sandvik for all assistance in the cell lab and for providing me with a steady supply of cells.

All the students and staff at the Biophysics group, for making my time as a master student a thoroughly delightful experience.

Finally, my dearest Steffen who means the world to me.

Table of Contents

Abbreviations and Designations

•OH	Hydroxyl radical
1400W	N-(3-(Aminomethyl)benzyl)acetamidine (Selective iNOS inhibitor)
ATM	Ataxia telangiectasia mutated
ATP	Adenosine triphosphate
BSA	Bovine serum albumin
CAC	Citric acid cycle
CCM	Cell conditioned medium
Cdk	Cyclin dependent kinase
CHA	Cyclic hydroxylamine
CMH	1-hydroxy-3-methoxycarbonyl-2,2,5,5-tetramethylpyrrolidine
Cu,Zn-SOD	Cytosolic superoxide dismutase (Membrane impermeable)
DEANO	Diethylamine nitric oxide sodium salt (NO•-donor)
DES	Desferroxamine (chelator)
DETC	Diethyldithiocarbamate (chelator)
ESR	Electron spin resonance
ETC	Electron transport chain
$FeSO_4$	Ferrous sulfate
GSH	Glutathione
GSSG	Glutathione disulfide
H_2O_2	Hydrogen peroxide
HDR	High dose rate
HRS	Hyper radiosensitivity
iNOS	Inducible nitric oxide synthase
IR model	Induced repair model
IRR	Increased radio resistance
KHB	Krebs HEPES buffer
KHB-D	KHB supplemented with chelators DES and DETC
LAP	Latency associated propeptide

LCCM	Low dose rate irradiated cell conditioned medium
LDR	Low dose rate
LET	Linear energy transfer
L-NAME	L-NG-nitroarginine methyl ester (NOS inhibitor)
LQ model	Linear quadratic model
MNIC	Mononitrosyl iron complex
N_2	Molecular nitrogen
NAD^+	Nicotinamide adenine dinucleotide
NADH	Reduced Nicotinamide adenine dinucleotide
NaOH	Sodium hydroxide
$NO^\bullet$	Nitric oxide
NOS	Nitric oxide synthase
NOx	NADPH oxidase
$O_2^{\bullet-}$	Superoxide anion
$ONOO^-$	Peroxynitrite
PBS	Phosphate buffered saline
PEG-SOD	Polyethylene glycol superoxide dismutase (Membrane permeable)
ROS	Reactive oxygen species
SOD	Superoxide dismutase
T-47D-P	T-47D cells given a protracted LDR priming dose
T98G-P	T98G cells given a protracted LDR priming dose
TCA	Trichloroacetic acid
TGF-β	Transforming growth factor-β

1 Introduction

Hyper radiosensitivity (HRS) is the phenomenon in which greater cell killing per unit dose of ionising radiation is achieved at lower doses (< ~0.3 Gy) than at higher doses. The HRS response to irradiation is thought to reflect a dose threshold for the induction of an early G2-checkpoint which arrests cells irradiated while in the G2-phase of the cell cycle. The failure to induce this checkpoint for doses below the threshold dose of ~0.3 Gy allows damaged G2-cells to enter into mitosis, resulting in increased cell death.

Several studies have shown the transient removal of HRS in cells after exposure to acute priming doses of ionising radiation upon subsequent challenge irradiation (Edin et al 2007, Marples & Joiner 1995, Short et al 2001). However, Edin et al. at our group discovered that HRS was permanently eliminated in T-47D mammary ductal carcinoma and T98G glioblastoma cells after a small, sub-lethal dose of 0.2-0.3 Gy given as a protracted exposure at low dose rate of [^{60}Co]-γ irradiation (Edin et al 2013, Edin et al 2007)[1]. Further work by Edin et al (2012) demonstrated that HRS was also transiently removed in reoxygenated cells after exposure to cycling hypoxia and that this removal of HRS could be made permanent by the supplementation of a nitric oxide ($NO^{\bullet}$) donor to cells before reoxygenation.

In light of these findings, Edin et al. put forward a hypothesis for the molecular mechanisms behind the sustained elimination of HRS, involving the action of reactive oxygen species (ROS) and nitric oxide; in short, protracted LDR priming is thought to incite a sustainable increased activity of inducible nitric oxide synthase (iNOS), which in conjunction with permanently elevated ROS (superoxide) levels forms peroxynitrite. Peroxynitrite then helps to activate TGF-β3 (transforming growth factor-β3), which is the factor hypothesised to be responsible for the elimination of HRS (Edin et al, unpublished data).

Research into ROS and nitric oxide is gaining interest as the implications of these reactive species in a vast range of pathological states as well as their roles in normal signal transduction are becoming known. Nitric oxide and superoxide are of major interest in cardiovascular and metabolic disease research. A range of different methods have been employed for the detection of reactive oxygen and nitrogen species *in vitro* and *in vivo*,

[1] This irradiation treatment is later in the text denoted as ”priming” or ”priming irradiation” and cells given such irradiation is said to have been ”primed”.

amongst others cytochrome c assays, fluorescence and chemiluminescence based techniques. Electron spin resonance (ESR) spin trapping is becoming increasingly popular for such studies in medical and biochemical research, especially with the arrival of table top ESR spectrometers and novel, more sensitive spin probes on the market.

With a view to probe the hypothesised mechanism for the sustained elimination of HRS in LDR primed cells, Edin wished to examine relative levels of superoxide/ROS and nitric oxide in primed cells as compared with unprimed controls. The measurements were outsourced to a lab at the German Heart Center in Munich, where they were carried out using a table top ESR spectrometer. ROS/superoxide was measured with cyclic hydroxylamine spin probe 1-hydroxy-3-methoxycarbonyl-2,2,5,5-tetramethylpyrrolidine (CMH) and nitric oxide was measured with colloidal iron-dithiocarbamate spin trap $Fe(II)(DETC)_2$. No significant difference was found in either case.

There were worries that the table top ESR spectrometer used did not provide the required sensitivity and it was therefore desirable to repeat these measurements using a larger, more involved ESR spectrometer which allows for more sensitive acquisition. The ESR lab at our group features two such instruments.

The purpose of this project was therefore to establish methods for ESR spin trapping of superoxide and nitric oxide in cultured cells, with the protocols used in Munich as basis for development. Once such methods were established, the initial aim was to compare qualitatively measured levels of superoxide and nitric oxide in primed and unprimed cells. The cell types examined are T98G glioblastoma cells and T-47D mammary ductal carcinoma cells.

The Munich protocol for superoxide/ROS measurement was found to be problematic, and an alternative protocol adopted from Deschacht et al (2010) with measurements on supernatant, as opposed to measurements on cell suspension with the Munich protocol, was extensively used. Measured levels of superoxide/ROS were compared for primed and unprimed cells. Superoxide/ROS levels were also examined in hypoxic and reoxygenated hypoxic cells, and in particular the development of superoxide/ROS levels with time after reoxygenation of hypoxic cells was investigated.

Although the Munich protocol for nitric oxide measurement with Fe(II)$DETC_2$ was successfully applied to samples of cells supplemented with an $NO^{\bullet}$-donor, measurements of basal nitric oxide proved to be considerably more challenging. Since no $NO^{\bullet}$ was conclusively detected in the samples prepared with the Munich protocol without $NO^{\bullet}$-donor, the $NO^{\bullet}$ -part of the thesis became concerned with exploring alternative variations of the standard method for elucidating the presence of nitric oxide in basal samples.

The thesis is structured as follows; Chapter 2 gives a theoretical background for the phenomena and topics to be discussed. In chapter 3, cell cultivation and general methods and materials common to the superoxide/ROS and nitric oxide measurements are presented along with some statistical considerations. Chapters 4 and 5 are devoted as wholes to respectively superoxide/ROS measurements with spin probe CMH and nitric oxide measurements with colloidal spin trap Fe(II)$DETC_2$, with establishment and development of method, results and analysis and discussion presented as subsections. Finally, the thesis is concluded in chapter 6.

2 Theory

2.1 Cell Biology

2.1.1 The cell cycle and cell cycle regulation

The following is based upon chapter 17*, Molecular Biology of the cell,* Alberts et al. (2008) and *Radiobiology for the Radiologist* (Hall & Giaccia 2012) unless otherwise stated. For a more detailed treatment the reader is referred to these texts.

The Cell Cycle

In order to proliferate, cells go through repeated growth and division, in the process known as the cell cycle. The cell cycle consists of four major stages; G1, S, G2 and M. See Figure 1. The first three make up interphase, during which the cell prepares for division. G1 and G2 are so called gap phases where the cell grows and synthesises proteins and other cell constituents, and monitors extracellular conditions. During S-phase, all DNA is replicated, giving a twin set of sister chromatids on completion. In M-phase the actual cell division, mitosis, occurs.

In the body, most cells are withdrawn from the cell cycle to a specialised, non-dividing, resting state, G0. The duration and reversibility of this state varies for different types of cells, depending on the need for renewal and external conditions. This variability accounts for the range of times needed to complete a cell cycle for different types of cells, the time taken to complete S, G2 and M-phase being fairly constant (12-24 h). In a 24 hour cell cycle, interphase typically takes up 23 hours, giving about 1 hour for mitosis.

Cell Cycle Regulation

All normally functioning organisms balance the loss of damaged or senescent cells through the continued replication of new, healthy cells in order to maintain structural homeostasis. This careful balance is maintained by the cell cycle control system, in which a multitude of signalling proteins act to initiate or hinder the production of new cells. Mutations in key genes involved in this control system can result in abnormal proliferation and pathogenesis.

Mitogenic stimulation is required for entry into the cell cycle and the further advancement through the cycle is regulated by cyclically activated cyclin-dependent protein kinases (Cdks). Fully active Cdk-cyclin complexes phosphorylate target proteins in order to trigger specific cell cycle events. Different classes of cyclin are synthesised and degraded at different stages of the cycle and a range of protein kinases and phosphatases act in self-regulating harmony to moderate Cdk activity, ensuring that all cell cycle events occur only once at the appropriate time and under the correct circumstances. See Figure 1 below.

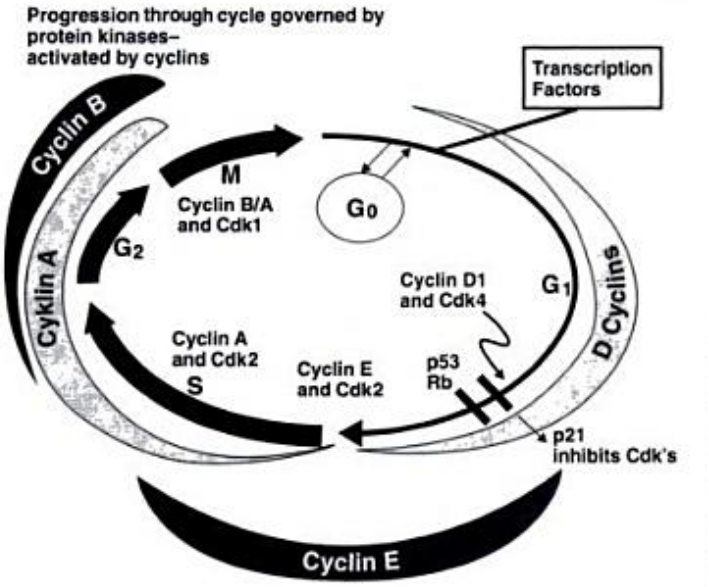

Figure 1
An overview of the different phases of the cell cycle and the various periodically activated cyclin-Cdk complexes which regulate key events, such as the initiation of DNA synthesis and the onset of mitosis (Hall & Giaccia 2006).

Checkpoints

There are several checkpoints in the cell cycle where cells are hindered from progression, if for some reason they are deemed unfit or conditions are found unfavourable. The major ones will be mentioned here. Firstly, G1k, or Start, is situated at the end of G1, where conditions are assessed and the cell is checked for DNA damage. If all is well, the cell is allowed to enter the cell cycle and duplicate its DNA content. Otherwise, it is either arrested from cycle progression to allow for repair, or apoptosis is triggered, in which the cell dies and is broken down in a contained manner. Secondly, G2/Mk is triggered in late G2 and cells are allowed to enter mitosis if all DNA is replicated properly and external conditions again are favourable.

Failure to arrest damaged cells may result in mitotic death and possible necrosis. A third checkpoint is found at the metaphase-to-anaphase transition of mitosis, where sister chromatids are separated if the mitotic spindle is correctly assembled. In addition, all of S-phase constitutes a sort of checkpoint, in which cells are continuously monitored for DNA damage and repaired during replication.

The protein kinase ATM (Ataxia telangiectasia mutated) is central in the triggering of the DNA repair machinery after recognition of double strand breaks, as well as the activation of cell cycle checkpoints throughout the cell cycle. The downstream effectors activated by ATM vary at different checkpoints. In G1, activation of ATM stabilises and activates tumour suppressor gene product p53. P53 binds to the site of damage and induces the expression of Cdk-inhibitor p21, which then inactivates G1/S- and S-Cdk-cyclins resulting in cell cycle arrest at G1k and Sk. Additional ATM-independent pathways are also thought to activate arrest during S-phase.

Two molecularly distinct checkpoints have been shown to act at the G2/M-interface following irradiation (Xu, Kim et al. 2002). An ATM independent, dose dependent checkpoint, known as the Sinclair or the late checkpoint, is induced hours after irradiation and has long been known to cause accumulation of damaged cells in G2 (Sinclair 1968). An ATM dependent checkpoint which acts rapidly and transiently after irradiation was more recently discovered (Xu et al 2002). This checkpoint has since been associated with the phenomenon of hyper radiosensitivity (HRS), and is further discussed in section 2.3.1.

2.1.2 Cellular Metabolism and Respiration

Metabolism

The cells of the body need energy in order to function normally and perform their various functions. Proteins, lipids and polysaccharides supplied through the dietary intake are reduced to their monomer constituents through enzymatic digestion and these subunits are then further broken down in a series of catabolic reactions to provide energy and building blocks for cellular activity. Energy is most notably harnessed in the form of ATP (adenosine triphosphate).

Glycolysis

The oxidation of sugars is a particularly important source of ATP. Glucose in the cytosol is converted to two molecules of pyruvate in a stepwise reaction, allowing most of the energy released in each step to be stored in activated carrier molecules. In this process, there is a net gain of two ATP and two molecules of the high energy electron carrier reduced coenzyme NADH (nicotineamide adenine dinucleotide) per molecule of glucose.

The Respiratory Chain and Oxidative Phosphorylation

Cellular respiration takes place in the mitochondria. Metabolic products are imported from the cytosol into the mitochondrial matrix. Pyruvate and fatty acids are broken down to acetyl CoA which is further oxidised in the citric acid cycle (CAC) to form mainly CO_2, a waste product which is removed by diffusion into the blood stream. The oxidation generates high energy electrons accepted by activated carrier molecules in the form of reduced coenzymes, most notably NADH. These reduced coenzymes go on to oxidise three major enzymatic complexes (complex I, III and IV) making up the Respiratory Electron Transport Chain (ETC) in the inner membrane of the mitochondria, finally terminating in the reduction of molecular oxygen to water. See Figure 2.

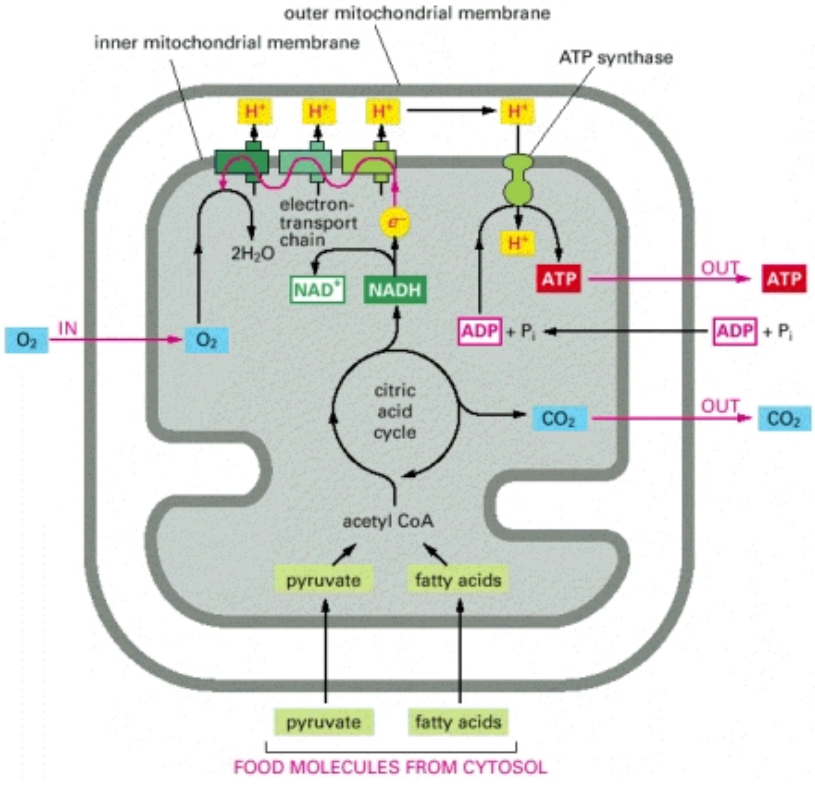

Figure 2
Overview of mitochondrial respiration. Metabolic products from the cytosol are broken down to acetyl CoA which is further metabolised in the citric acid cycle, yielding reduced coenzyme NADH. In the process of oxidative phosphorylation, high energy electrons are sequentially passed from NADH through the electron transport chain to molecular oxygen. The electron transport chain generates a proton gradient which drives the production of ATP by ATP synthase (Alberts 2008).

The respiratory complexes of the electron transport chain are shown in more detail in Figure 3. The large complex I is a NADH dehydrogenase complex, which accepts electrons from NADH and passes them on through a series of iron-sulfur (Fe-S) centres to ubiquinone (coenzyme Q), which then transfers its electrons to complex III, the cytochrome b-c1complex. This dimeric complex consists of two sets of hemes bound to cytochromes and a Fe-S protein. The electrons from ubiquinone are passed to cytochrome c in a series of reactions known as the Q-cycle, and cytochrome c in turn carries its electrons to complex IV, cytochrome oxidase, where the reduction of oxygen takes place. This complex accepts one electron at a time from cytochrome c, and passes them four at a time to oxygen.

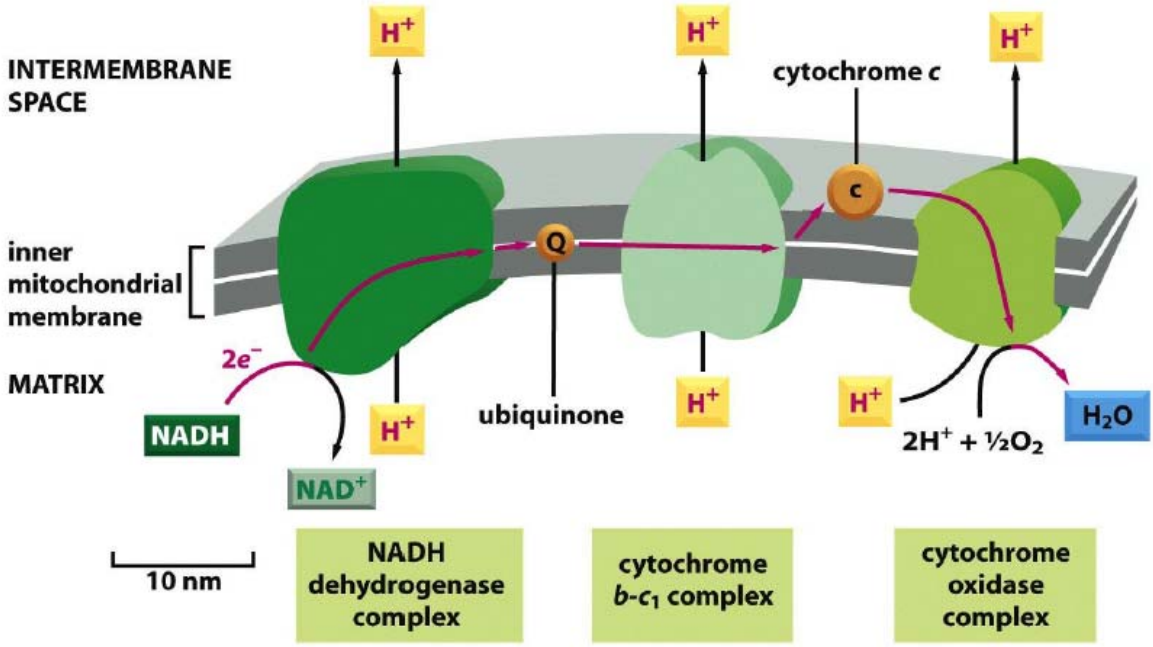

Figure 3
The electron transport chain respiratory complexes I, III and IV in the inner mitochondrial membrane. The red line indicates the flow of electrons through the electron transport chain from NADH to molecular oxygen. Ubiquinone and cytochrome c act as mobile carriers ferrying electrons from one complex to the next. As indicated, protons are pumped into the intermembrane space by each respiratory complex (Alberts 2008).

Cytochrome c oxidase traps O_2 at a special bimetallic centre until it is fully reduced, allowing the safe release of two molecules of water.

In addition, a fourth complex, succinate dehydrogenase or complex II, acts as a second funneling site of electrons into the ETC, coupling the oxidation of succinate, a product of the CAC, to the reduction of ubiquinone by complex III.

In each step of the ETC, electrons are passed to a more electronegative acceptor, giving a release of energy which is used to progressively generate a proton gradient across the inner membrane by actively pumping protons (H^+) into the intermembrane space. The enzyme ATP synthase in the inner membrane allows H^+ to flow back into the matrix down the electrochemical gradient which arises through specialised hydrophilic pathways, harnessing the potential energy released to assemble ATP from ADP and inorganic phosphate ion in the process of oxidative phosphorylation. Oxidative phosphorylation is responsible for ~90% of ATP synthesis in cells.

2.1.3 Hypoxic Metabolism

Under hypoxia, molecular oxygen is not as readily available for ATP production through mitochondrial respiration, and the majority of ATP is produced through lactic acid fermentation. Pyruvate from glycolysis is converted to lactate and NAD+ is regenerated so that it again is available for glycolytic oxidation. The energy yield of 2 molecules of ATP by fermentation is overall much lower than that achieved by complete oxidation, giving up to 38 ATP molecules. Hypoxic cells so require much more glucose to maintain metabolic function. This is also true of most tumour cells, regardless of oxygenation, and this phenomenon is known as the Warburg effect.

2.1.4 Reactive oxygen species (ROS) in the cell

Reactive Oxygen Species (ROS) is a term referring to a number of reactive molecules and free radicals derived from molecular oxygen. Cellular ROS may act as signaling molecules and influence many physiological processes including host defense, hormone biosynthesis, fertilization, and cellular signaling (Lund et al 2011). However, an increase or an imbalance in ROS production can lead to oxidative stress, which is implicated in the development of a panoply of pathophysiological states, including cancer, cardiovascular disease, neurological and mental disorders to mention but a few.

The main mechanism of ROS production in most biological systems is the sequential reduction of molecular oxygen to form superoxide, hydrogen peroxide and hydroxyl radicals. Formation of superoxide thus typically gives a cascade of ROS production (Hancock et al

2001). The following sections are largely based upon *Free Radicals and Other Reactive Species in Disease* (Halliwell 2005).

Superoxide ($O_2^{\bullet -}$)[2] is a primary ROS formed through the one-electron reduction of oxygen.

$$O_2 + e^- \rightarrow O_2^{\bullet -}$$

Superoxide is unstable in aqueous solution with a half-life of a few seconds. It is poorly membrane permeable, only able to cross the mitochondrial lipid membrane through anion channels and so is generally restricted to the cell compartment where it was produced (Li & Shah 2004).

Further reduction of oxygen gives hydrogen peroxide (H_2O_2), which can arise through the dismutation of superoxide in a spontaneous reaction with rate constant 8×10^4 $M^{-1}s^{-1}$.

$$2O_2^{\bullet -} + 2H^+ \rightarrow H_2O_2 + O_2$$

However, this dismutation is also catalysed by a family of enzymes known as superoxide dismutase (SOD), giving a significantly accelerated reaction with rate constant 2×10^9 $M^{-1}s^{-1}$. Under physiological conditions, formation of superoxide almost inevitably results in the formation of hydrogen peroxide.

Hydrogen peroxide is weakly oxidizing and cytotoxic, but is also increasingly found to be an important redox signaling molecule (Rhee 2006). H_2O_2 is more stable, diffusible and permeable in biological membranes than superoxide and so may be of higher relevance to the modulation of signal transduction pathways (Li & Shah 2004).

Hydrogen peroxide is relatively poorly reactive, but may form hydroxyl radical ($^{\bullet}OH$)[3] through the Fenton reaction, which is catalyzed by transition metal ions such as copper and iron.

$$H_2O_2 + Fe^{2+}/\ Cu^+ \rightarrow {}^{\bullet}OH + OH^- + Fe^{3+}/Cu^{2+}$$

Hydroxyl radicals are highly reactive radicals with short half-life and react with almost anything at diffusion limited rates, probably with the first molecule they encounter (Hancock

[2] The superscripted dot • denotes an unpaired spin, i.e. a free radical
[3] Hydroxyl radical is written with a preceding dot in order to emphasise the location of the unpaired spin on oxygen

et al 2001). Hydroxyl radicals thus cause severe harm to cells through lipid peroxidation, DNA base mutations and enzyme inactivation.

Additionally, superoxide readily reacts with nitric oxide ($NO^{\bullet}$) to form the powerful and toxic oxidant peroxynitrite ($ONOO^{-}$) at almost diffusion limited rates (6.7×10^{9} $M^{-1}s^{-1}$).

$$O_2^{\bullet-} + NO^{\bullet} \rightarrow ONOO^{-}$$

The protonated form ONOOH has $^{\bullet}OH$-like reactivity.

Nitric oxide is a fairly stable radical which diffuses readily between cells and is an important molecule involved in intracellular signal transduction. The half-life of $NO^{\bullet}$ depends on concentration, and in isolated systems, physiologically relevant concentrations of $NO^{\bullet}$ (nM) have a half-life in excess of 70 h (Beckman & Koppenol 1996). However, in biological systems, half-lives are much shorter.

The toxicity associated with nitric oxide is more likely to be due to the formation of peroxynitrite in the presence of superoxide. The reaction rate for the formation of peroxynitrite exceeds that of the dismutation of superoxide by SOD. Tissues do however commonly contain large amounts of SOD and peroxynitrite is only preferentially formed if the internal $NO^{\bullet}$ concentration approaches that of SOD, typically micro molar concentrations (Beckman & Koppenol 1996).

2.1.5 Cellular Sources of ROS

A schematic overview of some of the major generators of cellular ROS is shown in Figure 4 in the below.

Although various sources can generate superoxide in the cell, the majority is produced by autoxidation of components of the electron transport chain (ETC) (Imlay & Fridovich 1991). Mitochondrial superoxide generation occurs at two sites in the ETC; complex I, NADH dehydrogenase, and complex III, in the Q-cycle region. (Turrens 1997). Under physiological conditions, an estimated 1-5% of the total daily oxygen consumption contributes to mitochondrial superoxide formation (Davies 1995, Imlay & Fridovich 1991).

NADPH oxidases (NOx) are a family of oxidoreductases which act as dedicated ROS-producers through the oxidation of NADPH by molecular oxygen to form superoxide. NOx are instrumental in the bactericidal activity of immune cells, in which large quantities of superoxide and consequently hydrogen peroxide are formed at toxic (mM) levels. NOx are however not limited to phagocytic immune cells, but are found in a range of different cells and tissues. Several studies have indicated that NOx-dependent ROS-generation plays an important role in the modulation of redox-sensitive signaling pathways in mammalian cells. The primary biological functions of NOx remain largely unclear, but there is ample evidence for the implication of NOx in oxidative stresses which may lead to pathogenesis (Jiang et al 2011).

Nitric oxide synthases (NOS) are a family of enzymes which generate $NO^{\bullet}$ by the oxidation of the amino acid L-arginine to form citrulline, using NADPH and oxygen as co-substrates. There are three main isoforms of NOS; endothelial NOS (eNOS, first discovered in endothelial cells) and neuronal NOS (nNOS, first discovered in neurons) are constitutively expressed and produce low levels of $NO^{\bullet}$ in a calcium-dependent manner for the purposes of signal transduction. The inducible form (iNOS, originally discovered in cytokine-induced macrophages) is Ca^{2+}-independent and produces higher levels of $NO^{\bullet}$ in response to various stimuli, such as mechanic and oxidative stress, hypoxia and cytokines.

Expression of iNOS is regulated at the transcriptional level. The induction of iNOS in most cells appears to be dependent on the activation of the transcription factor NF-κB, which is known to occur in cellular responses to stress such as UV and ionizing radiation, free radicals, bacterial and viral antigens and cytokines (Förstermann & Kleinert 1995). Once activated, it remains so for several hours, generating large amounts of $NO^{\bullet}$ (Moncada & Higgs 2006).

NOS require five cofactors, one of which is the enzyme tetrahydrobiopterin (BH_4). The absence or inactivation of tetrahydrobiopterin causes NOS to dysfunction through the uncoupling of NADPH oxidation and $NO^{\bullet}$ synthesis, with oxygen instead of L-arginine as terminal electron acceptor, culminating in the generation of superoxide (Verhaar et al 2004). Peroxynitrite is known to oxidise BH_4 and thus cause uncoupling of NOS. NOS are then also potential generators of superoxide and so ROS in general.

Other potential sources of superoxide formation include xanthine oxidase (XO), cytochrome P450-type enzymes, cyclooxygenase (COX) and lipoxygenase (LOX).

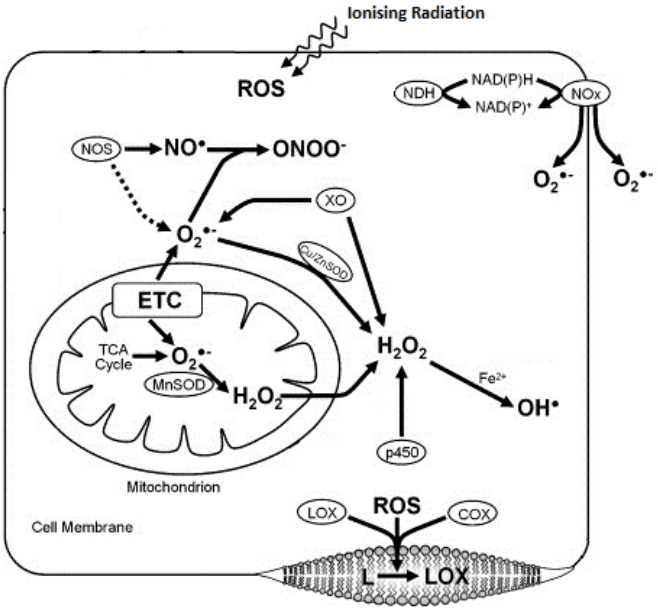

Figure 4
Schematic display of some of the major sources of cellular ROS. Adapted, from Sheu et al (2006).

2.1.6 Cellular Defences Against ROS

ROS are useful as signalling molecules and in host defence, but are detrimental if produced in an uncontrolled manner. It is therefore not surprising that there are several mechanisms for the elimination of ROS present in cells. As mentioned above, superoxide dismutase (SOD) is an important enzyme which catalyses the dismutation of superoxide to form hydrogen peroxide and molecular oxygen at almost diffusion limited rates.

$$2O_2^{\bullet -} + 2H^+ \xrightarrow{SOD} H_2O_2 + O_2$$

There are two different isoforms of SOD present in mammalian cells and these are differentiated by the metallic ions in the active site. Cu,Zn-SOD is present in the cytoplasm and mitochondrial intermembrane space, whilst Mn-SOD is present in the mitochondrial matrix. SOD is vital for the normal function and development of cells. For instance, Escherichia coli deficient or lacking in SOD, particularly mitochondrial Mn-SOD, display greatly elevated mutation rates during aerobic growth (Farr et al 1986). Tumour cells both in vitro and in vivo have been found to show altered SOD activities, specifically lowered total SOD activity and to be deficient or totally lacking in Mn-SOD. Cancer cells are also seen to generate higher levels of mitochondrial superoxide (Oberley & Buettner 1979).

Thiol group (-SH) containing compounds, particularly glutathione, are important cellular antioxidants. Glutathione acts as an electron donor to radicals and oxidants, thereby stabilising them. In this process, reduced glutathione (GSH) is converted to its oxidised form (GSSG). The enzyme glutathione reductase in turn recycles GSSG to GSH using NADPH as reducing agent. The ratio of GSH to GSSG is often used as an indicator for oxidative stress in cells. Glutathione peroxidases (GSHPX) are a vital class of enzymes which catalyse the reduction of hydrogen peroxide to water, using glutathione as cofactor.

A range of other enzymes participate in the defence against ROS, such as catalases and peroxiredoxins, which catalyse the reduction of hydrogen peroxide and peroxynitrite.

Additionally, antioxidant scavengers are rife in cells. Ascorbic acid (vitamin C), tocopherol (vitamin E), β-carotene and glutathione between them directly scavenge several reactive species such as $ONOO^-$,$^\bullet OH$, H_2O_2, radical centres on DNA, lipid peroxides etc.

2.1.7 ROS in Hypoxia/Reoxygenation

There has been some dispute in the literature as to whether ROS levels are elevated or decreased during hypoxia. The increase in $O_2^{\bullet -}$ generation during chronic, severe hypoxia has been found to originate mainly in mitochondria, through electron leakage, particularly from respiratory complexes I and III. The increased generation of ROS is coincident with the decline of mitochondrial membrane potential due to the breakdown of the ETC (see section 2.1.3), and is seen to cease with the loss of membrane potential. The ability to maintain the membrane potential, through e.g. reversal of ATP synthase, may vary for different cell types and conditions, giving differing patterns of ROS generation, and this variability may underlie the controversy of increased or decreased ROS generation under hypoxia (Abramov et al 2007). The decline in membrane potential is also thought to release into the cytosol $O_2^{\bullet -}$ normally compartmentalised in the matrix (Millar et al 2007). Additionally, a number of mitochondrial enzymes, such as Mn-SOD and cytochrome oxidase (complex IV) show decreased activity during hypoxia, also resulting in increased ROS levels. See the review paper by Li and Jackson (2002).

Mitochondrial autophagy has been observed in cells subjected to prolonged hypoxia and is thought to be an adaptive response to increased mitochondrial ROS generation (Zhang et al 2008).

ROS in reoxygenation has been thoroughly studied, particularly in relation to ischaemia/reperfusion injury in cardiovascular and cerebral tissues. Bursts of ROS production during reoxygenation has been shown in a range of cells and tissues, and NADPH oxidases, and xanthine oxidase in certain tissues, are thought to be the main culprits (Li & Jackson 2002).

2.2 Cellular Radiobiology

2.2.1 Radiological Physics

Ionising Radiation

Ionising radiation is characterised by its ability to ionise the atomic and molecular constituents of matter. A distinction is made between directly and indirectly ionising radiation. Charged particles such as electrons, protons and α-particles are directly ionising and deposit energy through many small Coulomb interactions. Photons and neutrons carry no charge and are indirectly ionising, depositing energy in relatively few interactions, but with potentially large transfers of energy (Attix 1986).

Interactions with matter

Photons deposit energy in mainly three ways; the photoelectric effect, Compton scattering and pair production. The cross sections for these interactions vary with the energy of the incident radiation and the effective atomic number of the absorber. For this thesis, only interactions pertaining to γ-irradiation from a ^{60}Co-source are of relevance. In the case of biological material irradiated with photons of mean energy 1.25 MeV, the predominant interaction is Compton scattering. In this type of interaction, the incident photon is deflected by an electron through an angle relative to its initial trajectory, transferring kinetic energy and momentum to the so called Compton electron. For a 1 MeV photon, the mean energy fraction transferred is roughly 45% (Attix 1986). The photon is successively scattered, steadily depositing energy until it is either absorbed in a photoelectric event, or it clears the material.

The Compton electrons which receive energy from the scattered photons carry charge and thus interact with the Coulomb fields of the atoms and molecules of the material. Energy is transferred in two possible ways; through so called soft/glancing collisions and hard/knock-on collisions. Glancing collisions involve the interaction of the charged particle with the Coulomb fields of atoms relatively far away, giving frequent but very small transfers of energy. Hard collisions, in which the charged particle interacts with an atomic electron, are on the other hand highly infrequent, but a large amount of energy is transferred per event. The fractions of energy transferred in the two processes are thus comparable.

The high energy transfers of hard collisions can give rise to so called δ-rays, which are energetic electrons with the ability to deposit their energy in secondary tracks to that of the primary particle.

Energy Deposition

The stopping power S of a charged particle of energy T is defined as the expected rate of energy loss per unit path length x, or mathematically; $S = (dT/dx)$. The stopping power thus expresses the amount of energy imparted in the absorbing material by the charged particle, and this value is dependent on the kinetic energy and charge of the particle and the effective atomic number of the absorbing material. However, high energy transfers, such as occur in hard collisions, may result in energy depositions outside of the primary interaction site, consequentially leading to the overestimation of local energy imparted by the stopping power. The use of restricted stopping power, or the related quantity, $L_\Delta = (dT/dx)_\Delta$, termed the linear energy transfer (LET) is therefore preferable. The LET for a charged particle is the fraction of the stopping power which is due to soft collisions and hard collisions which yield δ-rays with energies below some cut-off value Δ, and thus impart their energy in the local neighbourhood of the primary interaction. High LET radiation is termed densely ionising, whereas low LET radiation is termed sparsely ionising.

^{60}Co

^{60}Co decays by β-decay (half-life 5.27 years) emitting two γ-rays with energies 1.17 and 1.33 MeV (mean energy ~1.25 MeV), and a β-particle with maximum energy 0.31 MeV. These

low energy electrons are reabsorbed in the source and surrounding materials and are thus not of importance when considering energy transfer to the biological material irradiated.

[^{60}Co]- γ-radiation is sparsely ionising with LET = 0.2 keV/µm (Hall & Giaccia 2006).

2.2.2 Radiation Induced Radical Generation

As mentioned above, ionising radiation causes atoms and molecules to become ionised, thus creating free radicals. Biological material consists of large amounts of water, and so radiation-induced water radicals are of particular importance. Water molecules are ionised according to the below reaction equation.

$$H_2O \rightsquigarrow H_2O^+ + e^-$$

The ionisation products further dissociate or interact with other water molecules to create highly reactive hydroxyl ($^{\bullet}$OH) and hydrogen (H$^{\bullet}$) radicals, in the following reactions.

$$H_2O^+ \rightarrow H^+ + {}^{\bullet}OH$$

$$e^- + H_2O \rightarrow OH^- + H^{\bullet}$$

The electron may polarise the surrounding water molecules and become hydrated, termed e^-_{aq}, and thus be relatively stable and able to diffuse significant distances to inflict its damage.

Excited water molecules may also dissociate as follows

$$H_2O^* \rightarrow H^{\bullet} + {}^{\bullet}OH$$

The resulting radicals may recombine to form less reactive species, react with biomolecules and cause damage or be removed by antioxidant defences, as described in sections 2.1.4 – 6.

2.2.3 Cellular Damage and Repair

Ionising radiation causes damage to several cellular constituents and biomolecules, such as proteins, lipids and organelles, but abundant evidence gathered since the 1960s exists for DNA as the sensitive target for radiation-induced cell lethality. In terms of cellular survival then, cellular damage refers to chromosomal corruption.

Cellular damage is generally divided into three categories; lethal damage (LD), sublethal damage (SLD) and potentially lethal damage (PLD) (Hall & Giaccia 2006). Lethal damage is such that is irreparable and leads irrevocably to cell death. Potentially lethal damage is deathly under normal circumstances, but may be repaired if enough time is allowed. Sublethal damage is not by itself lethal and can under normal conditions be readily repaired, but may lead to death in conjunction with additional sublethal damage.

2.2.4 Cellular Survival and Dose Response

The response of a cell population exposed to ionising radiation is described by a so called cell survival curve, which relates the survival, in this context defined as the average fraction of cells retaining their reproductive integrity, with the dose absorbed. Clonal survival studies on such cell populations generally yield values which are consistent with linear quadratic (LQ) models, particularly when little data is collected in the low dose region (Bonner 2004).

The most popular of these linear quadratic models is the LQ-model due to Sinclair (1966) and Chadwick and Leenhouts (1973), which is of the form

$$S = e^{-(\alpha D + \beta D^2)}$$

where S is the surviving fraction of cells exposed to a dose D, and α and β are constants. Representative curves for densely and sparsely ionising radiation are shown in Figure 5.

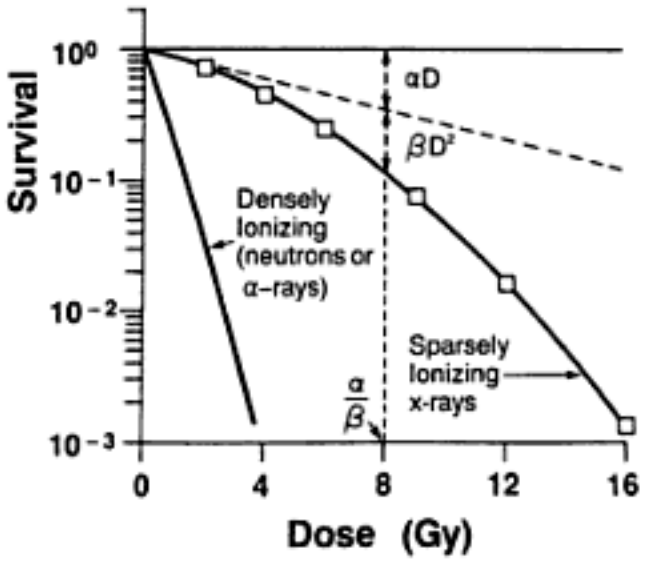

Figure 5
Typical LQ-fitted survival curves for cells exposed to different qualities of ionising radiation. Survival is plotted on a logarithmic scale against dose on a linear scale. Densely ionising radiation produces linear curves, whereas sparsely ionising radiation produces curves with initial linear slope followed by a shoulder region. The cell kill due to the linear (αD) and quadratic (βD^2) components are equal at the dose α/β. From Hall and Giaccia (2006).

The model is based on the assumption of double strand breaks in DNA as the mechanism for cell death, and the fact that these breaks may be repaired or restituted. The constants α and β represent two separate components of cell killing caused by double strand breaks resulting from a single event and interacting single strand breaks respectively (Chadwick & Leenhouts 1973). This simple equation thus expresses effects relating to total dose absorbed, the rate at which this dose is delivered, radiation quality (LET) and cellular capacity for repair. The initial shoulder characteristic for sparsely ionising radiation reflects repair of sublethal damage. A broad shoulder indicates a high capacity for such damage repair and the preference for such repairs to apoptosis. Densely ionising radiation gives rise to survival curves which are largely dominated by the linear α-component, reflecting the relative insignificance of sublethal damage.

The dose at which the cell killing due to the linear (αD) and quadratic (βD^2) components are equal is given by the ratio α/β. This ratio is an important parameter indicating dose response for a given tissue and the differing dose response for healthy and cancerous tissues is exploited in radiotherapy. Tumours tend to have a high α/β-ratio (~10 Gy) indicating reduced ability for repair, whilst normal tissues tend to have a low ratio (~3 Gy).

2.2.5 Effects of Dose Rate on Survival

Dose rate effects are only of real relevance for sparsely ionising radiations such as x- or γ-rays, which display significant components of multiple-track cell kill, since the component of cell killing due to single-track damage is the same whether the radiation is delivered acutely or at lower dose rates.

Acutely delivered radiation doses (high dose rate, HDR) cause ionisations to occur more closely in space and time, giving rise to more sublethal damage with the potential to interact, thus resulting in greater cell death. The dose response to HDR radiation is fairly uniform between cell lines.

Reducing the dose rate allows the repair of sublethal and potentially lethal damage, improving survival, due to the protracted exposure time. Different cell lines show a great variability in dose response at low dose rates, reflecting differences in the time needed to repair sublethal damage.

However, some cell lines have been shown to display increased lethality with declining dose rate in a limited dose rate interval (~0.3 - 1 Gy/h). This phenomenon is known as the inverse dose rate effect and is thought to be a manifestation of redistribution of cells during low dose rate (LDR) radiation exposure. In this limited dose rate interval, cells are arrested and accumulate in the more radiosensitive G2 phase (see section 2.1.1), thus giving a more efficient cell killing per unit dose. Lower dose rates allow cells to keep cycling during exposure, whereas for higher dose rates cells are frozen in the phase of the cycle they were in at the onset of irradiation (Hall & Giaccia 2006).

It has also been hypothesised that the inverse dose rate effect reflects the phenomenon of hyper radiosensitivity (HRS), see section 2.3 below. Mitchell et al (2002) noted the presence of an inverse dose rate effect in HRS proficient cell lines, but not in HRS deficient ones. This relation however has since been shown not to be valid for all cell lines.

2.3 Hyper Radiosensitivity

2.3.1 The Induced Repair Model

Many cell lines exposed to ionising radiation *in vitro* display a dose response at low doses which deviates from that predicted by the LQ-model. Specifically, for doses below ~0.4 Gy, the amount of cell killing per unit dose is elevated, giving a so called low dose hyper radiosensitive (HRS) response. The initial hyper sensitive response is followed by a region of increased relative survival in the dose range ~0.4 – 1 Gy, which is termed increased radioresistance (IRR) (Joiner et al 2001). For doses above ~1 Gy, the dose response coincides with that described by the LQ-model. The HRS/IRR-type response is not unique for cultures exposed to ionising radiation, but is also seen in relation with chemical and UV exposure in a number of cell systems, both *in vitro* and *in vivo*. The extent of the HRS response varies greatly between cell lines, being more prominent for malignant cells than for normal tissues (Joiner et al 2001).

A modification to the LQ-model was proposed (Denekamp & Dasu 1999, Joiner & Johns 1988, Marples & Joiner 1993) to more satisfactorily describe the dose response in the HRS/IRR region. The resulting induced repair (IR) model accomplishes this through the introduction of an expanded α-component.

$$\alpha = \alpha_r \left(1 + \left(\frac{\alpha_s}{\alpha_r} - 1\right) e^{-D/d_c}\right)$$

where α_r is the α-component from the LQ-model, whilst α_s is that representing the initial, sensitive part. d_c represents the dose level at which the IRR response arises. See Figure 6.

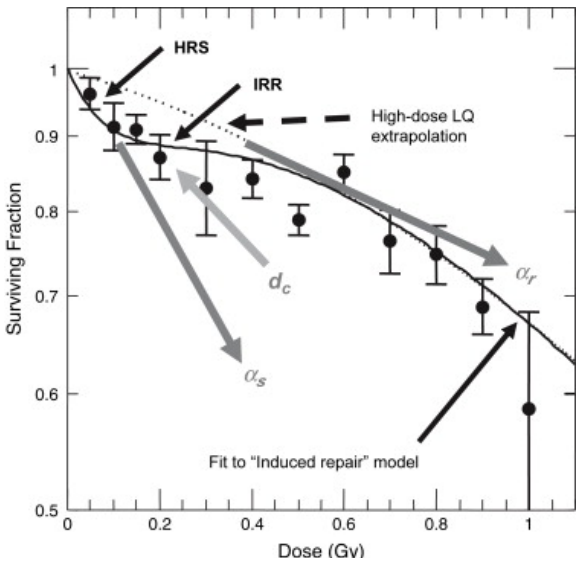

Figure 6
Typical cell survival curve for dose response at low doses (<1 Gy). The solid line gives the fit to the IR model, whilst the broken line gives the low-dose extrapolation from the LQ model applied to high-dose data. α_s is the initial slope, which changes into α_r as the response transitions through the HRS/IRR region into that described by the LQ model. d_c indicates the level at which the transition between the HRS and the IRR region occurs (Marples, Collis 2008).

Experiments performed with cell populations enriched in the different stages of the cell cycle have shown that the HRS/IRR response is especially marked in the G2-phase (Krueger et al 2007, Marples et al 2003, Short et al 2003). This indicates that the mechanism regulating the HRS/IRR response is connected with checkpoint events in G2-phase. As mentioned in section 2.1.1, two distinct radiation-induced checkpoints act at the G2/M interface. The first, the Sinclair checkpoint or the late checkpoint, is ATM independent and prevents damaged cells irradiated in G1- and S-phase from entering mitosis. It fails however to arrest cells which were in G2 at the time of irradiation. The second checkpoint, referred to as the early checkpoint, is ATM dependent, transient (active 0-2 h post irradiation) and acts much more rapidly, so that cells irradiated in G2 are also hindered from entering mitosis. Most notably, it has a distinct activation threshold of ~0.3 Gy. The coincidence in dose level required for the activation of this checkpoint with the transition from HRS to IRR strongly suggests that HRS is a consequence of the failure to induce the early checkpoint for cells in G2 exposed to doses lower than ~0.3 Gy. Damaged cells are then allowed to attempt mitosis, resulting in increased cell death.

An analysis of the fraction of mitotic cells after exposure to a range of radiation doses rather elegantly demonstrates the induction of the G2 checkpoint at the onset of IRR. The fraction of mitotic cells in a population may be determined by staining of the mitotic marker histone H3. In Figure 7 below, the survival curve for a population of glioblastoma cells (T98G) is shown for doses in the HRS/IRR region (■, A). The mitotic ratio for the same cells, indicating the fraction of mitotic cells in a population irradiated with a certain dose to that of an unirradiated one, is shown on the right (■, B). As can be seen, the dose level (~0.3 Gy) at which the mitotic ratio starts to decline below unity coincides with the transition from HRS to IRR.

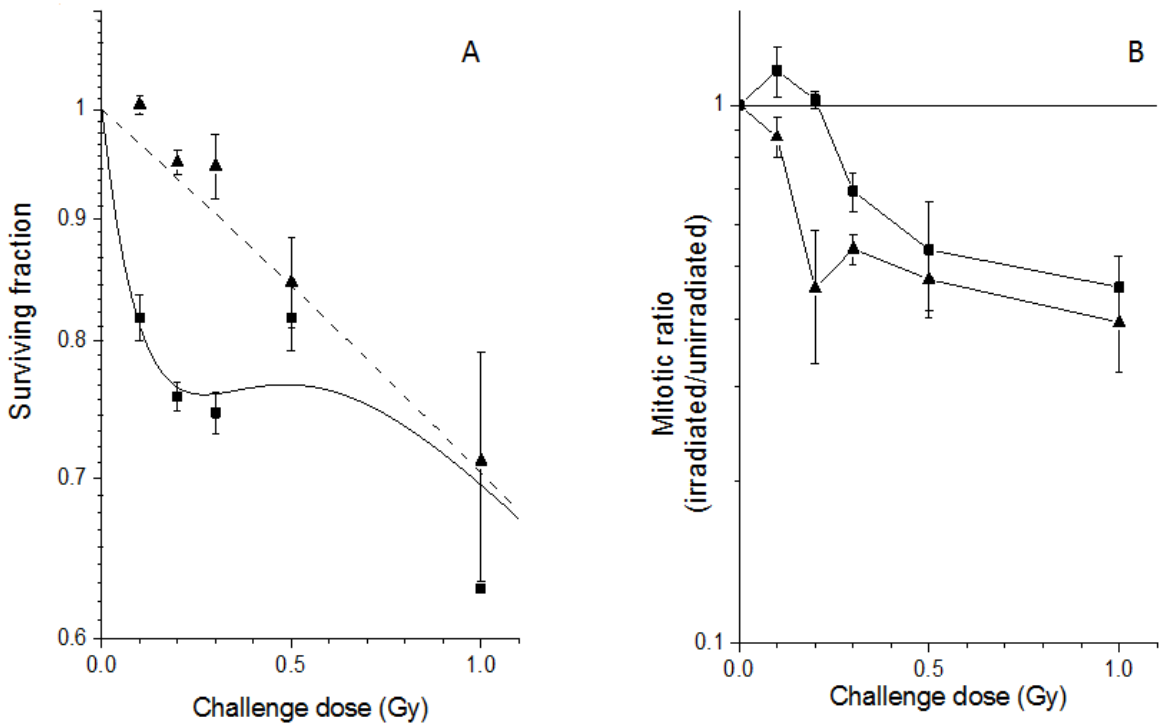

Figure 7
Panel A shows the survival curves for two cell populations in response to HDR challenge irradiation. Squares (■) represent HRS proficient T98G cells and triangles(▲) represent HRS deficient T98G cells which have had their HRS response eliminated by priming (see section 2.3.2). In panel B the ratios (irradiated/unirradiated) of mitotic cells for both cell populations are shown as a function of radiation dose. Adapted, from Edin et al (2013)

The triangles (▲) in both panels represent the corresponding curves for a HRS deficient cell population (low dose rate (LDR) primed T98G, see section 2.3.2). The mitotic ratio falls immediately with radiation exposure even at the smallest doses, indicating the activity of the G2 checkpoint also for doses below 0.3 Gy.

2.3.2 Mechanisms for the Elimination of HRS

The phenomenon in which cells exposed to a small radiation dose (priming dose) exhibit increased resistance to a subsequent larger radiation dose (challenge dose) is known as the adaptive response (AR). This was first described in mammalian cultures by Olivieri et al. in relation with the increased clonal survival of tritium-labeled cells compared with unlabeled cells after exposure to external ionising radiation (Olivieri et al 1984). This is similar to the effect seen in HRS proficient cell lines given a priming dose, in which the hypersensitive response is eliminated and the survival approaches, or even surpasses, that of the LQ-model also for the lowest challenge doses (Edin et al 2007, Marples & Joiner 1995). See Figure 7A (▲) above.

Several studies have shown the transient removal of HRS in cells exposed to HDR priming doses of 0.2 - 0.3 Gy in response to subsequent challenge irradiation (Edin et al 2007, Marples & Joiner 1995, Short et al 2001). This is thought to be associated with the preferential killing of radiosensitive G2 cells. However, Edin et al. discovered that protracted LDR irradiation eliminated HRS permanently in T-47D mammary ductal carcinoma and T98G glioblastoma cells (Edin et al 2013, Edin et al 2007). HRS may also be transiently removed by transfer of medium from LDR irradiated cells to unirradiated cells, indicating that the removal of HRS is mediated through bystander effects (BE). Edin et al. found that indeed no cells needed be present during irradiation for the HRS/IRR response to be eliminated in recipient cells, provided the medium had first been in contact with cells (cell conditioned) and the priming dose was given at low dose rate (0.3 Gy/h for 1 h). This LDR irradiated cell conditioned medium is termed “LCCM” in the following. LDR priming doses as small as 0.05 - 0.06 Gy given over an hour eliminated HRS, but not when given over 15 min, indicating that time is an important factor (Edin et al 2013).

The cells thus seem to secrete some factor into the medium during cell conditioning, and this is dependent on the presence of serum in the medium (Edin et al 2009). A small priming dose then seems to modify this factor, which can thereafter interact with cells, resulting in the elimination of HRS.

2.3.3 Proposed Molecular Mechanisms for the Elimination of HRS

The Role of TGF-β3 in the Elimination of HRS

Edin et al. hypothesised that the factor secreted during cell conditioning is a member of the TGF-β (transforming growth factor beta) family, which are cytokines known to be involved in the regulation of cellular growth and differentiation, immune function, and in particular the inhibition of cellular proliferation (Koli et al 2001). Specifically, TGF-β3 was shown to remove HRS in cells otherwise untreated when added to culture medium and the specific inhibition of TGF-β3 recovered HRS in cells in receipt of LCCM. Additionally, significantly elevated levels of TGF-β3 were found in the cytosol of primed T98G and T-47D cells as compared with unprimed cells (Edin, unpublished data). The binding of TGF-β3 thus appears to activate a pathway for the induction of the early G2 checkpoint for doses in the HRS region.

TGF-βs are initially translated as dimers consisting of the TGF-β domain and a so called latency-associated propeptide (LAP) domain. Proteases, such as furin, cleave the prodomain from the bioactive TGF-β domain, leaving LAP non-covalently associated with the TGF-β. This latent complex is then secreted by the cell. In order to be fully activated, TGF-β must be dissociated from LAP. This may be accomplished in various ways, such as increased temperature, low/high pH, irradiation or more generally events resulting in increased ROS in the extracellular space (Hyytiainen et al 2004). See Figure 8 below. The activation however is reversible and application of recombinant LAP reduces the amount of active TGF-β (Böttinger et al 1996). Active TGF-β binds to transmembrane serine/threonine kinase receptors for signal transduction.

LDR irradiation of CCM removes HRS in recipient cells, but HDR irradiation does not. LDR seems to be able to modify TGF-β3 whilst HDR is not. An important difference between LDR and HDR is the time needed for dose delivery.

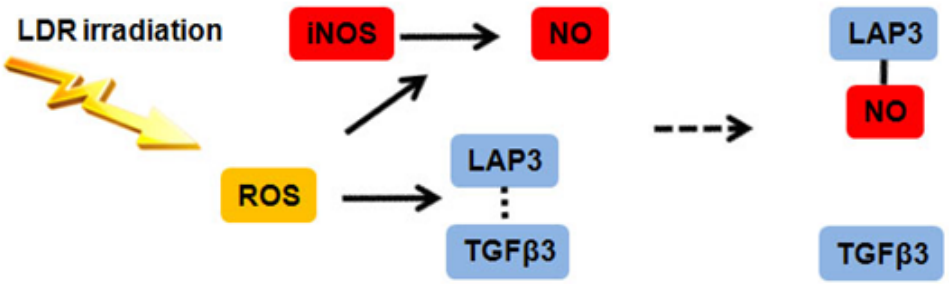

Figure 8
Proposed mechanism for the activation of TGF-β3 during LDR irradiation. Increased levels of ROS dissociate TGF-β3 from the latency associated protein (LAP-3), and nitric oxide (NO) scavenges the LAP, resulting in full activation of the TGF-β3. From Edin, unpublished work (2013).

The role of iNOS in the Elimination of HRS

As mentioned above, a major difference between the LDR and HDR irradiation is the time needed for dose delivery. Edin et al. have hypothesised that the mechanism by which LDR irradiation removes HRS in cells recipient of LCCM (transiently) and in directly irradiated cells (permanently) involves the activity of inducible nitric oxide synthase (iNOS).

Evidence in support of this hypothesis includes the inhibition of the removal of HRS by LDR priming by the addition of iNOS inhibitor 1400W during priming. Moreover the effect of permanent removal of HRS by LDR priming was found to be mimicked by the addition of $NO^{\bullet}$-donor diethylamine nitric oxide sodium salt (DEANO) in combination with either HDR priming or reoxygenation after cycling hypoxia. Addition of the iNOS inhibitor 1400W was seen to recover HRS in LDR primed cells, indicating the need for continued iNOS activity for the elimination of HRS. Indeed, the addition of 1400W was found to induce HRS in the normally HRS-negative cell line NHIK 3025 (Edin et al 2013).

Edin has put forward two closely related hypotheses for the molecular mechanisms behind the transient and permanent removal of HRS. Protracted ROS production during LDR priming of CCM activates TGF-β3 in the medium and LAP is thought to be scavenged by $NO^{\bullet}$ due to increased iNOS activity. A limited supply of active TGF-β3 is then free to act on recipient cells, giving a transient removal of HRS. Figure 8 above demonstrates this mechanism.

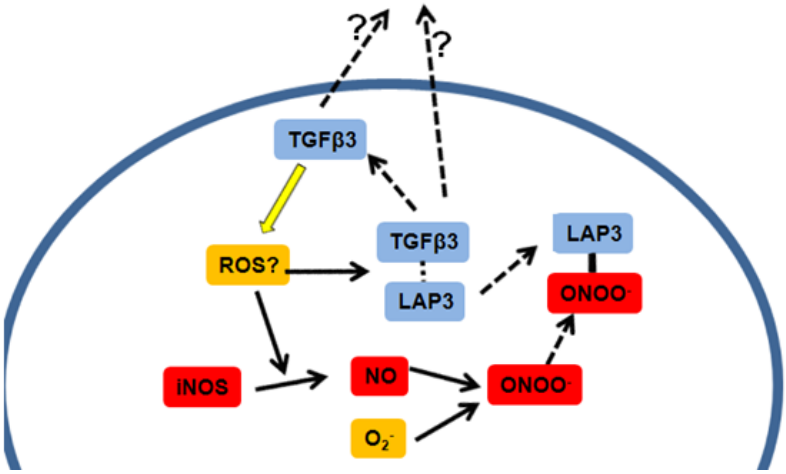

Figure 9
Hypothesised mechanisms for the permanent elimination of HRS after direct, protracted LDR irradiation of cells. An unknown mechanism gives heightened levels of ROS which activate TGF-β3. Increased levels of NO combine with superoxide to form peroxynitrite, which may scavenge LAP-3, allowing stable TGF-β3 to be secreted and act on cellular receptors. From Edin, unpublished work (2013).

The hypothesis proposed for the permanent removal of HRS involves the induction of a persistent activation of TGF-β3 inside cells. How this may occur is illustrated in

Figure **9**.

Protracted LDR is thought to incite a permanently increased iNOS activity together with increased ROS production, resulting in generation of peroxynitrite which scavenges LAP-3. Active TGF-β3 is then continuously secreted by the cells to persistently induce the early G2-checkpoint, resulting in the permanent elimination of HRS.

HRS and Hypoxia

Cells continuously cultured under hypoxic conditions for several passages experience a cyclic variation in pericellular oxygenation. In an atmosphere of 4% O_2, the pericellular oxygen concentration cycles from 4% after reculturing to below 0.1% at the maximal cell density (Pettersen et al 2005).

Cells subjected to cycling hypoxia for several weeks lose HRS, but regain the HRS response within two weeks of reoxygenation. Edin has speculated that the removal of HRS is linked to increased ROS generation upon reculturing due to reoxygenation, and that these radical bursts are able to activate the factor responsible for the induction of the G2-checkpoint (Edin et al 2012). As mentioned above, reoxygenation after cycling hypoxia in conjunction with DEANO could mimic the effect of LDR irradiation.

Medium transfer from hypoxic cells also transiently eliminates HRS in recipient cells cultured at ambient oxygenation (Edin et al 2012). This is closely reminiscent of the response seen in cells in receipt of LCCM, in which HRS is eliminated, but regained within two weeks, suggesting a common mechanism at play.

2.4 Electron Spin Resonance

The following is based upon the texts *Principles and Applications of ESR Spectroscopy* (Lund et al 2011) and *Principles of Electron Spin Resonance* (Atherton 1993), unless otherwise stated in the text.

2.4.1 Basic Principles of Electron Spin Resonance

Electron spin resonance (ESR) spectroscopy is utilised to study paramagnetic species in the presence of an external magnetic field. Paramagnetic substances are such that they contain permanent magnetic dipoles in the form of unpaired electrons.

Electrons possess an intrinsic spin angular momentum, S (= $1/2\,\hbar$), which gives rise to a magnetic moment analogous to that of classical orbital angular momentum. The electron magnetic moment is given by

$$\boldsymbol{\mu_e} = -g_e\mu_B\boldsymbol{S}$$

where $\mu_B = e\hbar/2m_e$ is the Bohr magneton, and g_e is the so called electron g-factor, which for free electrons has a magnitude of 2.00232. Here, the unit of spin, $\hbar$, is included in the Bohr magneton so that the spin is considered as dimensionless in the following text.

The Hamiltonian for the electron spin magnetic moment in an external magnetic field B applied in the z-direction ($\boldsymbol{B} = B\widehat{\boldsymbol{k}}$) is then given by

$$\boldsymbol{\mathcal{H}} = -\boldsymbol{\mu_e}\cdot\boldsymbol{B} = g_e\mu_B\boldsymbol{S}\cdot\boldsymbol{B} = g_e\mu_B S_z B$$

with eigenvalues

$$E = g_e\mu_B B m_s = \pm\frac{1}{2}g_e\mu_B B$$

where $m_s = \pm 1/2$ is the spin quantum number, referring to the two zeroth-order eigenstates |α> ('spin up') and |β> ('spin down'), respectively. Thus, the energy is split in 2s+1 = 2 Zeeman levels, with energy difference

$$\Delta E = g_e \mu_B B.$$

The above relation, which is illustrated in Figure 10, is commonly referred to as the *resonance condition*. An alternating electromagnetic field with a frequency ν which fulfils the resonance condition in terms of having $\Delta E = h\nu$, applied perpendicularly to B, induces transitions between the two spin states. This is called stimulated absorption or stimulated emission of electromagnetic energy.

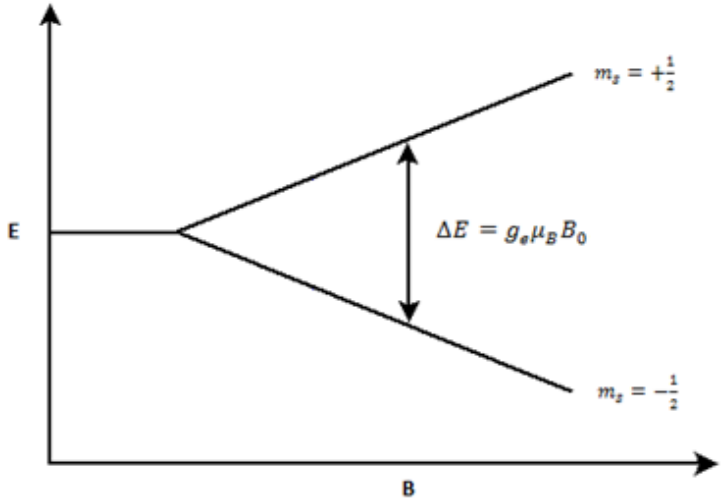

Figure 10
Zeeman splitting of energy levels for electrons in an external magnetic field B. An alternating electromagnetic field of constant frequency υ is applied, whilst the magnetic field is swept. At resonance, the energy difference ΔE equals the energy hυ of the applied electromagnetic field (arrow). The magnitude of the energy difference increases with increasing field strength.

According to Fermi's golden rule, the probability of stimulated emission equals that of stimulated absorption. The rate of transition from a state is proportional to the population of that state. At thermal equilibrium, the energetically upper and lower spin states (N_+ and N_- respectively) are populated according to Maxwell-Boltzmann statistics

$$\frac{N_+}{N_-} = e^{-\Delta E/kT} = e^{-g_e \mu_B B/kT} < 1$$

where k is the Boltzmann constant and T is the absolute temperature. There is thus a greater population of spins in the lower energy state. If at resonance, as the system is stimulated, a greater number of spins transition from the N_- to the N_+ state, giving a net absorption of

energy from the electromagnetic field. This net absorption accounts for the detectable ESR signal. In order to maintain the signal, the population difference must be upheld, and this happens through relaxation mechanisms (spontaneous transitions) in the system. With excessively high power of the alternating field, these relaxation mechanisms are rendered inadequate in restoring any population difference between the two levels, resulting in saturation and consequently the loss of signal.

Spectrometers are commonly operated at frequencies of roughly 9.5 GHz (X band), whilst the corresponding magnetic field strength (at g=2.0023) is about 340 mT. An ESR spectrum is acquired by sweeping the magnetic field keeping the microwave frequency constant, and detecting the absorption of energy as a function of B. The energy difference between the two Zeeman levels can then be determined.

2.4.2 Molecular Environments – The Spin Hamiltonian

The atomic environment also influences the local field experienced by the electron, contributing to the further splitting and shifting of energy levels. The total spin Hamiltonian for a molecular system is given by[4]

$$\boldsymbol{\mathcal{H}} = \boldsymbol{\mathcal{H}}_{Ze} + \boldsymbol{\mathcal{H}}_{ZN} + \boldsymbol{\mathcal{H}}_{hf}$$

The different terms are explained in the following.

- The electron Zeeman term - $\boldsymbol{\mathcal{H}}_{Ze} = \mu_B \boldsymbol{S} \cdot \boldsymbol{g} \cdot \boldsymbol{B}$

  Describes the electronic Zeeman effect as explained in the above, with the slight modification that the g-factor is replaced by the g-tensor, which couples the spin angular momentum with its own orbital momentum.

- The nuclear Zeeman term - $\boldsymbol{\mathcal{H}}_{ZN} = -g_N \mu_N \boldsymbol{I} \cdot \boldsymbol{B}$

  This term is directly analogous with the electronic case, and describes the splitting of the nuclear energy levels in the external magnetic field *B*. g_N is the nuclear g-factor (which varies for different isotopes), $\mu_N = e\hbar/2m_p$ is the nuclear magneton and **I** is the nuclear

[4] Neglecting quadrupole and electron-electron interactions, which are not of relevance here

spin operator (considered dimensionless). The sign is negative as compared to the electron Zeeman term due to the positive charge of the nucleus.

- The hyperfine interaction term – $\boldsymbol{\mathcal{H}_{hf} = S \cdot A \cdot I}$

The hyperfine interaction term describes the coupling between the electronic spin and the nuclear spin of nuclei in the vicinity of the electron. This interaction gives rise to so called hyperfine structure which provides information about the local environment of the electron. $\boldsymbol{A = a\mathbf{1} + A^0}$ is the hyperfine coupling tensor, with isotropic part a and anisotropic part $\boldsymbol{A^0}$. The isotropic part is commonly referred to as the Fermi contact coupling, since it arises when the electron has a finite probability of appearing at the nucleus, and is given by

$$a = \frac{2}{3}\mu_0 g_e \mu_B g_N \mu_N |\psi|^2$$

where $\mu_0$is the permeability of free space and $|\psi|^2$ is the unpaired electron spin density at the nucleus, $[a]$ = J. The anisotropic part arises from the electron-nuclear dipolar interaction, and averages to zero by rapid tumbling in solution.

The g-tensor

The g-factor relates to the coupling between the external magnetic field and both of the electron spin and orbital angular momenta for an unpaired electron as well as the coupling between the two angular momenta themselves (spin-orbit coupling). In the solid state, the orbital moment is mostly quenched (Weil & Bolton 2007). Then the extent of the difference from the value for free electrons reveals information about the molecular orbitals describing the unpaired electron spin distribution. Radicals with S < 1 typically yield g-values quite close to that of the free electron. For many metal-containing compounds, the total spin S > 1. Here, quenching of the spin angular moment is less effective. The resonance will then exhibit far larger g-values and g-anisotropy due to extensive spin-orbit coupling.

The g-anisotropy, reflecting the orientation dependency with respect to the direction of the external field is more generally given by the g-tensor, which is a second rank Cartesian tensor. The three principal components of g are denoted by g_X, g_Y and g_Z.

If $g_X = g_Y = g_Z$, the g-tensor is isotropic, g_{iso}. Similarly, for radicals rapidly tumbling in solution, the observed g-value will be an average equal to the isotropic g-value g_{iso}. Solid samples (powders) however exhibit g-anisotropy due to an orientation distribution of radicals between all possible directions. If $g_X = g_Y = g_\perp$ and $g_Z = g_\parallel$, then the system is of axial symmetry. In this case, and if $g_\perp > g_\parallel$, the spectrum around $g_\perp$ (at lowest field) is somewhat similar to the normal derivative shape, whilst that at $g_\parallel$ is reminiscent of an upside-down absorption peak. See Weil and Bolton (2007), p. 102 - 103. If $g_\perp < g_\parallel$, the spectrum around $g_\perp$ (now at highest field) is somewhat similar to the normal derivative shape, whilst that at $g_\parallel$ is reminiscent of an absorption peak. In general, the intensity of the signal around $g_\perp$ is stronger than at $g_\parallel$ since more radicals are oriented in the plane perpendicular to the parallel axis than along it (Lund et al 2011).

Basic ESR Spectrum

For the purpose of describing a basic ESR spectrum, one may consider the case of a collection of electrons interacting with a single nucleus, and further assume isotropic g-tensor and hyperfine coupling tensor, giving a considerably simplified spin Hamiltonian;

$$\boldsymbol{\mathcal{H}} = g_e \mu_B B \boldsymbol{S} - g_N \mu_N B \boldsymbol{I} + a \boldsymbol{S} \cdot \boldsymbol{I}$$

with first order energy eigenvalues

$$E(m_s, m_I) = g_e \mu_B B m_s - g_N \mu_N B m_I + a m_s m_I$$

with eigenfunctions $|m_s, m_I\rangle$, $[a]$ = J.

For coupling to a nucleus with spin I = 1, which is of particular relevance for this project, each m_s level will be split in three, corresponding to $m_I = -1, 0, +1$. These energy levels are denoted by (m_s, m_I).

Allowed transitions between energy states are such that $\Delta m_s = 1, \Delta m_I = 0$.

Shown below in Figure 11 is the development of a basic ESR spectrum for a system with $S = 1/2$, $I = 1$, as the magnetic field is swept, keeping the microwave frequency ν constant.

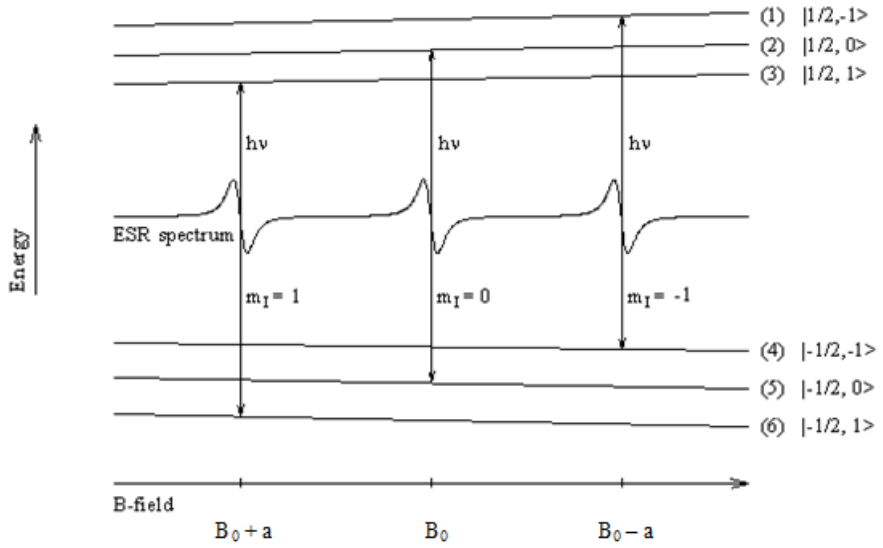

Figure 11
Basic ESR spectrum for a system with $S = 1/2, I = 1$ and small, negative hyperfine coupling constant ($-g_N\mu_N B < a/2 < 0$). The magnetic field is swept through the resonance condition for each allowed transition ($\Delta m_s = 1, \Delta m_I = 0$), giving stimulated absorption for three values of magnetic field strength; B_0, $B_0 \pm a$. Adapted, from Vestad (1999).

The resonance condition is fulfilled when the energy difference between allowed transition states, which depends on B, equals that of the microwave field of constant frequency ν.

$$m_I = -1: h\upsilon = g_e\mu_B B - a$$

$$m_I = 0: h\upsilon = g_e\mu_B B$$

$$m_I = +1: h\upsilon = g_e\mu_B B + a$$

Solving for B, one gets

$$B = \begin{cases} B_0 \\ B_0 \pm a \end{cases}$$

where $[a]$ = mT in magnetic field units.

This gives a three line ESR spectrum with hyperfine splitting *a* (see Figure 11). The isotropic hyperfine splitting can thus be deduced directly from measurements of the line separations (in magnetic field units) in the ESR-spectrum.

2.4.3 Spin Trapping

Radicals can be notoriously reactive and unstable, making it difficult or even impossible to make direct measurements by ESR spectroscopy. Some radicals may be sufficiently stable, but yield impractical spectra, for instance in that they are too broad. The use of spin traps facilitates the measurement of such radicals. Spin traps are compounds which intercept short-lived radicals, forming a covalent bond with the radical by an addition reaction, giving rise to a so called spin trap adduct with an enhanced lifetime and hence detectable by ESR spectroscopy. The reaction follows the simple principle below:

$$R^{\bullet} + ST \rightarrow R - SA^{\bullet}$$

where $R^{\bullet}$ is the radical under inspection, ST is the spin trap and $R - SA^{\bullet}$ is the spin trap adduct (Kleschyov et al 2007).

Generally, the intensity of the signal is proportional to the amount of spin adduct formed.

In recent years, the use of cyclic hydroxylamines for the ESR detection of certain reactive species in biological systems has become increasingly popular. These compounds are not spin traps in the usual sense in that they do not form adducts, but rather become oxidised by the reactive species, thus transferring the unpaired spin from the radical to the so called spin probe. The reaction is summed up in the below:

$$R^{\bullet} + XH \rightarrow RH + X^{\bullet}$$

where $R^{\bullet}$ again is the radical under inspection, XH is the spin probe, RH is the reduced radical in question and $X^{\bullet}$ is the oxidised spin probe.

Spin probes are thus not uniquely specific, and the initial presence of a certain oxidising radical must be validated by the addition of scavengers/inhibitors to the system (Dikalov et al 2011).

3 General Methods and Materials

In this chapter, methods and materials generally relating to cell cultivation are presented. Additionally, protocols, techniques and considerations common to the two main groups of experiments; 1. Superoxide/ROS measurement with spin probe CMH and 2. Nitric oxide measurement with spin trap $Fe(II)(DETC)_2$, are also described here.

Techniques and protocols specific to superoxide/ROS and nitric oxide experiments are presented in the methods sections of the chapters devoted as wholes to their treatment, chapters 4 and 5 respectively.

3.1 The Cell Lines

The experiments in this thesis were performed on two immortalised cell lines of human origin, T-47D and T98G. These are adapted to proliferate in culture at ambient oxygen concentration (20% O_2). Fresh cells are taken out of cryostorage twice a year (summer/Christmas) and kept in continuous culture.

T-47D

T-47D is a mammary ductal carcinoma cell line isolated from a pleural effusion from a 54 year old woman in 1974 (Keydar et al 1979). T-47D has normal Rb function, but contains only single copies of mutant p53 (Amellem et al 1998, Casey et al 1991).

T98G

T98G was isolated in the 1970s from glioblastoma multiforme tumour tissue from a 61 year old man (Stein 1979). T98G also has mutant p53.

Primed Cells

Experiments were also performed with so called primed cells, which have been γ-irradiated with a shielded Theratron 780-C ^{60}Co-source at the Norwegian Radium Hospital, at low dose rate ~0.2 Gy/h over 1 h to give a total priming dose of ~0.2 Gy. New batches of primed cells

are made biannually with cells relatively fresh out of cryostorage. Primed cells are indicated by a suffix "–P", giving T-47D-P and T98G-P. See section 2.3.2.

3.2 Cell Cultivation

Cells kept in continuous culture constantly grow and divide, and so need vigilant care in the form of subculturing, fresh supplementation of nutrients and growth factors and removal of waste products. Suboptimal conditions, such as too high or low density of cells, or depletion of nutrients may inhibit proliferation and/or cause cell death. Therefore, cells are passaged twice a week (Monday and Friday) and receive an additional change of medium once weekly (Wednesday).

Cells are cultured in monolayers in sterile, disposable plastic cell flasks with bottom surface area of either 25 cm^2 or 75 cm^2. The medium used is RPMI (Roswell Park Memorial Institute), buffered with $NaHCO_3$ and supplemented with 10% foetal calf serum, 1% streptomycin, 1% penicillin, 1% l-glutamine and 0.2% insulin. The addition of phenol red gives an indication of the pH in the medium. Cells are incubated at 37 ºC.

3.2.1 Subculturing

Cells are washed twice with ~1.5 ml trypsin supplemented with EDTA, and then left to incubate at 37 ºC until cells start to detach from the bottom of the cell flask. This is expedited by giving the flask a brisk tap. Fresh RPMI medium is then added to cease the action of trypsin and cells are thoroughly resuspended before reseeding of a certain fraction in new flasks with fresh medium. The reseeding fraction depends on the proliferation rate of the cells in question and the number of days until the next subculturing, typically being1/4 – 1/6 for T-47D and 1/13 – 1/16 for the more quickly proliferating T98G. For 25 cm^2 and 75 cm^2 cell flasks, the total volume of fresh medium supplied is 5 ml and 15 ml respectively. Cell flasks are incubated with open caps in 5% CO_2 and 20% O_2.

3.2.2 Sterile Technique

Cell cultures are prone to infection by a host of microorganisms, and it is essential to keep equipment and working environment clean and sterile whenever possible.

All sterile work with cells in ambient air was performed in a LAF (laminar air flow) bench, which hinders airborne particles from reaching the working environment inside the bench. Working surfaces are routinely cleaned with 70% ethanol to ensure sterility. Hands are always clean (gloved) and washed with 70% ethanol before work with cells commences.

Bottle caps and necks for sterile solutions are burnt with a propane flame before and after use. Disposable equipment, such as pipettes, syringes and plastic test tubes, are kept in sterile packaging/condition and only exposed under laminar flow.

3.2.3 Cell Cultivation in the Hypoxia Box

Cell cultivation in hypoxic atmosphere (4% O_2, 5% CO_2) was performed in an IN VIVO$_2$ 400 glove box hypoxia workstation (Ruskinn, UK). The hypoxia box does not tolerate sterilisation with ethanol and it is vital to keep it as clean as possible by ensuring good manual hygiene through the use of gloves, and immediately removing any potential spills with sterile gauze towels.

Cultivation of cells in the hypoxia box is much like that in ambient air under laminar flow, with a few exceptions.

To avoid oxygenation of hypoxic cells, medium and trypsin must be placed in the hypoxia box in advance of usage. This allows the oxygen concentration of the solution to equilibrate with the hypoxic atmosphere. The time needed for equilibration depends on the volume, and larger flasks with medium are usually placed in the box a day in advance, whereas small quantities of trypsin need no more than a few hours.

Plastic equipment such as cell flasks and test tubes require longer equilibration periods due to slow diffusion in such materials, and these are given at least a few days before use.

3.3 Seeding of Experimental Samples

Experiments measuring nitric oxide with Fe(II)(DETC)$_2$ were performed on 75 cm^2 cell flasks of T-47D and T98G cells, which were ordered in advance from the regular stock of continuous cell culture at the lab.

All experiments with CMH were performed on samples of T-47D cells cultured in 25 cm^2 cell flasks, which were seeded personally. The following subsection (section 3.3.1) therefore concerns samples for superoxide measurements only.

In this case it was desirable to seed an approximately equal number of cells in parallel samples and also to seed roughly the same number of cells per flask from experiment to experiment.

3.3.1 Counting of Cells in Suspension

Two techniques were used to count cells in suspension in order to seed an approximate number of cells for samples; the disposable Bürker chamber and flow cytometry. The Bürker chamber was used to count cells in the earlier experiments, but was found to be unsatisfactory, and so its function was entirely replaced by flow cytometry in later experiments.

In both cases, approximate single cell suspensions were made. Cells were washed with trypsin once, and then incubated with 3 ml (25 cm^2) or 5 ml (75 cm^2) trypsin until cells started to detach. A 10 ml syringe with 2.10×80 mm hypodermic needle was then used to create turbulence in the suspension in order to separate cells from each other. Care was taken to avoid pumping air through the suspension, as this may damage the cells. When the suspension was seen to consist of mostly single cells when placed under the microscope, an equal amount of RPMI was added to the cell/trypsin suspension. The cell suspension was then transferred to a 15 ml test tube and centrifuged at 2000 rpm for 3 minutes. Thereafter, the medium/trypsin solution was aspirated and the cell pellet resuspended in a suitable volume of medium using a 2 ml pipette with rubber teat.

Bürker Chamber Method

A sample of the cell suspension was further diluted (typically 1:10) by transferring a small amount of suspension to another test tube containing fresh medium. The diluted cell suspension was then thoroughly resuspended and a sample examined in a disposable Bürker chamber. The Bürker chamber is etched with a 3×3 matrix with squares of volume 10^{-4} ml. The number of cells in each square was counted, the highest and lowest number disregarded

and the average calculated. This was done for two sets of squares and the average of these was then multiplied by 10^4 to give the number of cells per ml.

Flow Cytometry Method

The flow cytometer measures laser light scattered from particles in a fluid stream. Light scatter is detected in the forward direction of the particle (forward scatter, FSC) and perpendicular to the direction of movement (side scatter, SSC), yielding information about respectively size and granularity of the particle, as well as the total number of particles passing the detector. Viable, single cells in a given suspension may then be identified and counted.

A small, undiluted cell suspension sample was transferred to another test tube, and from this a 500 µl sample was filtered through the cap of a flow tube using an auto pipette (100 – 1000 µl). The two step process was used to prevent contamination of the cell suspension by the non-sterile auto pipette. The cell suspension sample was then vortexed and analysed with an Accuri C6 flow cytometer. A 200 µl sample was analysed at fast fluidics speed. Histograms of FSC-A vs. FSC-H and SSC-A were gated for viable single cells to give the number of such cells in the drawn sample. The reader is referred to the thesis by Jensen (2013) for an explanation and discussion of this method. Another gate was applied to the area representing doublet cells, and the number of cells in this gate was multiplied by two. The total number of cells in the 200 µl sample was then multiplied by five to give the concentration of cells per ml.

Counting of Cells in the Hypoxia Box

Cells (T-47D) which have been exposed to hypoxia for extended periods of time do not tolerate prolonged treatment with trypsin and/or handling with syringe and so the protocol here is slightly different. Cells were washed twice with trypsin and left until they started to detach, much like the routine for subculturing, see section 3.2.1. A suitable volume of medium was then added and a 5 ml pipette used to the flush the cells off the flask surface and suspend them in the medium. The resulting cell suspension was quickly transferred to a test tube and thoroughly pumped using a 2 ml pipette with rubber teat in order to separate cells as well as possible. This is important, as insufficient separation can give local areas of overly

dense cells, which are extra susceptible to detachment/death under oxygen deprived conditions. A sample of this suspension was then transferred to another test tube, which was taken out of the hypoxia box to be counted with the flow cytometer.

Seeding

When the concentration of cells in suspension was determined, a suitable amount of cell suspension was added to experimental cell flasks to give a known number of cells per flask.

Samples for superoxide measurements were seeded at ~400 000 – 600 000 cells per flask. When seeded at ~600 000 cells per flask, the samples would typically be ready for harvesting after three to four days. Cell flasks would receive a medium change after two days, and hypoxic samples which were required to continue in culture for one day more would receive an additional medium change after three days, due to accelerated glucose consumption.

3.3.2 Oxygen Measurements

Oxygen measurements were made using an oxygen sensor (Unisense, Denmark) in order to determine the pericellular oxygen concentration in a representative sample before commencing an experiment with hypoxic cells.

The sensor was calibrated before each use by two-point calibration at ~0% and 4% oxygen. A fresh zero solution was made each time by dissolving 1 g Na_2SO_3 in 50 ml milli-Q water. After calibration at 0%, the sensor was rinsed in milli-Q water and 70% ethanol. The 4% calibration was then made in the hypoxic atmosphere and the calibration curve calculated and applied using the Unisense software.

The sensor was maneuvered into a cell flask using a computer controlled micromanipulator. Oxygen profiles were acquired by measuring the oxygen concentration at 100 μm increments from the atmosphere above the medium surface, down through the medium to the cell layer at the bottom. The data were automatically saved in an excel file.

3.4 Preparation of Chemical Solutions

Krebs HEPES Buffer (KHB)

Krebs HEPES buffer (KHB) was prepared as concentrated stock (×10) containing 0.99 M NaCl, 46.9 mM KCl, 10.3 mM KH_2PO_4, 25 mM $CaCl_2$ (×2 H_2O), 12 mM $MgSO_4$ (×7 H_2O).

Chemicals were weighed using an AG245 dual range analytical balance and dissolved in milli-Q water. This stock could then be kept refrigerated at 4°C.

The concentrated stock was then diluted 1:10 and supplemented with 25 mM $NaHCO_3$, 5.6 mM D-glucose and 20 mM Na-HEPES. The pH was measured in the KHB with an Argus pH meter and NaOH and HCl solutions were used to adjust the pH so that it reached ~7.35. The pH meter was regularly calibrated using pH 4 and 10 standard solutions. The complete buffer solution was finally filtered using a 0.2 μm syringe filter with 50 ml syringe. This buffer could then be kept refrigerated up to three days or frozen at -20°C for longer storage. A more instructive recipe is given in Appendix C.

3.5 ESR Spectroscopy

All ESR work was done in the ESR lab at the University of Oslo with a Bruker EleXsyS 560 Super X X-band ESR spectrometer. A rectangular TE_{102} cavity was used for all experiments.

The spectrometer was always turned on a couple of hours before any measurements were made to allow it to warm up and stabilise.

For every sample, the cavity was tuned and the phase adjusted to provide optimum sensitivity before recording of spectra. The spectrometer was always set to TUNE and the microwave power reduced by increasing the attenuation to 50 dB when changing samples. In TUNE, the resonant frequency was then set by centring the dip. In OPERATE the coupling between the waveguide and cavity was optimised by adjusting the iris screw for a range of increasing power settings so that the diode current was kept stable. The phase was then adjusted for each sample to give the maximum diode current reading.

3.5.1 Placement of Samples in the Cavity

The cavity was fitted with a top collet which held the sample tube in place, making sure it was straight and not moving. A plastic rod was fitted from beneath to ensure that the position of the sample in the cavity was the same from experiment to experiment.

3.5.2 ESR Spectrometer Settings

All ESR-spectra were recorded using a modulation frequency of 100 kHz and a spectrum resolution of 1 k (1024 data points). Additional settings depend upon the system under inspection. Centre field and sweep width (mT) were set so that the complete ESR spectrum of interest would be recorded and appear roughly centred on the screen.

An explanation of the different settings is given below, with abbreviations used elsewhere in the text:

P = microwave power (mW)	-	Increasing the power improves the signal, but may cause saturation.
MA = modulation amplitude (mT)	-	A higher setting increases the signal, but also increases distortion.
#scans = number of added scans	-	The addition of *n* scans ideally improves the signal-to-noise ratio by a factor $\sqrt{n}$.
TC = time constant (ms)	-	Controls electronic filtering of noise. A higher setting will improve signal-to-noise ratio, but may cause loss of fine structure.
CT = conversion time (ms)	-	Time spent on each data point.

3.5.3 Measurement of ESR Signal Intensity

Signal intensity for a line was measured in terms of the peak-to-peak height. See Figure 12 below. This was done using inbuilt software.

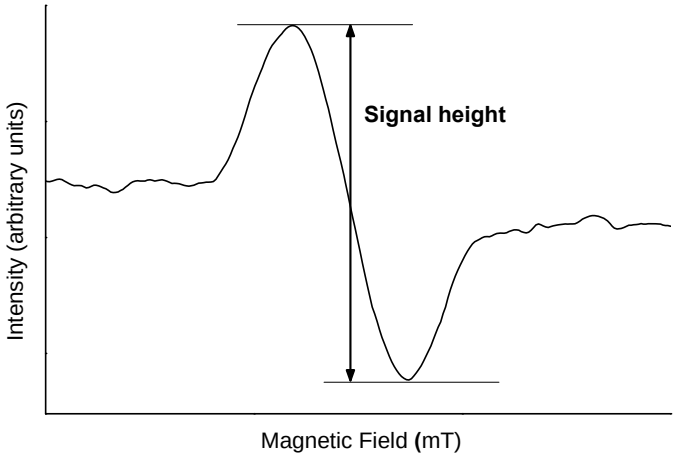

Figure 12
The signal intensity was measured as the height from peak to peak of the low-field line.

3.5.4 Presentation of ESR Spectra

Variations in microwave field frequency from experiment to experiment, and to a lesser degree from sample to sample within an experiment, would cause recorded spectral lines to appear at slightly varying values of magnetic field strength.

In order to more instructively display and compare spectra, these were shifted along the abscissa so that lines of matching g-values fall at the same magnetic field strength value. ESR spectra may so not be positioned in the magnetic field as they were in fact recorded.

Spectra are presented with ESR settings, with the abbreviations explained above.

3.6 Some Statistical Considerations

This section is based as a whole on *Introduction to the Practice of Statistics* (Moore et al 2012).

Quantification of Uncertainties in Measurements

The experimental measurements will be summarised by empirical means, plus/minus the standard error of the mean (SEM). When the observations are assumed to be Normally distributed and statistically independent, this corresponds to a 68% confidence interval for the population mean, imagined to be the limit of the empirical mean when an infinite number of

repetitions of the experiment are performed. There seems to be no reason to doubt the statistical independence between repetitions of any of the experiments presented in this thesis. However, due to the small sample size, there is no basis for assessing the assumption of Normality. However, even if the observations are not Normal, the empirical mean plus/minus the SEM does give a reasonable quantification of how uncertain the empirical mean is as an approximation of the population mean.

The empirical mean is given by

$$\bar{x} = \frac{\sum_{i=1}^{n} x_i}{n} \quad (1)$$

where $x_1,\ldots,x_n$ are the observations and n is the sample size.

Irrespective of the distribution of the observations, the standard deviation of the mean equals

$$\frac{\sigma}{\sqrt{n}}$$

where σ is the standard deviation of the observations.

The standard deviation of the mean is approximated by the standard error of the mean (SEM), given by

$$SEM = \sqrt{\frac{\sum_{i=1}^{n}(\bar{x} - x_i)^2}{n(n-1)}} \quad (2)$$

Testing of Significance

In section 4.4, the two-sample t-test procedure will be used. Because the sample sizes of these experiments are all of the order 3-5, the measurements will be assumed to be Normally distributed. Without any distributional assumptions on the data, statistical tests cannot be performed when the sample size is this small.

Suppose one observes $n_x$observations $x_1,\ldots,x_{n_x}$with population mean μ_x and $n_y$observations $y_1,\ldots,y_{n_x}$with population mean μ_y. To test the null hypothesis $\mu_x = \mu_y$ versus the alternative hypothesis $\mu_x \neq \mu_y$, one may use the two sample t-test statistic

$$t = \frac{\bar{x} - \bar{y}}{\sqrt{\frac{s_x^2}{n_x} + \frac{s_y^2}{n_y}}}$$

where

$$s_x = \sqrt{\frac{\sum_{i=1}^{n_x} (\bar{x} - x_i)^2}{(n_x - 1)}}$$

is the empirical standard deviation of the x-observations and

$$s_y = \sqrt{\frac{\sum_{i=1}^{n_y} (\bar{y} - y_i)^2}{(n_y - 1)}}$$

is the empirical standard deviation of the y-observations.

Under the null hypothesis, this statistic is t-distributed with a complicated degree of freedom formula, computed by statistical software. This test is valid even when the standard deviations of the two populations are not equal.

If the standard deviations of the two populations are assumed to be equal, the pooled t-statistic

$$t = \frac{\bar{x} - \bar{y}}{s_p \sqrt{\frac{1}{n_x} + \frac{1}{n_y}}} \quad (3)$$

where

$$s_p = \sqrt{\frac{(n_x - 1)s_x^2 + (n_y - 1)s_y^2}{n_x + n_y - 2}}$$

may be used and is t-distributed with $n_x + n_y - 2$ degrees of freedom under the null hypothesis that $\mu_x = \mu_y$. If the assumption of equal variances is correct, this test has higher statistical power than the standard t-test.

4 Superoxide/ROS Measurement with Cyclic Hydroxylamine Spin Probe 1-hydroxy-3-methoxycarbonyl-2,2,5,5-tetramethylpyrrolidine (CMH)

As reviewed in section 2.3.3, Edin et al. have proposed a number of mechanisms responsible for the elimination of hyper radiosensitivity (HRS) featuring the involvement of reactive oxygen species (ROS). In particular, the process of LDR priming is thought to induce a state of permanently elevated ROS in the so called P-cells, giving activation of TGF-β3 and subsequent elimination of HRS. Additionally, reoxygenation after hypoxia is thought to generate a burst of ROS which mimics the effect of irradiation, again giving elimination of HRS. This is permanent if $NO^{\bullet}$-donor is supplemented before reoxygenation and transient otherwise.

As discussed in section 2.1.4, initial formation of superoxide is the main source of cellular ROS. Therefore, in order to probe ROS levels, superoxide is measured.

4.1 Cyclic hydroxylamine CMH as spin probe for $O_2^{\bullet-}$ /ROS

Cyclic hydroxylamines (CHAs) were recently found to be efficient probes for the detection of ROS in biological systems and enjoy several advantages over older methods.

Cyclic hydroxylamines react rapidly with superoxide ($k \sim 10^3 – 10^4\ M^{-1}s^{-1}$, pH = 7.4) to form stable nitroxides with half-lives of several hours. This efficient scavenging of superoxide allows CHAs to compete with intracellular antioxidants and therefore low concentrations of spin probe may be used (0.05 – 1 mM), minimising potential adverse effects in cells or tissue. Additionally, the spin probe is oxidised in a one-step reaction, thus avoiding potential artefacts which may arise from methods of detection requiring more steps. In contrast to some fluorescent and chemiluminescent techniques, cyclic hydroxylamines do not engage in redox

cycling, which otherwise may lead to problems with artificial $O_2^{\bullet -}$ production (Dikalov et al 2011).

Cyclic hydroxylamines are however not specific to one radical species, but can potentially be oxidised by several ROS. The identification of a specific oxidising species is accomplished through supplementary experiments using parallel samples including agents which inhibit or scavenge that particular species.

CHAs generally do not react with hydrogen peroxide, but transition metal ions (Cu, Fe) may catalyse their oxidation in the presence of H_2O_2, by formation of hydroxyl radical (Dikalov et al 2007b). The use of chelating agents such as desferroxamine (DES) and DETC is therefore essential for the elimination of artificial signals caused by such reactions.

A range of cyclic hydroxylamines are available as spin probes for ROS, which display varying degrees of cellular and mitochondrial permeability, allowing the quantification of superoxide produced by various cellular compartments both *in vitro* and *in vivo*.

CMH

The cyclic hydroxylamine spin probe 1-hydroxy-3-methoxycarbonyl-2,2,5,5-tetramethylpyrrolidine (CMH) is highly cell permeable and can detect both extracellular, intracellular and even mitochondrial ROS. CMH reportedly has the highest affinity for $O_2^{\bullet -}$ of the CHAs ($k \sim 1.2 \times 10^4\ M^{-1}s^{-1}$) (Dikalov et al 2007a). Its chemical structure before and after oxidation is seen in Figure 13.

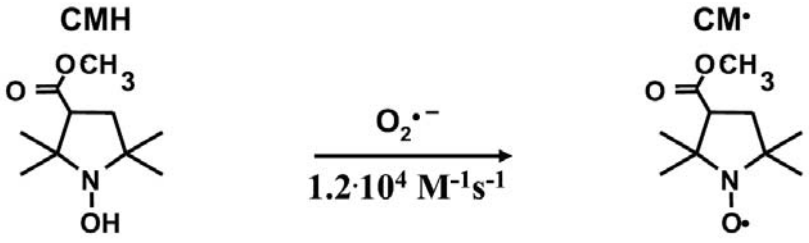

Figure 13
The chemical structure of cyclic hydroxylamine spin probe 1-hydroxy-3-methoxycarbonyl-2,2,5,5-tetramethylpyrrolidine (CMH). CMH reacts with superoxide with rate constant $1.2 \times 10^4 M^{-1}s^{-1}$ to form stable nitroxide $CM^{\bullet}$ detectable by ESR. The oxidation of CMH to $CM^{\bullet}$ is not specific to $O_2^{\bullet -}$. Adapted, from Dikalov et al (2007a).

Although nominally indicated to be localised at the ^{16}O nucleus, the unpaired spin is delocalised over the ^{14}N – ^{16}O fragment (the ^{16}O-nucleus has I = 0) and the resulting Fermi-coupling to the ^{14}N-nucleus (I = 1) yields a 1:1:1 three-line isotropic spectrum at ambient temperature, with g = 2.004 and a = 1.5 mT. This is illustrated in Figure 14.

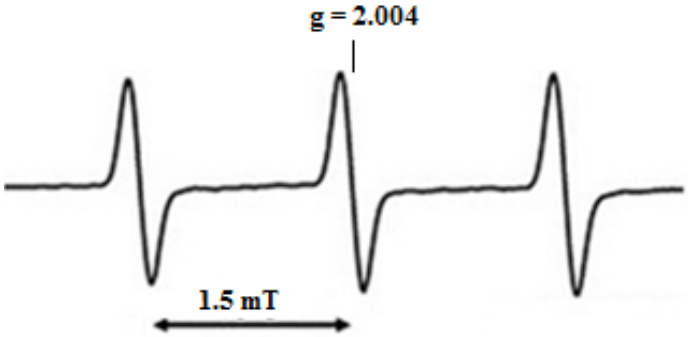

Figure 14
The ESR spectrum of the oxidised spin probe CM• at ambient temperature (293 K), showing the triplet splitting due to coupling to the nitrogen (I = 1) nucleus. g = 2.004 and a = 1.5 mT.

4.2 Chemical Solutions

Krebs HEPES buffer (KHB) prepared as described in section 3.4, p. 42, was used for all experiments with the spin probe CMH with the addition of chelating agents desferroxamine (DES) and diethyldithiocarbamate (DETC) at concentrations of 25 µM and 5 µM respectively. KHB was either prepared fresh or thawed from storage at -20 °C. DES and DETC were always freshly prepared by dissolution in milli-Q water. The abbreviation "KHB-D" will in the following always signify KHB supplemented with DES and DETC.

NOS-inhibitor L-NG-nitroarginine methyl ester (L-NAME) was dissolved in milli-Q water to give an 18.5 mM stock solution. This was always prepared fresh and kept on ice. For experiments with L-NAME, which is the vast majority, L-NAME was added to KHB-D before deoxygenation.

The spin probe CMH was weighed and dissolved in deoxygenated KHB-D to give 1 or 10 mM stock solutions. This was either used fresh, kept on ice under N_2-bubbling, or stored at -80 °C in aliquots giving enough for two samples per tube.

For more detailed quantities, see Appendix C**.**

4.3 Establishment and Development of Method

The following gives a description of various experimental methods and protocols used in experiments relating to measurements of superoxide/ROS using the spin probe CMH. Samples for use in the experiments were seeded as described in section 3.3, p. 38. The experiments were performed when the flasks were subconfluent with ~3 - 4×10^6 cells per flask.

4.3.1 Primary Protocols for Measurement with CMH

Munich Protocol

Cell flasks were rinsed with phosphate buffered saline (PBS). Deoxygenated KHB-D was added and the cells scraped with a rubber policeman. The cell suspension was transferred to an eppendorf tube. CMH was then added at final concentration 100 μM and cell suspension was immediately drawn into a capillary tube and measured in the ESR spectrometer. For samples to be treated with L-NAME this was added to cell suspension in KHB-D at 300 μM and samples were incubated on ice for 10 min. CMH (10 mM) was kept in frozen aliquots at -80 °C and thawed and kept on ice during experiments.

The first measurements replicated this protocol, using 450 μl KHB-D and 50 μl CMH solution.

Supernatant Protocol

This protocol was adopted from Deschacht et al (2010).

Cell flasks were rinsed with PBS and supplemented with deoxygenated KHB-D. CMH was added at final concentration 100 μM and samples were incubated for 50 minutes at 37°C. The incubation time was later shortened to better suit the experiments at hand. Supernatant was then drawn in 50 μl capillaries, stopped with putty and placed in an ESR quartz tube for insertion in the cavity. This method was employed with the following range of total volumes of KHB-D with CMH; 500, 1000 and 1500 μl.

In both cases, one sample at the time was prepared and spectra were recorded after a set amount of time after addition of spin probe, allowing for tuning of the cavity. This time varied somewhat from experiment to experiment due to varying degrees of cooperation on the part of the spectrometer.

4.3.2 Supplementation of NOS-inhibitor L-NAME

Cell flasks were supplemented with 300 μM L-NAME before preparation with spin probe. For hypoxic samples, L-NAME was deoxygenated by bubbling with N_2.

1. For experiments with cells cultured at ambient oxygenation (with the exception of reoxygenated such cells, which were treated as in point 2.), cell flask medium was supplemented with L-NAME ~20 min before sampling.

2. For larger experiments with cells cultured under hypoxia, L-NAME was added to cell culture medium 20 – 60 min before sampling. This was added to batches of four with auto pipette to the medium, taking care not to disturb the cell flask any more than necessary in order to avoid a small reoxygenation of cells by higher concentrations of oxygen in layers closer to the surface. The batch of flasks was then left to incubate for ~20 min before sampling began.

3. For flasks sampled in hypoxic atmosphere (oxygen concentration set to 0.1%), see section 4.3.5, cell flasks cultured in parallel with experimental samples were harvested for medium which was supplemented with L-NAME, deoxygenated and donated to experimental samples. Flasks were quickly turned upside down, and medium was removed and replaced with deoxygenated medium equilibrated to the hypoxic atmosphere. Flasks were then turned right side up and incubated for ~20 min.

L-NAME was also supplemented in KHB-D at 300 μM. For reoxygenation experiments, 300 μM L-NAME was also present in fresh medium.

Samples which were not to be treated with L-NAME were given an equivalent volume of ice cold milli-Q water.

4.3.3 Determination of Pericellular Oxygenation for Hypoxic Cells

Hypoxic cells were monitored for pericellular oxygen concentration with an oxygen sensor as described in section 3.3.2. Oxygen profiles were set to run until the pericellular oxygenation was seen to have reached ~0.1%. This typically took three days, depending on the number of cells seeded and handling of cells.

In later experiments, an oxygen sensor was not available. However, cell flasks were viewed under a microscope and harvested when seen to be sufficiently dense to have reached a pericellular oxygenation of ~0.1%, judging by experience.

Cells received a change of medium after two days of hypoxic culture and again after three days if they had to run for an additional day to reach a pericellular oxygenation of ~0.1%.

4.3.4 Reoxygenated Samples

Cells were reoxygenated by two main methods:

- Reoxygenation with fresh medium

  Flasks were removed from the hypoxia box and reintroduced to 20% O_2, whereupon they were replenished with fresh medium equilibrated to the ambient atmosphere. Flasks were allowed to reoxygenate for a set amount of time (min) and then prepared for sampling.

  "0" min reoxygenation samples were not replenished with fresh medium, but directly rinsed with PBS. Samples with reoxygenation times below or equal to 2 min were reoxygenated in the incubator room and the sample was prepared with KHB-D and CMH in the basement before being brought up during the spin probe incubation time. Otherwise, the flask was brought up during reoxygenation with medium and allowed to spend the remainder of the time in the incubator at 37°C before sampling.

- Reoxygenation without change of medium

  Flasks were brought out of the hypoxia box, the caps removed and they were then allowed to reoxygenate in an incubator room (37°C) on a gently rocking tray.

4.3.5 Preparation of Samples in Hypoxic Atmosphere

For sampling with CMH in KHB-D in hypoxic atmosphere, filter caps were exchanged with solid caps, and these were closed so that the flasks retained an atmosphere of just below 4% O_2. The oxygen concentration was then turned down from 4% to 0.1%, the lowest setting available, and the box allowed time to reach this value.

Deoxygenated PBS, KHB-D and CMH were brought into the box, and samples were prepared according to regular protocols for supernatant or cell suspension, but the entire process took place in the hypoxia box. Regular stopping putty did not function in the hot, humid atmosphere, and an air curable malleable rubber (Sugru) was used for these samples to seal both ends of the capillary tubes. These were then inserted in the quartz tube, which was sealed with a plastic cap. Only then was the sample brought out of the hypoxia box for regular measurement with the ESR spectrometer.

4.3.6 Protein Measurement With the Bradford Assay

Protein measurements were carried out using the Bradford assay in order to normalise detected ESR signal to the protein content of samples.

The Bradford assay is a colorimetric assay which is based on the binding of Coomassie Brilliant Blue G-250 dye to proteins. In acidic conditions, the dye mostly exists in its cationic doubly protonated red form. Binding to protein converts the dye to a stable unprotonated blue form with maximum absorption spectrum at 595 nm. A purified protein, in this case bovine serum albumin (BSA), diluted at known concentrations is used to create a standard curve in order to relate the optical density measured in samples to protein content.

Preparation of Samples

- Supernatant protocol

  Two main methods for preparation of supernatant samples for protein measurement were used:

1. Supernatant with spin probe was removed and cells rinsed with PBS. 20 ml 0.2 N sodium hydroxide (NaOH) was then added and samples were incubated on a tray for about an hour, until protein suspensions appeared to be sufficiently dissolved. Flasks were agitated to help the process along. This method was not very good and the resulting lysed cell suspension contained gel-like filaments even after prolonged incubation with NaOH. This inhomogeneity was obviously an issue. Therefore, trichloroacetic acid (TCA) was used to extract protein in later experiments, which is, as was belatedly realised, the common method for preparation of cells for protein measurement.

2. Supernatant with spin probe was removed and cells rinsed with ice cold PBS. Cells were then left to fixate in 2 ml of 10% TCA for 10 – 15 min. The 10% TCA was then removed and rinsed out with 2% TCA. The cells were then stored in 2% TCA in a refrigerator overnight or for up to two days. When protein measurements were to be made, TCA was removed and flasks were rinsed with PBS. 20 ml 0.2 N NaOH was then added and samples were incubated for at least ten minutes, but no longer than two hours on a rocking incubator tray.

- Suspension protocol

Samples were centrifuged and the supernatant removed. 200 µl 10% TCA was added and the tubes vortexed. After 10 – 15 min, 800 µl milli-Q water was added to give 2% TCA. Samples were then stored as above.

Tubes with cells in TCA were then centrifuged again and 900 µl supernatant aspirated, leaving 100 µl to minimise loss of protein. 900 µl 0.2 N NaOH was then added and samples were incubated for at least ten minutes, but no longer than two hours. Lysed cell samples were then diluted 1:10 in 0.2 N NaOH.

Protein Measurement

BSA was diluted in 0.2 N NaOH at 50 µg/ml. A series of dilutions of BSA were made in a 96 well-plate, 0, 10 – 50 µl in a total of 100 µl per well to give a standard curve of 0 – 25 µg/ml. Supernatant protein samples were diluted at 20 or 30 µl per 100 µl total, whilst suspension samples were added undiluted at 100 µl per well, so that the resulting absorbance values fell

within the linear region of the spectrometer. All dilutions were made with NaOH and everything was done in triplicate. 100 µl Bradford stock dye was then added to each well, for a total volume of 200 µl. The well-plate was then allowed to incubate for at least five minutes, but no longer than an hour. The absorbance was measured at 595 nm using a micro plate reader.

A simple linear regression model was fitted to the standard curve (the linear part) and the protein content of the samples deduced from this.

4.3.7 ESR Spectroscopy

Capillary samples in quartz tubes were inserted in the cavity and spectra were recorded at ambient temperature (~295 K). The capillary tube was positioned such that the entire cavity was covered by a cylinder of cell suspension/supernatant. The bottom part containing ESR signal yielding stopping putty was kept well below the cavity. Added scans were recorded.

The low-field line of the spectrum was then measured as shown in section 3.5.3. The measured intensity is proportional with the amount of oxidised spin probe ($CM^{\bullet}$) formed.

4.3.8 Presentation of Data

For added scans, the recorded intensity (see section 3.5.3) was divided by the number of scans to give an average value per scan. This average signal intensity per scan represents the relative amount of oxidised spin probe present in the sample, which again is proportional with the amount of detectable ROS (superoxide) present in the sample.

Results are either presented as scatter plots or as column plots. All data are plotted as empirical averages with standard error of the mean (SEM) error bars (see section 3.6, equations (1) and (2)). Means plotted against time are presented as scatter plots, whereas means for categories for comparison of cell types or treatment are presented as column plots.

All experimental results are presented in two versions side by side; in the left panel, the ordinate axis represents the average ESR signal per scan (“ESR signal”), whilst in the right panel it represents the average ESR signal per scan normalised to protein content (“ESR signal/µg protein”). The abscissa is the same in both panels.

4.4 Results and Analysis

4.4.1 Preliminary Experiments

T-47D cells were prepared according to the Munich method in eppendorf tubes and cell suspension with CMH was drawn in 100 µl capillaries.

ESR Settings

The initial ESR spectrometer settings used were immediately successful in detecting a signal from the oxidised spin probe CM•. These were as shown in Table 1 below.

Centre Field (mT)	Sweep Width (mT)	Mod. Amplitude (mT)	Conversion Time (ms)	Time Constant (ms)	Mod. Frequency (kHz)
348	6	0.27	81.92	655.36	100

Table 1 *ESR settings used for recording of spectra for superoxide samples with spin probe CMH.*

A representative spectrum is shown in Figure 15.

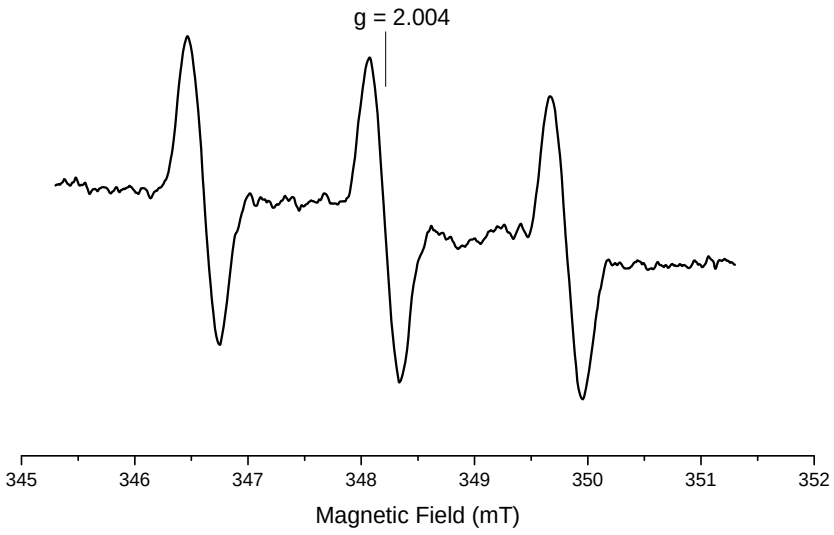

Figure 15
Representative ESR spectrum for the oxidised spin probe CM• in cell suspension of T-47D cells with 100 µM CMH in KHB-D. ESR settings: P=25 mW, MA=0.27 mT, #scans=3, TC= 655.36 ms, CT= 81.92 ms.

During recording of ESR spectra, the cells would sink and accumulate at the bottom of the capillary tube. This was a concern, since it was then uncertain what one was actually measuring superoxide in, making normalisation of ESR signal to protein content dubious. Some scraped cell suspension samples which had been stored at 4°C for two days were centrifuged and a sample of supernatant drawn for inspection with the ESR spectrometer. This supernatant sample also yielded a strong ESR signal and the development of this signal with time was examined at irregular intervals over three days. The results are shown below in Figure 16.

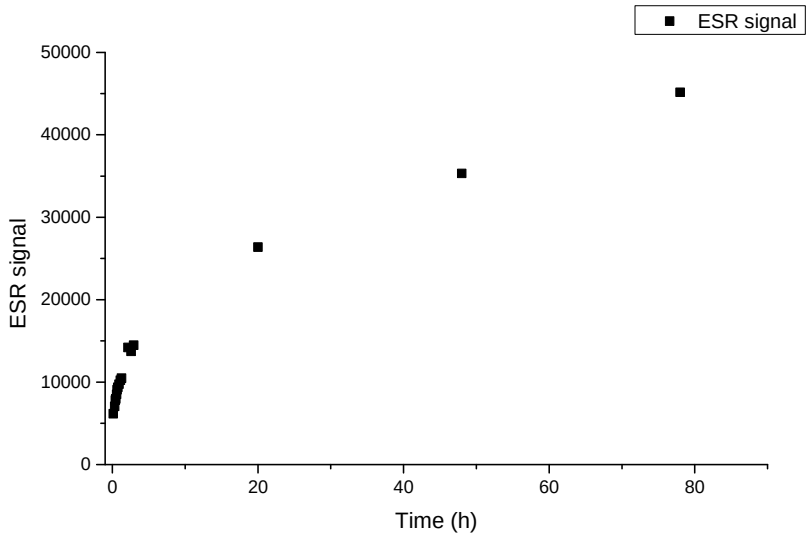

Figure 16
The time development of the ESR signal detected from the oxidised spin probe CM˙ in supernatant from centrifuged cells after preparation with the Munich protocol. ESR spectra were recorded at irregular intervals over three days with the ESR settings given in Table 1.One single scan per time was recorded.

The ESR signal increases logarithmically with time, indicating continued oxidation of CMH. Since no cells were present in the sample, the increase in oxidised spin probe present was attributed to diffusion of molecular oxygen into the sample.

Apart from the apparent ability of molecular oxygen to oxidise CMH, what is indicated by the data shown in Figure 16 is that oxidation of CMH forms a highly stable nitroxide radical since no decrease in signal is seen even after three days. The decrease in the rate of growth with time may reflect the fact that there are progressively lower concentrations of CMH available for oxidation, thus causing the reaction to proceed at a slower rate.

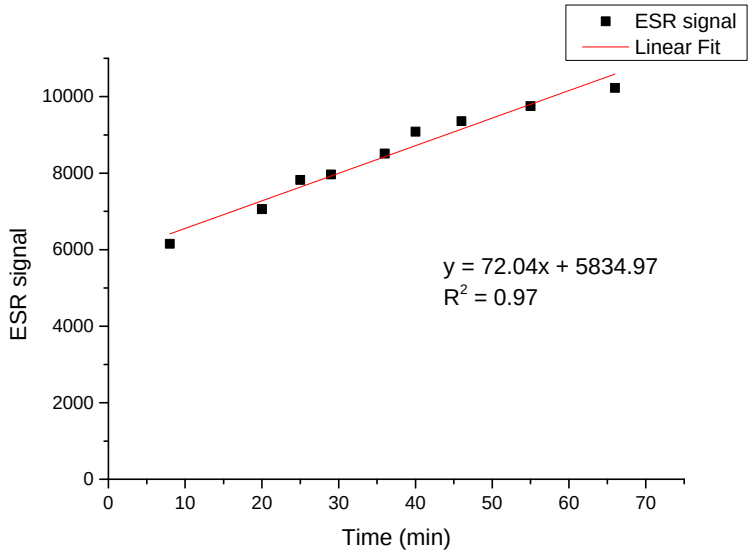

Figure 17
Shown is the development of ESR signal with time detected in the same sample as that of Figure 16, but for the first data points only. The increase in signal with time is linear over the first hour (R^2 = 0.97).

In Figure 17 the same data as shown in Figure 16 is plotted, but for the first data points only. There is a linear increase in signal over the first hour (R^2 = 0.97), indicating that there is a sufficient concentration of CMH available for oxidation to occur in proportion with the concentration of oxidising species present.

Please note that this result was inappropriately applied to conclude that a concentration of 100 µM CMH was sufficient to use for incubation of cells for 50 minutes with spin probe. The oxidation of the spin probe in a cellular system would most probably be much greater than that of background oxidation due to molecular oxygen. However, the samples used had been exposed to air and stored in plastic eppendorf tubes for two days, making a rather high background oxidation likely.

The Munich protocol utilised a microwave power of 25 mW, and no saturation was seen when using this setting. It was however noticed after a while that the cavity was somewhat difficult to tune, and that the diode current would drift during recording of spectra. This was assumed to be due to heating of the sample through the high microwave effect. The power was therefore reduced to 10 mW in later experiments. The time constant was also changed in later experiments from 655.36 ms to 1310.72 ms. This setting afforded ESR signals with a greater signal-to-noise ratio without loss of spectral features.

4.4.2 Test of ESR Signal in Supernatant with Known Number of Cells

5 × 2 cell flasks were seeded with an increasing number of cells in order to examine how the cell density affected the ESR signal as recorded in supernatant. The flasks were seeded and

incubated for two days without change of medium, and prepared for measurement according to the supernatant protocol. Samples were supplemented with L-NAME (in medium for 20 min and in KHB-D) and incubated for 50 minutes with 100 µM CMH. ESR spectra were recorded at 25 mW.

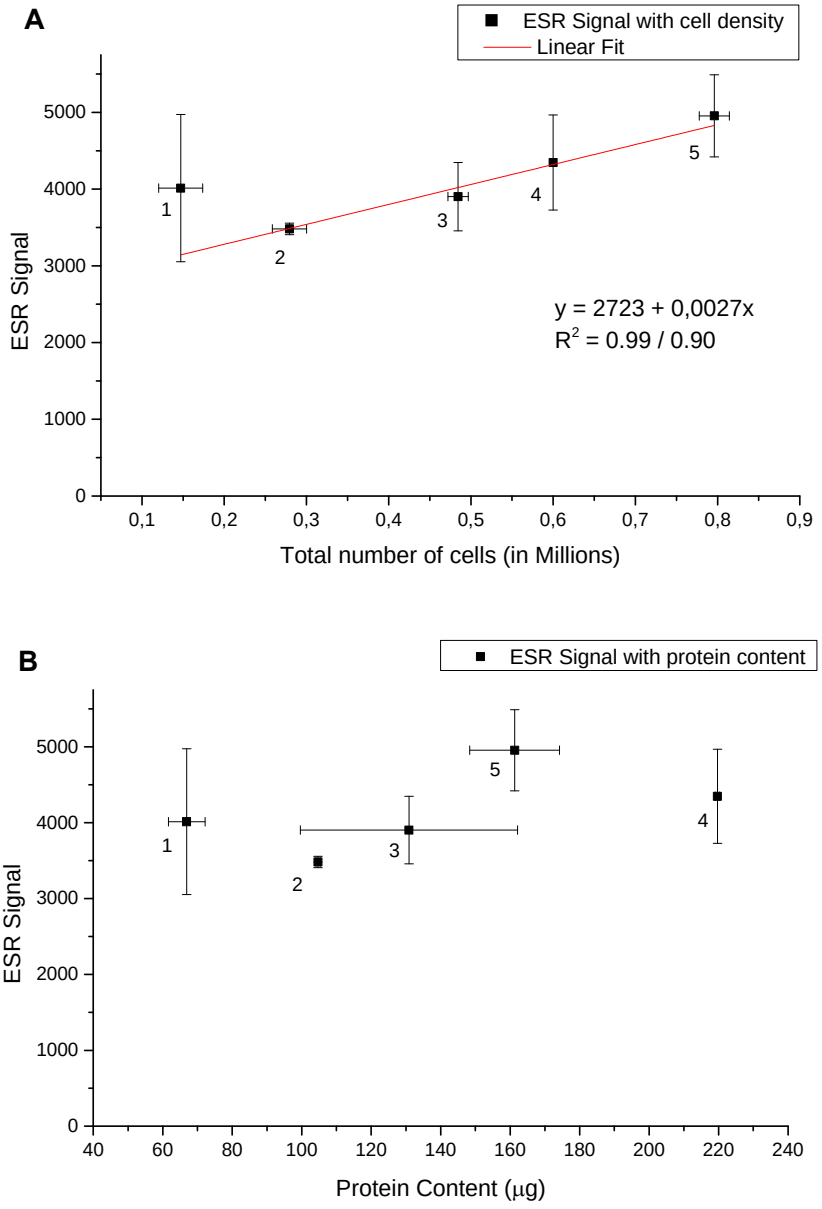

Figure 18
The variation in ESR signal as recorded in the supernatant of cell flasks of known cell density after 50 min incubation with 100 µM CMH. Panel A shows the ESR signal as a function of the number of cells in the flask, which was deduced by counting of cells in 4 pictures per cell flask and taking the average.
A linear regression model was fitted to the sample means, with (R^2 = 0.90) and without (R^2 = 0.99) the data point labelled "1".
Panel B shows the ESR signal as a function of protein content as measured by the Bradford assay. Data points are labelled 1 – 5 in rising order of seeded cell density. ESR spectra were recorded at 25 mW.

The cell flasks used for these measurements were not very densely seeded, with flasks containing between 120 k and 820 k cells as compared with the roughly 3000 k cells per flask generally used for experimental samples.

The number of cells per flask was deduced from counting of cells in four pictures per flask, taking the average and multiplying with a factor to give the total number per flask. The pictures were taken immediately before the experiment began.

As can be seen in Figure 18A, the ESR signal detected in the supernatant is very well approximated by a linear function of the number of cells present in the flask during incubation with spin probe. Although the sample size for each data point is very small (n = 2), when modeled on all the data points, a linear fit gives an $R^2 = 0.90$, whereas when the first data point is removed, an almost perfect linear fit is obtained ($R^2 = 0.99$). The corresponding correlation between ESR signal and protein content as measured with the Bradford assay is shown in Figure 18B. There is no immediately evident linear relationship in this case. However, the data point marked "5" could be too low due to detachment of cells before/during preparation for protein measurement, resulting in a fewer number of cells being measured, as compared with the number of cells present in the flask during incubation with the spin probe (The optical density values obtained for the samples representing the data point "5" fell within the linear part of the standard curve). A linear fit to the data points 2, 3 and 4 (not shown) gives an $R^2 = 0.92$, with equation $y = 2622 + 8.25x$.

4.4.3 Reoxygenation Experiments on Supernatant

A series of experiments were executed in order to investigate ROS generation from reoxygenated cells at a succession of times after exposure to ambient air and reoxygenation with fresh medium. Five separate experiments with hypoxic cells (designated by #1 - #5) and one with aerated cells (cultured at 20% O_2) were conducted to this end. Three different batches of CMH in aliquots stored at -80°C were used for the different experiments.

Hypoxic Cells

All cell flasks were incubated under hypoxia for a total of three days with medium change on the second day, with the exception of the cell batch used in experiment #3. These were trypsinised too harshly and some of the cells damaged. There was some difficulty in estimating the number of viable cells present and a smaller number of such cells were consequently seeded. Cells would also take longer to enter the cell cycle due to damage. These flasks required a change of medium after one day to remove debris and again on the third day, before harvesting on the fourth. It is therefore likely to be slightly more variation in cell density between flasks for this experiment.

Cell flasks were allowed to reoxygenate with medium for 1 – 20 min (also 60 and 120 min), before the medium was removed and the flask rinsed with PBS before sampling. The exception is the "0" min reoxygenation, which was directly rinsed with PBS and prepared for sampling. All samples were treated with L-NAME.

Cells Cultured at Ambient Oxygenation

Cells cultured at 20% O_2 were also examined for reoxygenation response. These were treated and prepared for sampling exactly as the hypoxic cells, but everything was done at ambient oxygenation.

In these experiments, batches of four flasks at the time were supplemented with L-NAME. This would mean that they were incubated with the NOS-inhibitor for different lengths of time. The effect of different incubation times with L-NAME was informally tested. A batch of cell flasks were contemporaneously supplemented with L-NAME to the medium and incubated for at least 20 min. Flasks were then prepared and incubated with spin probe at regular intervals after initial supplementation of L-NAME. No apparent change in recorded signal intensity was observed within 120 minutes, which was the greatest time examined (data not shown).

For these experiments, the incubation time with spin probe was shortened from 50 to 5 minutes (#1 and #2), and later to 1 minute and 40 seconds (#3, #4, #5 and #20%), in order to better separate the effect of superoxide/ROS generation with time. The rather conspicuous time of 1 minute and 40 seconds was that required to transport a sample from the hypoxia workstation in the basement to the ESR laboratory on the 3rd floor.

Experiment	Incubation time with CMH	CMH batch	Microwave Power (mW)	#scans
#1	5 min	1	25	3
#2	5 min	1	10	3
#3	1 min 40 s	2	10	3
#4	1 min 40 s	3	10	2
#5	1 min 40 s	3	10	2
#20%	1 min 40 s	3	10	2

Table 2 *Variations in ESR settings and protocols used for the different reoxygenation experiments performed on supernatant.*

The variations in ESR settings and protocols used for the different experiments can be seen in Table 2. These variable settings largely explain the differences in overall level of ESR signal seen for the different experiments. The pericellular oxygen concentration was measured in a representative cell flask for all measurements with hypoxic cells. The pericellular oxygenation before commencement of measurements was ~0.1% for all experiments.

Sampling of flasks for different reoxygenation times was done in relatively random order.

Experimental Results

Reoxygenation time is plotted against both average signal recorded per scan, "ESR signal", and against this signal normalised to measured protein content. The results for the reoxygenated hypoxic samples of experiments #1, #2, #3, #4 and #5 are seen in Figure 19. Please note the differences in scale used to present the various data sets.

There is a certain trend present in these curves. Three out of four curves display an initial heightened signal at "0 min" reoxygenation, before a dip for 1 – 2 minutes, whereupon the curve is seen to rise again to a plateau of sorts at between 5 – 8 minutes. Thereafter the signal is seen to decline in an erratic manner. Experiment #3 also featured measurements at 60 and 120 min, which are not shown here for ease of viewing. Complete data sets are given in Appendix D.2

These reoxygenation experiments were repeated with the aim of increasing the sample size and thus build stronger statistics. However, the trend seen in the plots of Figure 19 could not be reproduced to any satisfaction when amalgamating data from the different experiments. The differences in incubation time with spin probe between experiments #1 and #2 (5 min) and the remaining experiments (1 min 40 sec) would also give a more smeared out relation of signal with time for the former as compared with the latter.

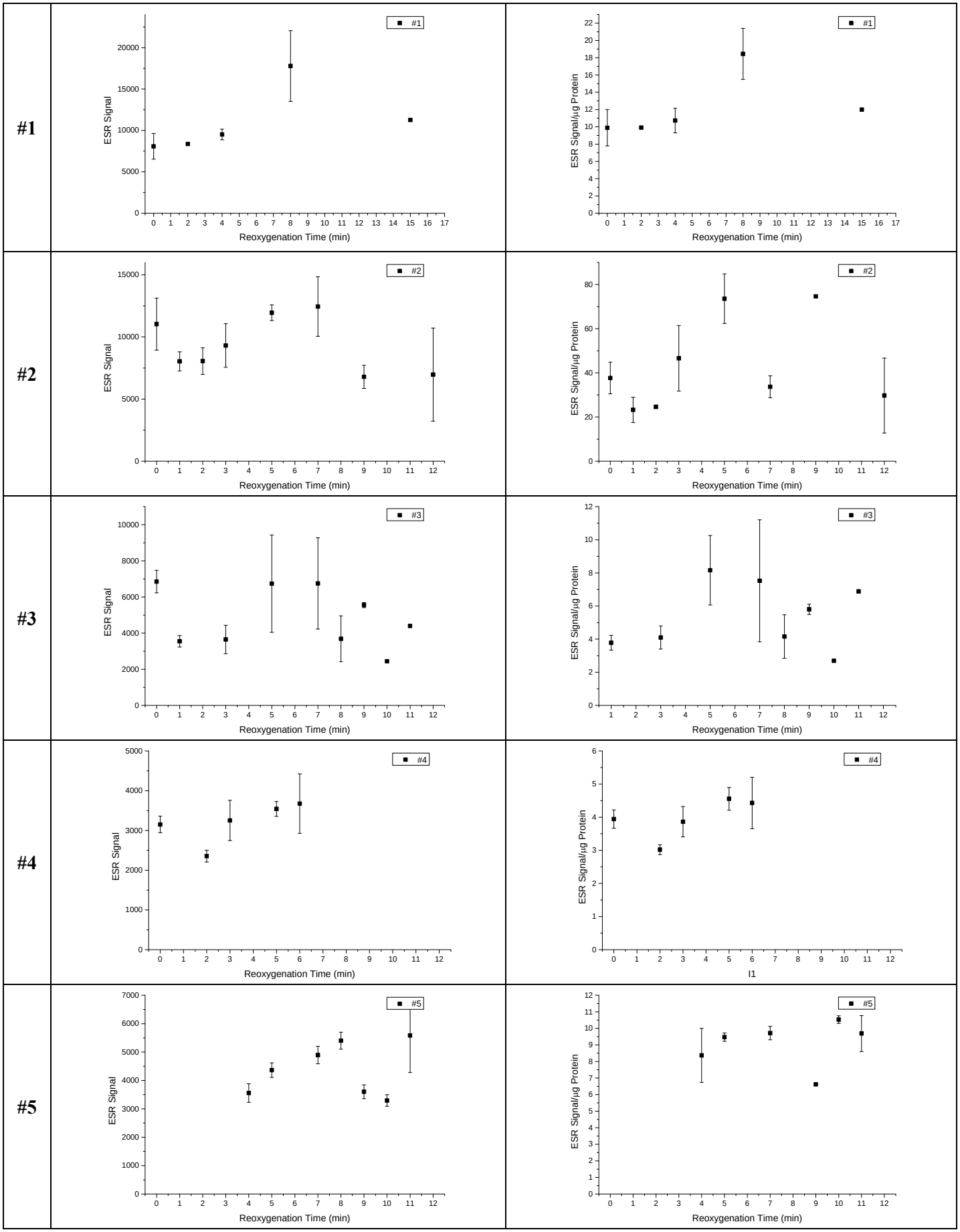

Figure 19

Reoxygenation experiments#1 - #5 performed on supernatant from hypoxic cells reoxygenated with fresh medium. The panels on the left show the variation in ESR signal detected with reoxygenation time. The panels on the right show the same results, but with ESR signal normalised to protein content. Please note the differences in scale used for the various panels. See Table 2 for variations in ESR settings and protocols used for the different experiments.

The change in ESR signal with time detected in the supernatant of reoxygenated cells cultured at 20% O_2 can be seen below in Figure 20. In this case there appears to be a relatively steady increase in levels of oxidised spin probe present in samples with increasing reoxygenation time, and no decline in signal is seen in the first 12 minutes. The initial levels of superoxide/ROS detected are similar to those seen for experiment #4, which used CMH from the same batch and otherwise the same protocols and ESR settings.

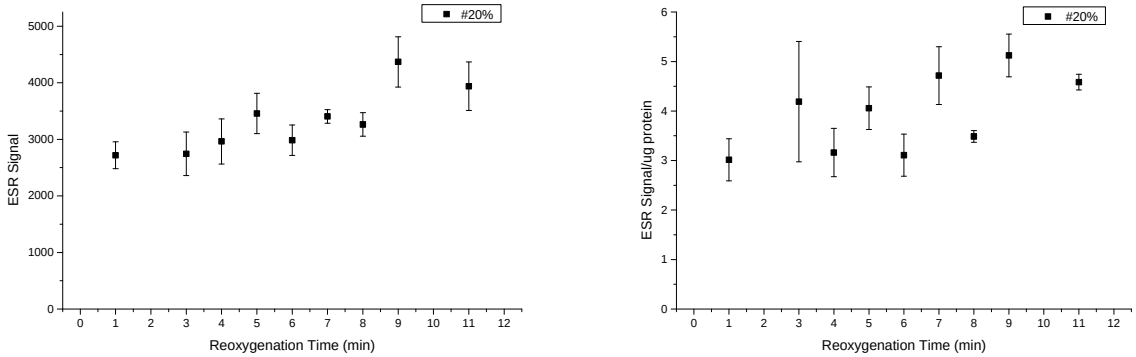

Figure 20
Reoxygenation experiment performed on cells cultured at ambient oxygenation (20% O_2). The panel on the left shows the development of ESR signal with reoxygenation time, whereas the panel on the right shows the same but for ESR signal normalised to protein content.

4.4.4 Hypoxic and Reoxygenated Cyclic Hypoxic Cells Sampled in Hypoxic Atmosphere

An experiment was carried out in order to examine the change in superoxide/ROS levels upon reoxygenation to 20% O_2 of cells cultured under cycling hypoxia as compared with unreoxygenated hypoxic controls.

Cells were cultured under hypoxia (4%) for over four weeks. Samples were supplemented with L-NAME as described in point 3. of section 4.3.2 and samples of supernatant were prepared according to section 4.3.5. Samples were reoxygenated without change of medium for five minutes at ambient oxygenation and then returned to the hypoxic atmosphere for preparation with spin probe. This reoxygenation time was chosen based upon the reoxygenation curves shown above in section 4.4.3. Samples were incubated for 5 min with spin probe.

The results obtained for hypoxic and reoxygenated cells are shown in Figure 21.

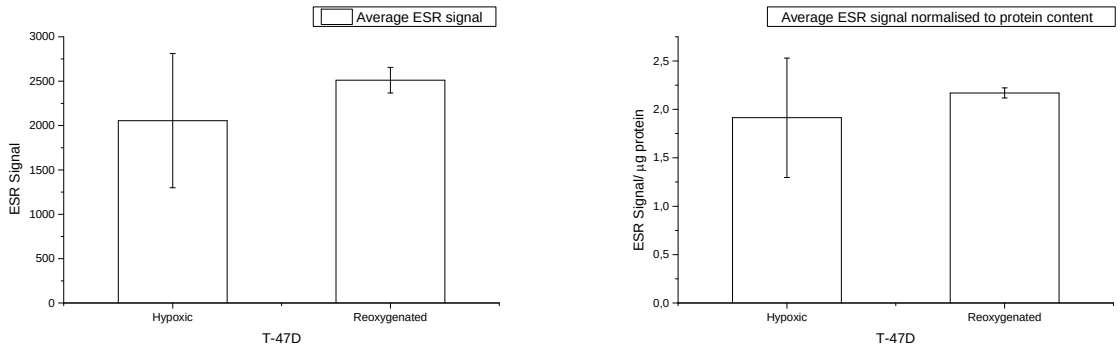

Figure 21
Levels of oxidised spin probe detected in the supernatant of cells cultured under cycling hypoxia for over four weeks. Reoxygenated cells were introduced to ambient atmosphere for 5 min before return to hypoxic atmosphere for sampling. Shown on the left is the average ESR signal detected in hypoxic and reoxygenated samples, on the right the ESR signal normalised to protein content. Sample sizes are: n(hypoxic)=n(reoxygenated) = 3.

The level of superoxide/ROS detected in reoxygenated cells appears to be somewhat higher than that detected in hypoxic cells which have not been reoxygenated. Upon inspection of the data presented in Figure 21, it is however immediately apparent that no significant difference between levels of oxidised spin probe was found for hypoxic and reoxygenated cells. The sample size is however very small, so only very great group mean differences would be statistically significant.

4.4.5 Comparison of Superoxide/ROS Levels in Primed and Unprimed Cells

A series of experiments were performed in order to compare levels of oxidised spin probe measured in primed and unprimed cells of type T-47D and T98G.

These experiments were carried out using either of the two protocols described below:

- Supernatant protocol with freshly thawed spin probe solution CMH in aliquots with enough for two samples. All samples were incubated for 50 min with CMH, before recording of added ESR spectra at 25 or 10 mW microwave power.

  This method was used for three separate experiments, which are designated; T-47D_1, T-47D_2 and T98G.

- Cell suspension (Munich) protocol with fresh CMH continuously bubbled with N_2 on ice. ESR signals were measured as relative levels of oxidised spin probe present at the time of recording of spectra. One experiment was carried out with this method; T-47D_suspension.

All experiments except T-47D_1 also compared the effect of L-NAME treatment with untreated controls.

All results obtained are shown as column plots of ESR signal per scan, as well as ESR signal normalised to protein content, for categories of samples. Columns represent mean values obtained for a particular category of samples with SEM error bars. The sample size is always $n \geq 3$, and is specified in figure legends.

Experiments on Supernatant

Shown below are the results obtained with the supernatant protocol. The first experiment (T47D_1) was made with primed and unprimed T-47D cells, all of which had their culture medium supplemented with 300 μM L-NAME 20 min before sampling.

ESR spectra were recorded at 25 mW of microwave power, 3 added scans.

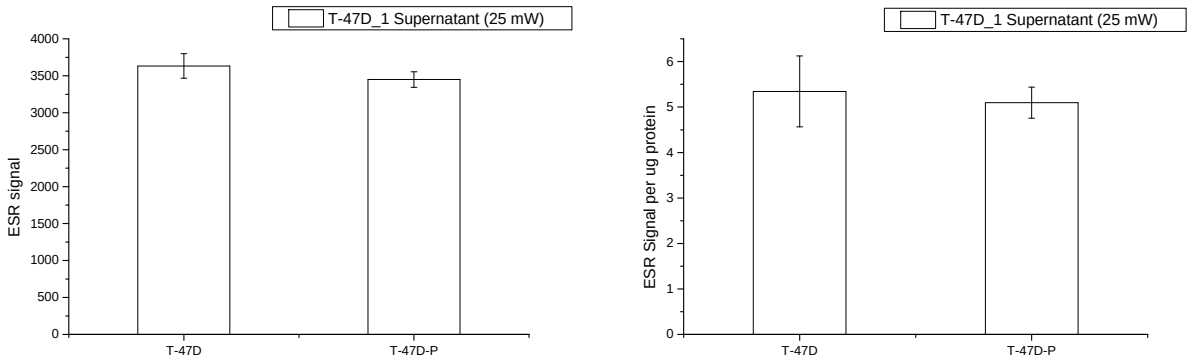

Figure 22
Relative levels of oxidised spin probe (ESR signal) detected in supernatant of primed and unprimed T-47D cells. Data are means ± SEM from one experiment, with sample sizes n(T-47D) = 5, n(T-47D-P) = 4. ESR spectra were recorded with microwave power of 25 mW.

Another two experiments with supernatant were carried out with primed and unprimed T98G and T-47D cells as above, with the added effect of L-NAME on recorded signal under inspection. This was administered to cell culture medium 20 min before sampling, and was

also present in KHB-D. Samples not to be treated with L-NAME were given an equal volume of milli-Q water and L-NAME free KHB-D. ESR spectra were recorded at 10 mW. The results are seen in Figure 23. Top panels represent T-47D cells whilst bottom panels represent T98G cells.

The general level of ESR signal detected in the T98G samples is ~1.5 times higher than that detected in T-47D samples. Whether this reflects a more oxidative environment in T98G cells as compared with T-47D cells, or whether it is simply due to a higher background oxidation or stock concentration of the spin probe solution used, is uncertain.

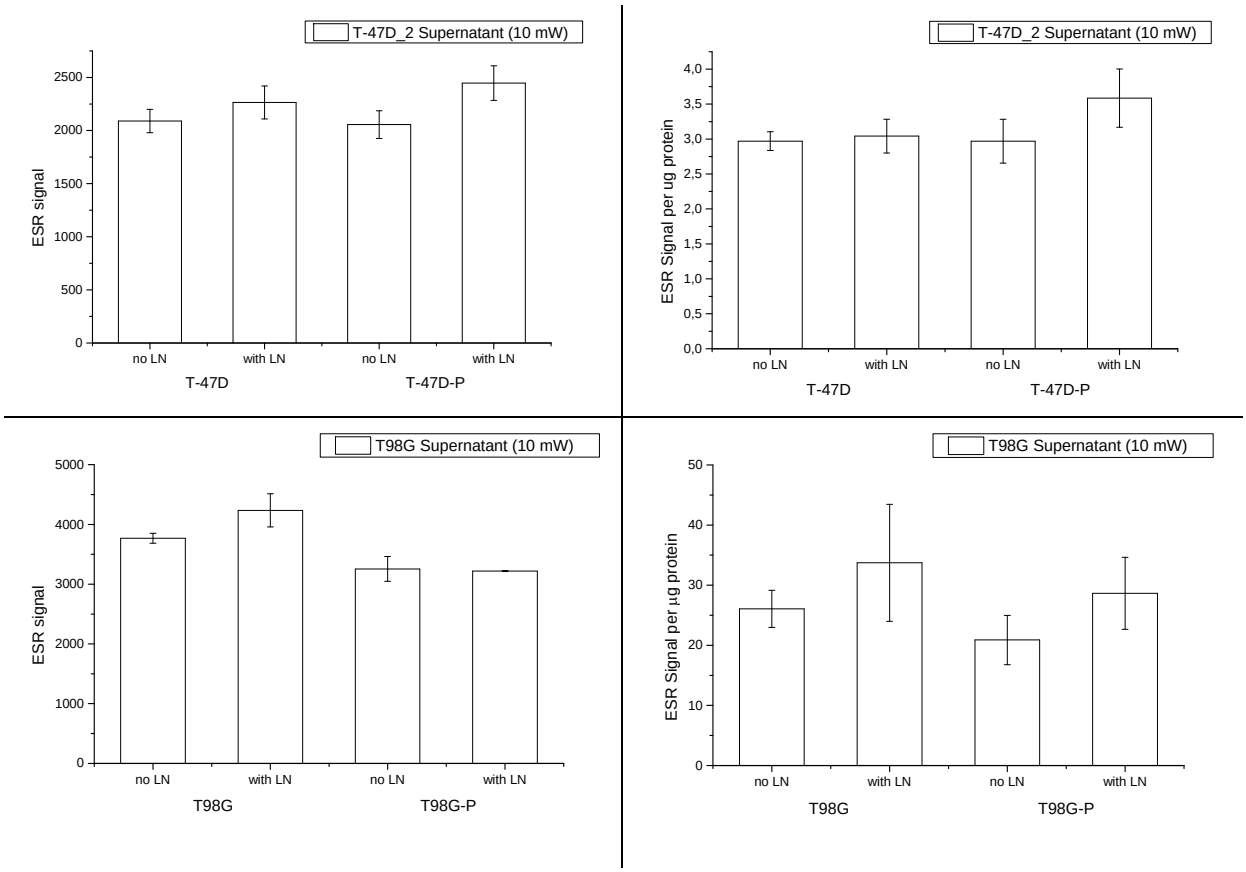

Figure 23
Relative level of oxidised spin probe (ESR signal) detected in the supernatant of primed and unprimed T-47D (topmost panels) and T98G cells (bottom panels).The experiments with T-47D and T98G cells were conducted separately. The label "with LN" signifies addition of 300 µM L-NAME to cell culture medium and KHB-D 20 min before and during incubation with KHB-D and spin probe. The label "no LN" signifies controls treated with an equal volume of milli-Q water. Data are means ± SEM from one experiment, with sample sizes n(T-47D)= n(T-47D-P) = n(T98G) = n(T98G-P) = 3. ESR spectra were recorded with microwave power of 10 mW.

Experiment on Cell Suspension

The fourth experiment was carried out on cell suspensions of T-47D cells. The CMH used for this experiment was made fresh and bubbled continuously with N_2 on ice during the course of the experiment.

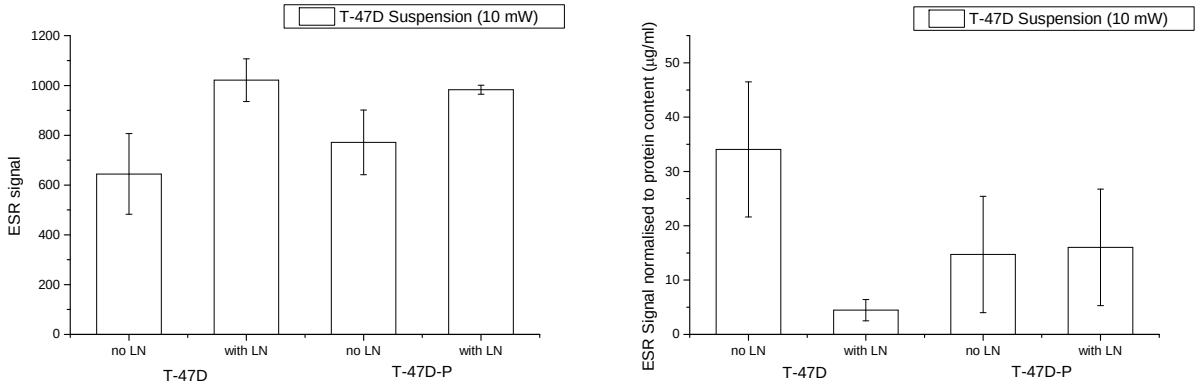

Figure 24
Relative levels of oxidised spin probe (ESR signal) detected in cell suspensions of primed and unprimed T-47D cells. The label "with LN" signifies addition of 300 µM L-NAME to cell culture medium 10 min before rinsing and scraping of cells.

Statistical Analysis

A number of t-tests (see section 3.6) were carried out on the data to examine whether the ESR signal and the ESR signal were significantly different as measured in primed and unprimed cells. The effect of L-NAME vs. untreated controls was also examined for significance.

T-tests for pooled data as given by equation (3), p. 46, were used since there was no reason to believe that the assumption of equal standard deviations for the two populations to be tested against each other did not hold. The same variation in measurement would be expected whether measuring on primed or unprimed cells or cells treated or untreated with L-NAME.

Nothing was significant at the 5% level, apart from for the T98G cells. The ESR signal (*not* normalised to protein content) detected for unprimed cells without L-NAME was found to be statistically higher than that detected for primed cells. The same was found for treatment with L-NAME. Treatment with L-NAME of unprimed cells was also seen to yield a statistically significantly higher signal as compared with untreated cells of the same type (T98G) ($p < 0.05$). However, since comparisons between different types of cells seeded from two stocks of

cell suspension were used, comparisons without consideration of protein should not be made lightly. Indeed, when comparing the signal normalised to protein content, there is no statistically significant difference.

The cell suspension samples of Figure 24 also yielded one statistically significant relation, namely the normalised ESR signal for T-47D samples supplemented with L-NAME was found to be statistically significantly lower than that of untreated controls ($p < 0.05$). This result, and indeed the entire experiment, is however of a dubious nature, as partially seen from Figure 25.

Please note that the p-values are calculated based on the assumption that the observations are Normally distributed. Because the sample size is so small, this cannot be assessed, and the p-values obtained must be interpreted in light of this. However, as the differences in means are not statistically significant, this is of little practical concern.

The dependence of ESR signal detected on sampling order was also examined. Shown below in Figure 25 is the variation in ESR signal detected in samples arranged in the order in which they were prepared and measured.

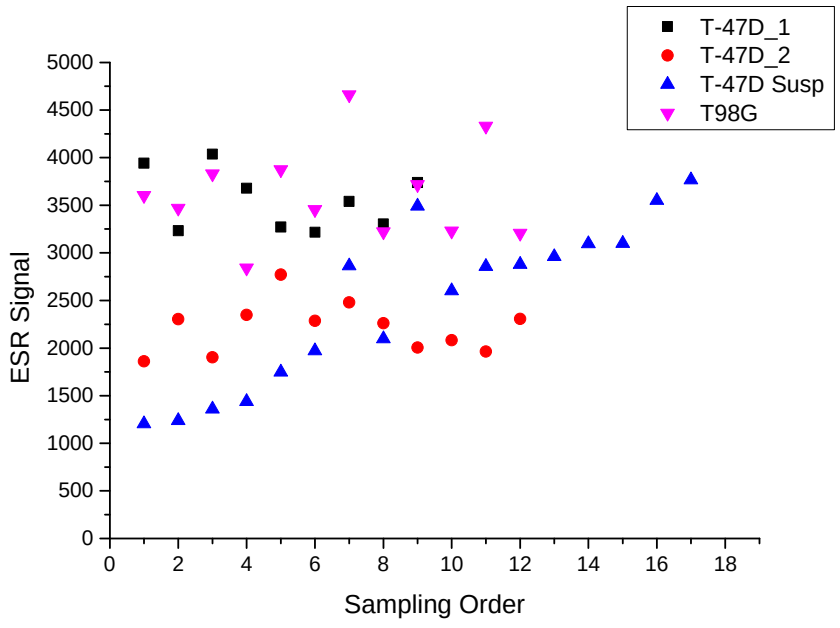

Figure 25
The variation in ESR signal detected in samples arranged in the order in which they were prepared with spin probe and sampled for all four experiments. Shown in black (■), red (●) and pink (▼) are the three experiments performed on supernatant with freshly thawed spin probe CMH, whilst the experiment performed on cell suspension with continuously N_2-bubbled CMH is shown in blue (▲).

The three experiments performed on supernatant do not display any noteworthy dependence of ESR signal on sampling order. The experiment performed on cell suspension with fresh CMH does however display a strong dependence, with a steadily increasing trend in ESR signal recorded.

4.5 Discussion

4.5.1 Establishment of Method

ESR signals from the oxidised spin probe $CM^{\bullet}$ were immediately detected in samples incubated with CMH. Both cell suspension and supernatant protocols were used to measure superoxide/ROS in cells.

Reger (Munich) measured the rate of ROS/superoxide generation in cells in suspension by monitoring of the low-field line over a time period of ten minutes. This protocol has, as later realised, the advantage of being more or less invariant to background oxidation, since only the rate of oxidation of the spin probe is of relevance. Diffusion of oxygen into the cell suspension in the capillary tube may be considered to be constant between samples.

This kind of measurement is naturally not possible with the supernatant protocol obtained form Deschacht et al (2010), since the only development of signal with time during recording of ESR spectra in this case is due to diffusion of molecular oxygen into the sample. The adoption of this protocol was in this way in retrospect perhaps unfortunate.

However, there are also several advantages to conducting measurements on supernatant as opposed to cell suspension. For one thing, the method is easier to use, requiring no scraping of cells. Since measurements are performed on cells as seeded, there is little variation in the cell content upon which the measurement is based. This largely makes measurements of protein content obsolete within experiments on one cell type. As seen in Figure 19, right panels, the normalisation of ESR signal to protein content generally yields the same overall shape of curve with time as that obtained by plotting ESR signal as a function of time (Figure 19, left panels). The data points which deviate from this rule are more than likely results of inadequacies of the Bradford assay than actual deviations in cell content. Cell flasks were inspected before experiments began and were seen to be relatively evenly seeded.

Samples using cell suspension were initially drawn in 100 µl capillaries. In this case cells would tumble down and accumulate in the bottom of the capillary. Later suspension samples were drawn in 50 µl capillaries, and the cells would in this case aggregate at uneven intervals along the sides of the capillary tube. In both cases, relating the signal to the material in the cavity by protein measurement on practically homogenous suspension is problematic.

As for the efficiency of detection of superoxide/ROS for the two protocols with cell suspension and supernatant, there are varying views reported in the literature. Deschacht et al (2010) found no significant difference in ESR signal detected in samples of supernatant and cell suspension of cells stimulated for superoxide production after 50 min incubation with spin probe CMH. Dikalov et al (2011) however found that nitroxide ($CM^{\bullet}$) formation was significantly higher in samples of cell suspension than in buffer (supernatant) of stimulated cells. I only recently realised the importance of the chemical used for stimulation of superoxide generation. Deschacht et al. used phorbol myristate acetate (PMA), an NF-κB activator, which gives generation of extracellular superoxide. Dikalov et al. however used antimycin A, a mitochondrial uncoupling agent, which gives generation of mitochondrial superoxide.

The supernatant method should give acceptable results when applied to reoxygenated cells, since the superoxide generating sources in this scenario are thought to be NADPH oxidases (NOx) and xanthine oxidase (XO), which both generate extracellular superoxide. This assumption is corroborated by the measurements made by Fabian et al (2004) on extracellular superoxide generated in reoxygenated cortical tissue using a cytochrome c reduction assay, see Figure 26A.

How this fact relates to measurements on supernatant from primed and unprimed cells cultured at ambient oxygenation is uncertain. The ROS hypothesised to be responsible for formation of peroxynitrite with nitric oxide and pro-activation of TGF-β3 is of unknown origin. The results obtained in section 4.4.4 indicate that at least some of this superoxide is detectable extracellularly.

Experiments performed in order to compare the ESR signal originating in cell suspension with that of supernatant indicate that the cell suspension protocol gives a higher signal per amount of protein (data not shown). This is not surprising in light of the above, since the cell suspension protocol would also detect mitochondrial superoxide.

CMH

The spin probe solution was originally aliquoted with enough for two samples per tube and frozen at -80 °C. However, due to concerns about the unnecessarily high background oxidation of the spin probe solution with this protocol raised by Dikalov et al (2002), a protocol in which CMH was prepared fresh in glass ware and continuously N_2-bubbled on ice was adopted.

However, as can be seen from Figure 25, this method was not successful. The level of the signal recorded started out almost indiscernible, and increased steadily with time. The variable level of background oxidation with this protocol was far more deleterious than the high one obtained when using thawed aliquoted CMH.

4.5.2 Issues with Protein Measurement by the Bradford Assay

All experimental results are shown as plots of both ESR signal and ESR signal normalised to protein content as measured by the Bradford assay. This setup was chosen due to variable results obtained with the normalisation of ESR signal recorded to measured protein content.

For experiments using the supernatant protocol with one cell type, protein measurement is more likely to introduce artefacts than to improve the accuracy of the measurements. Cells are seeded evenly, and there is not a great spread in the number of cells per flask. As seen in Figure 18A, even with a sample size as small as n = 2, the ESR signal recorded in supernatant from cell flasks seeded at increasing density corresponds with the number of cells present during incubation with spin probe in a perfectly linear fashion. Experimental samples seem to contain roughly 800-900 μg protein. The corresponding picture for ESR signal with protein content as measured with the Bradford assay, seen in Figure 18B, is not as clear. For one thing, the SEM error bars are quite a bit more variable and larger, indicating disparate results. Admittedly, the sample size is very small (n = 2), and so this alone cannot be considered in judgment of the Bradford assay.

However, when comparing measurements on different cell types in the same experiment, the protein measurements may be of some use, if not only to give an idea of the level of number of cells seeded of the different types. The method of counting cells from pictures taken before

experiments is however superior in any case when using the supernatant protocol. The only drawback of this method applied in this case is that it is time consuming and tedious.

Uncertainties with Protein Measurements for Suspension Protocol

For measurements on cell suspension, measuring protein content in samples is necessary, but also problematic. As noted above in section 4.5.1, the uneven aggregation of cells in the capillary tube makes relation of ESR signal recorded to protein content unsatisfactory.

It is also difficult to identify outliers since the spread in values obtained is so great. As can be seen from the raw data in Appendix D, the amounts of protein measured for suspension samples is far more variable than those measured for supernatant samples.

Jensen (2013) at our lab undertook a study of the correspondence between different techniques used for quantification of cells and protein, namely the Bürker chamber, flow cytometry, scintillation counting and the Bradford assay. Her report concludes that the Bradford assay is of dubious use and that comparisons of measured protein content between different cell types using this method cannot be trusted. In comparing protein measurements between T-47D and T98G cells, she found that the much larger T98G cells apparently yielded significantly lower quantities of protein than T-47D cells. This rather unlikely result was also found in this thesis.

Additionally, her report finds that the disposable plastic Bürker chamber is practically useless, which was also the conclusion drawn at an early stage in the work with this project, in the process of seeding cells for experimental samples.

4.5.3 Superoxide/ROS in Reoxygenated Cells

The reoxygenation experiments on supernatant from reoxygenated hypoxic cells of section 4.4.3, see Figure 18, show a trend of an initial increase in signal with time before plateauing around 5 – 8 minutes and subsequent decline. Four experiments (#1 - #4) included a “0 min” reoxygenation time, and three out of four of these showed a heightened level for these data points in relation to the following data points obtained for 1 and 2 minutes reoxygenation.

Abramov et al (2007) report that different mechanisms of ROS generation act at different times during hypoxia and reoxygenation. The heightened levels seen for the “0 min” data

points may be a remnant of some other ROS generating mechanism than that seen for the rest of the curve. However, these data points are not directly comparable with the rest obtained for greater reoxygenation times since these were not supplemented with fresh medium upon reoxygenation, as were the others.

Shown in Figure 26A is the change in extracellular superoxide generation with time upon hyperoxic reoxygenation after hypoxia in cortical tissue of rats *in vivo*, as measured with a cytochrome c electrode (Fabian et al 2004). Triangles represent the data obtained for samples treated with polyethylene glucose conjugated SOD (PEG-SOD), which is cell permeable. Circles represent data obtained for untreated controls.

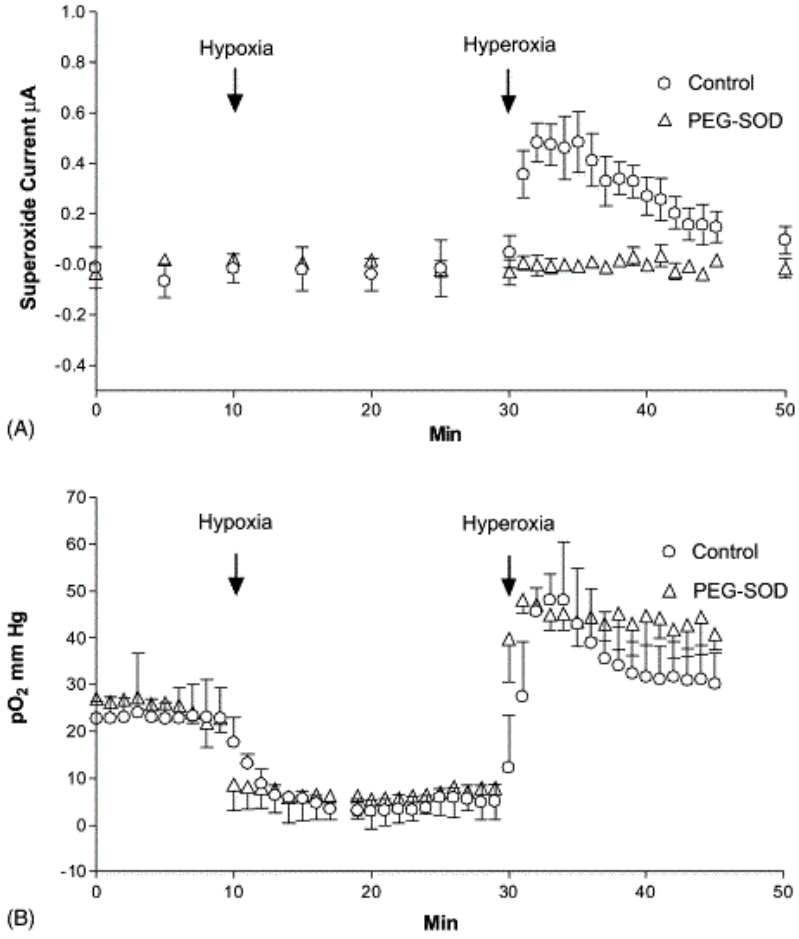

Figure 26
Measurements made on cerebral cortex of rats. Some animals were treated with 1 U/g PEG-SOD (△), whilst controls were injected with carrier only (○). Hypoxia signifies inspiration of 10% O_2, whilst hyperoxia signifies inspiration of 100% O_2.
Panel (A) shows cortical surface superoxide current as measured by a cytochrome c coated electrode, during breathing of ambient air and after onset of hypoxia and hyperoxia. Panel (B) shows cortical tissue oxygenation measured by fluorescence quenching.
Adapted, from Fabian et al (2004).

After seeing the reoxygenation curve of Figure 26A, the focus of the reoxygenation experiments became on the first 12 – 15 min, trying to get enough data points in this range for the change in ESR signal with time to become clearer. The reoxygenation curves seen in Figure 19 also display an initial rise in signal after which the signal seems to plateau.

However, the following decline of signal is not as clear as that seen in Figure 26A. This may be due to the fact that there is a rather high background oxidation.

Please note that the data obtained by Fabian et al (2004) differ from those obtained in the reoxygenation experiments of section 4.4.3 in that the former were made in real time. Each data point represents the average current measured at a certain moment in time. The reoxygenation measurements represent the average level of spin probe oxidised over a period of 5 min (#1 and #2) or 1 min and 40 sec (#3, #4, #5) after reoxygenation for a certain time.

Data obtained by Fabian et al. also differ from those obtained here in that they are collected as a sequence of measurements on the same sample, whereas for the latter, each data point represents a measurement on an individual sample. In order to get as good approximations to the true population means as those of Figure 26, far more samples would be needed with the individual sampling method. Unfortunately, it was not practically possible to increase the sample size much beyond what was done for the larger experiments, with 21 samples for hypoxic and 29 for aerated reoxygenation. The fact that data from different experiments could not be amalgamated was a major drawback.

The results shown in Figure 21 seem to indicate that there are indeed heightened levels of superoxide/ROS generated in reoxygenated cells as compared with hypoxic cells, however the difference was not statistically significant. The sample size (n = 3) was small and so no definite conclusions can be drawn on this basis. The levels of ROS detected upon reoxygenation of hypoxic cells was however found to be similar to that obtained for reoxygenation of cells cultured at ambient oxygenation. In this case, the oxidation of the spin probe was seen to rise somewhat erratically with time and no definite decline in ESR signal was seen within 12 minutes. These results suggest that it is not the absolute level of ROS but rather the sudden increase after reoxygenation of hypoxic cells that is responsible for the observations by .One may speculate that the cellular defence mechanisms are down-regulated during hypoxia when ROS-levels seem to be low, resulting in reduced capacity for handling of the same ROS-levels which were seen for aerated cells.

It is also evident from Figure 26 (panel B) that the oxygenation of cortical tissue changes upon reoxygenation in a similar manner to the superoxide current. Since molecular oxygen may also oxidise CMH, the oxidation of CMH with time after reoxygenation seen in Figure

19 may in part be due to increased levels of oxygen in cells. Superoxide is far more reactive though. This cannot be decided without the use of SOD.

Unfortunately, SOD was not successfully used in these experiments. Early attempts to use SOD gave highly strange results. This turned out to be due to a mix up featuring the SOD stock solution, resulting in something other than SOD mistakenly being supplemented to cells. Later experiments with SOD were conducted in conjunction with the unsuccessful method of continuously N_2-bubbled fresh CMH and sampling in hypoxic atmosphere (data not shown), and any potential effects of SOD were obscured by the severe background oxygen contamination seen in this case.

4.5.4 Issues with the Unspecific Oxidation of CMH

Since a general increase in oxidative species is what is thought to be behind the elimination of HRS in reoxygenated cells, the nonspecific nature of CMH oxidation is not a major issue. The major contributors to oxidation of CMH are thought to be superoxide and to a lesser degree peroxynitrite. Since peroxynitrite is generated downstream from initial superoxide production in a 1:1 ratio, the oxidation of CMH by peroxynitrite could be viewed as a second order oxidation by superoxide. Both reactions occur with large rate constants.

The use of SOD would also cancel both the oxidative contribution from superoxide and peroxynitrite. The formation of hydrogen peroxide resulting from dismutation of superoxide does not affect the oxidation state of the spin probe. Hydroxyl radical formation, which would oxidise CMH and cause artefacts, is avoided with the use of chelating agents.

Dikalov et al (2007b) have studied the efficiency of different spin traps and spin probes in cell systems, both unstimulated and stimulated for superoxide generation. In stimulated samples, they find a drastic decrease of signal due to $CM^{\bullet}$ when supplemented with SOD, up to 70 – 90%. However, in unstimulated basal samples, although no numbers for the reduction in signal is given, the change in signal as deduced from representative ESR spectra is not great. One may then infer that basal superoxide production in unstimulated cells is not very high.

4.5.5 Results Obtained in Munich

Reger prepared samples of primed and unprimed T-47D and T98G cells according to the Munich protocol in 50 µl capillaries. L-NAME (presumably deoxygenated) was supplemented by addition to scraped cell suspension in KHB-D at 300 µM concentration before incubation on ice for 10 min, with subsequent addition of CMH and immediate recording of ESR spectra with a table top ESR spectrometer at 25 mW. Results are seen in Figure 27.

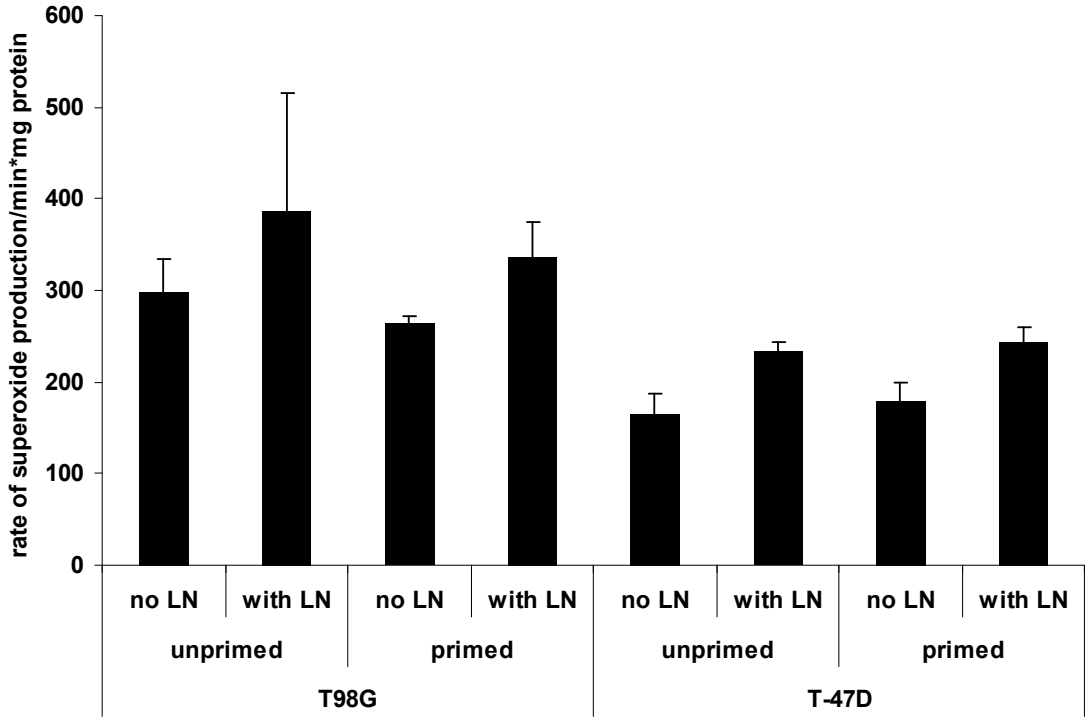

Figure 27
Rate of superoxide production measured in unprimed and primed T98G and T-47D cells using the Munich protocol, normalised to protein content. The label "with LN" signifies addition of 300 µM L-NAME to cell suspension in KHB-D and incubation on ice for 10 min before addition of CMH. "no LN" signifies direct addition of CMH after scraping of cells in KHB-D. The number of experiments and sample size is unknown. From Reger (unpublished data) .

Reger found no significant difference in levels of oxidised spin probe normalised to protein content between primed and unprimed cells, neither for T-47 D nor T98G cells. However, the treatment of cells with NOS-inhibitor L-NAME gave an increase (not statistically significant at the 5% level) in rate of superoxide (ROS) production detected. This result was taken to indicate that nitric oxide in cells scavenges superoxide to form peroxynitrite. This peroxynitrite is hypothesised to be responsible for the persistent activation of TGF-β3 with subsequent sustained elimination of HRS. As described in section 5.4.8, p. 101, Edin recently

showed that peroxynitrite is indeed present in cells and that HRS is reinstated in primed cells after treatment with peroxynitrite scavenger uric acid, see Figure 39.

This effect of L-NAME was not consistently seen in the corresponding experiments conducted in this thesis, as shown in Figure 23 and Figure 24. The statistics are admittedly poor, with sample sizes of merely n = 3 for the three experiments using L-NAME.

The units are not directly comparable. The measurements of Figure 27 were done on cell suspension and the rate of spin probe oxidation was deduced from the increase in signal with time during recording of spectra. The corresponding experiments carried out in this project were performed on supernatant and relative levels of oxidised spin probe present after incubation for a certain time were compared for primed and unprimed cells (this was also done for the one such experiment with cell suspension).

L-NAME

In addition to functioning as a NOS-inhibitor, L-NAME also scavenges radical species. Rehman et al (1997) found that L-NAME is a powerful scavenger of $^{\bullet}OH$ ($k \sim 7\times10^{9}\ M^{-1}s^{-1}$), even at concentrations as low as 300 μM.

Therefore, the addition of L-NAME could potentially (especially if there is not a lot of $NO^{\bullet}$ present to scavenge superoxide) lower the signal originating from $CM^{\bullet}$, since unspecific oxidation of CMH may decrease in the absence of hydroxyl radical.

Rehman et al. advice the careful usage of L-NAME as a specific NOS-inhibitor, and suggest the use of the inactive enantiomer of L-NAME, D-NAME, in control experiments to determine the true contribution by NOS-inhibition to the change in signal.

5 Nitric Oxide Measurement with Colloidal Iron-diethyldithiocarbamate Spin Trap $Fe(II)(DETC)_2$

In order to explore the hypothesised mechanisms for the removal of hyper radiosensitivity (HRS) in primed cells mediated through increased generation of nitric oxide by iNOS (see section 2.3.3, p.27 - 28), attempts were made to qualitatively measure nitric oxide in cultured cells using ESR spin trapping with colloidal iron-diethyldithiocarbamate spin trap $Fe(II)(DETC)_2$. Working from the assumption that chronically increased levels of $NO^{\bullet}$ stabilise TGF-β3 to remove HRS in protracted LDR primed cells (P-cells), the ultimate goal of the undertaking would be to compare levels of nitric oxide measured in P-cells with those measured in unprimed controls.

5.1 Trapping of $NO^{\bullet}$ with $Fe(II)(DETC)_2$

Spin trapping is extensively used for the quantification of nitric oxide in a range of cells and tissues both *in vitro* and *in vivo*. Nitric oxide reacts readily with transition metals, particularly iron, and so mononitrosyl iron complexes (MNICs) have been successfully employed for this purpose. The use of the chelating agent diethyldithiocarbamate (DETC) with iron yields the hydrophobic spin trap $Fe(II)(DETC)_2$, which is a potent scavenger of nitric oxide ($k \sim 1.1 \times 10^8\ M^{-1}\ s^{-1}$). The structure of the resulting spin trap adduct is seen in Figure 28. The lipophilic property of the spin trap is regarded as an asset as $NO^{\bullet}$ is thought to partition into the hydrophobic interior of lipid membranes (Kleschyov & Munzel 2002).

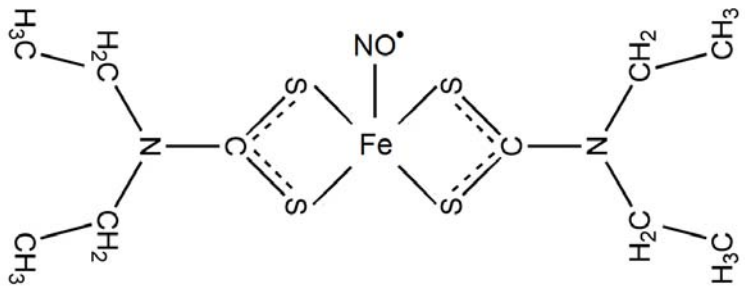

Figure 28
The structure of the spin trap complex with nitric oxide radical, $NO^{\bullet}$-$Fe(II)(DETC)_2$.

As mentioned above, the rate constant for the reaction between $NO^{\bullet}$ and $Fe(II)(DETC)_2$ is $1.1\times 10^{8}\ M^{-1}\ s^{-1}$, whilst that for $NO^{\bullet}$ and superoxide is higher, $6.7\times10^{9}\ M^{-1}\ s^{-1}$. However, the concentration of $Fe(II)(DETC)_2$ used is far higher than that of superoxide even at elevated levels, so the $Fe(II)(DETC)_2$ should still trap $NO^{\bullet}$ quite efficiently. Experiments performed by Kleschyov et al (2000) indicate that spin trapping with a colloid trap is quite insensitive to ambient levels of superoxide.

The detection limit of $NO^{\bullet}$- $Fe(II)(DETC)_2$ is reportedly ~10 nM (Cadenas & Packer 2005), but Kleschyov reports detected levels as low as picomolar in aortic tissue (Kleschyov et al 2007).

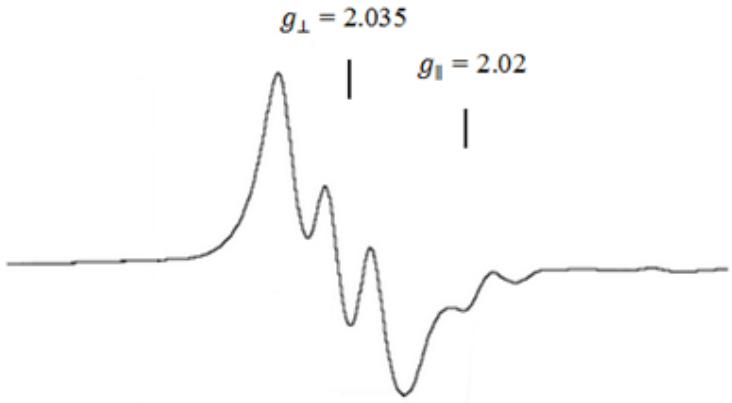

Figure 29
Typical ESR spectrum for the spin adduct $NO^{\bullet}$-Fe(II)$(DETC)_2$ (in fresh blood) recorded at liquid nitrogen temperature (77 K). Adapted, from Takizawa et al (2002).

In frozen solution (77 K), the resulting spin adduct, $NO^{\bullet}$-$Fe(II)(DETC)_2$, yields an anisotropic ESR signal with axially symmetric g-tensor exhibiting a triplet structure at $g_{\perp}$. See Figure 29 above. $g_{\perp} = 2.035$ and $g_{\parallel} = 2.02$, a = 1.26 mT (Kleschyov et al 2007, Vanin & Poltorakov 2009). At 293 K, the spin adduct yields an isotropic spectrum with g = 2.04, a = 1.25 mT (Vanin & Poltorakov 2009).

5.2 Establishment and Development of Method

Sub-confluent 75 cm^2 cell flasks of ~8 – 10×10^6 cells were used for nitric oxide measurements.

5.2.1 Standard Sample Preparation (Munich Protocol)

Krebs HEPES buffer (KHB) was thawed/prepared and bubbled with N_2 for at least 10 minutes. If using, Cu,Zn-SOD was added to medium (~30 min before sampling) and to KHB at 50 – 100 U/ml.

$FeSO_4 \times 7H_2O$ (4.50 mg) and DETC (7.2 mg) were dissolved separately in two 10 ml volumes of deoxygenated ice cold KHB and kept on ice. Colloidal spin trap was prepared immediately before addition to cell flasks by 1:1 mixing of these parent solutions, giving a 0.8 mM $Fe(II)(DETC)_2$ solution. This should be yellow/brownish with no precipitates. The formation of black aggregates indicates oxidation of Fe(II) to the diamagnetic and ESR-silent Fe(III).

The medium was removed and the cells rinsed with phosphate buffered saline (PBS). Three ml of KHB was carefully pipetted into the flask, avoiding getting any air into it. One ml of colloidal spin trap $Fe(II)(DETC)_2$ was then carefully added to each flask and these were set to incubate for an hour at 37°C with closed caps.

During incubation of samples, tip-less 1 ml syringes with KHB cushion were prepared. The plunger was retracted, 250 µl KHB pipetted in and the syringe was then frozen in liquid nitrogen.

After complete incubation with spin trap, the buffer was removed, leaving behind approximately 200 µl. The aspirated buffer was always clear, indicating the delivery of hydrophobic trap to cellular membranes. Cells were then collected using a rubber policeman (TPP, Switzerland), taking care to avoid air bubbles, and transferred to the cushioned syringe using a glass pipette with rubber teat. The cell/spin trap suspension must be quickly delivered into the syringe, keeping a steady flow to avoid the suspension freezing inside the thin glass pipette tip. Syringes with sample were then refrozen in liquid nitrogen and stored at -80°C.

5.2.2 Alternative Methods of Sample Preparation

Different variations of the standard method presented above were explored in the process of trying to measure nitric oxide in cells:

DEANO Samples

$NO^{\bullet}$-donor diethylamine nitric oxide sodium salt (DEANO) dissolved in buffer releases two molecules of $NO^{\bullet}$ and one molecule of diethylamine, with a half-life of about two minutes at 37°C, pH 7.4. Two different types of samples were examined:

1. A cell-free system of KHB was supplemented with 0.4, 0.2 and 0.05 mM colloidal spin trap and ~1 mM DEANO. Samples were immediately drawn in 100 µl capillaries and spectra were recorded at ambient temperature (as for superoxide samples).
2. T98G cells were supplemented with ~1.8 mM DEANO before 1 h incubation with spin trap. Samples were otherwise treated as described above in the standard sample preparation section.

DETC Samples

Samples supplied with only DETC in place of spin trap $Fe(II)(DETC)_2$ were prepared to look at spectra due to chelation of intracellular transition metal ions. In this case, DETC was diluted 1:1 with KHB and added to samples. Compared with the $Fe(II)(DETC)_2$ samples which in frozen condition appeared pinkish in colour, the DETC samples appeared white transparent.

Capillary Tube Samples

To reduce boiling from where the sample touches the side of the Dewar flask (see section 5.2.3 below), some samples were incubated and scraped as above, but drawn into 100 µl capillary tubes, stopped with putty and frozen in liquid nitrogen.

These capillary tube samples were however prone to breaking and the boiling did not subside, making the sample still more unstable.

[^{60}Co]-γ Irradiated Samples

A batch of T98G cells was LDR primed (see section 2.3.2) with the spin trap present in order to try and improve the signal. The aim was to have the nitric oxide preferentially trapped by $Fe(II)(DETC)_2$ as its generation was induced, due to the high rate constant of the reaction, thus avoiding $NO^{\bullet}$ being "lost" to LAP (see Figure 8, p. 27).

Cell flasks were supplemented with 100 U/ml Cu,Zn-SOD and prepared with colloidal spin trap as above, but allowed to incubate under ^{60}Co-γ irradiation at 0.18 Gy/h for one hour. 37°C was maintained by a circulating water-heated plate.

KHB was bubbled with N_2 at the University of Oslo (UIO) and kept in a glass bottle with plastic cap which had been stored for two days in 4% oxygen to minimise diffusion contamination. Spin trap chemicals were weighed and kept dry in deoxygenated glass vials with screw caps, and only dissolved shortly before addition to samples. Cell flasks were transported in a polystyrene box for isolation. Samples were irradiated at the Norwegian Radium Hospital. After irradiation, flasks were brought back to UIO and samples were prepared as described above. Total incubation time with spin trap was then 2 h 15 min.

5.2.3 ESR Spectroscopy

Samples were transferred to a Dewar flask filled with liquid nitrogen. The syringe was briefly warmed in the palm of the hand and the sample was then dislodged with the plunger and transferred to a chilled glass tube of slightly greater inner diameter. The sample was then guided through the glass tube down into the Dewar finger, see Figure 30. This had to be done quickly to hinder the sample from thawing and lodging inside the glass tube.

The Dewar flask features a vacuum layer enclosing the inner volume for cryogenic fluids. The isolation is however not perfect, and water in the samples boiled incessantly where they made contact with the wall of the Dewar flask. This would make the sample highly unstable, making tuning and recording of spectra practically impossible.

In order to remedy this, a motorised vacuum pump was used to subcool the liquid nitrogen. Suction was applied for a minute or two and the sample would then be stable for the period necessary to allow tuning of the cavity. The Dewar flask would then be pumped again before commencing with recording of as many added spectra as would be allowed before the sample

again became too unstable. A glass straw was placed on top of the sample in the Dewar flask to generally provide stability and to avoid it being sucked out of the finger part during pumping.

Figure 30
The Dewar flask used for experiments with spin trap Fe(II)(DETC)$_2$ in liquid nitrogen (77 K).The sample (not present) would be situated in the finger part of the Dewar flask during recording of spectra, as indicated by the arrow. The thin glass straw would also be inserted into the finger part on top of the sample to provide stability. The sealed cap with hose for the motorised vacuum pump can be seen fitted over the top of the Dewar flask.

Spectra were recorded at 5 or 10 mW of microwave power, 100 kHz modulation frequency, 0.5 or 1.0 mT of amplitude modulation. The sweep width was set to 18 mT unless otherwise stated. The conversion time was always 81.92 ms, giving a sweep time of 84 s. The time constant was set to 327.68 ms for all measurements except for DEANO samples recorded at ambient temperature, in which a setting of 655.36 ms was used.

5.3 Results and Analysis

In the following the various spectra obtained with the different methods described in section 5.2.2 above are presented. These are merely qualitative since, with the exception of the DEANO samples, the signal attributable to the $NO^{\bullet}$-Fe(II)$(DETC)_2$ complex was not recognised for any of the samples.

5.3.1 Samples Supplemented with $NO^{\bullet}$-donor DEANO

In order to examine the spectrum due to the $NO^{\bullet}$-Fe(II)$(DETC)_2$ complex without any confounding background signals, ~0.4 mM colloidal spin trap was allowed to react with ~1 mM $NO^{\bullet}$-donor DEANO in KHB. Spectra were recorded at ambient temperature and a representative spectrum is shown in Figure 31 below (legend 0.4 mM, in black).

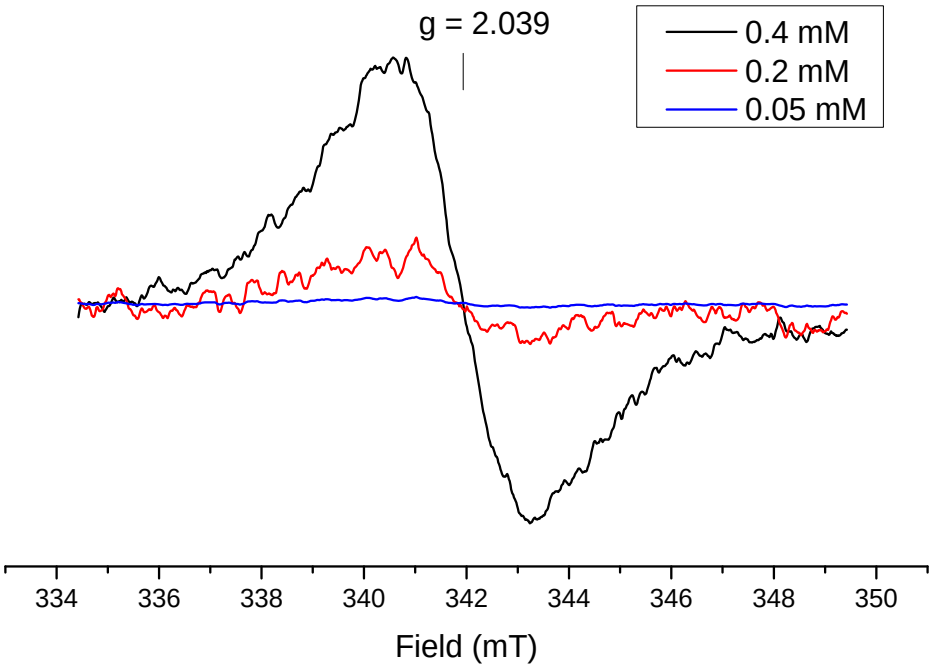

Figure 31
Qualitative ESR spectra of colloidal spin trap Fe(II)$(DETC)_2$ in a cell-free system (buffer) with 1 mM $NO^{\bullet}$-donor DEANO at ambient temperature (295 K). These display one line without resolved hyperfine structure at g = 2.039.Three different concentrations of spin trap complex were utilised; 0.4, 0.2 and 0.05 mM. Decreasing the spin trap concentration resulted in increasingly lowered intensity of the signal. ESR settings: P=20 mW, MA=0.16 mT, #scans=4, TC= 655.36 ms, CT= 81.92 ms.

The sample at ambient temperature yielded a spectrum at g = 2.039, which is consistent with that reported for the $NO^{\bullet}$-Fe(II)$(DETC)_2$ complex at 293 K. There was however no resolved triplet structure. A possible reason for this was speculated to be Heisenberg spin exchange due to high concentrations of radical in the solution, broadening the lines, thus potentially giving

an overlap of lines and so an unresolved triplet structure. A dilution of spin trap concentration (0.2 mM and 0.05 mM) however only resulted in reduced intensity of the one-line signal. The lowest concentration yielded very little signal. See Figure 31 (red and blue).

It was also realised that the lipophilic property of the spin trap was very likely to affect the spectrum. Hydrophobic forces could lead Fe(II)$(DETC)_2$ to aggregate, yielding a spectrum with powder-like properties rather than the solution-like properties one might expect. Rather than displaying an average value of g, the spread in g-values with a range of orientations could well obscure the triplet structure.

In order to overcome the issue of hydrophobicity, the spin trap was allowed to incubate with ~1.8 mM DEANO in a cellular system of T98G cells. Spectra were recorded at 77 K. Figure 32 shows the resulting triplet spectrum characteristic of $NO^{\bullet}$-Fe(II)$(DETC)_2$. This signal was highly intense, and the receiver gain had to be reduced from the standard setting of 80 to 70 in order to contain the spectrum.

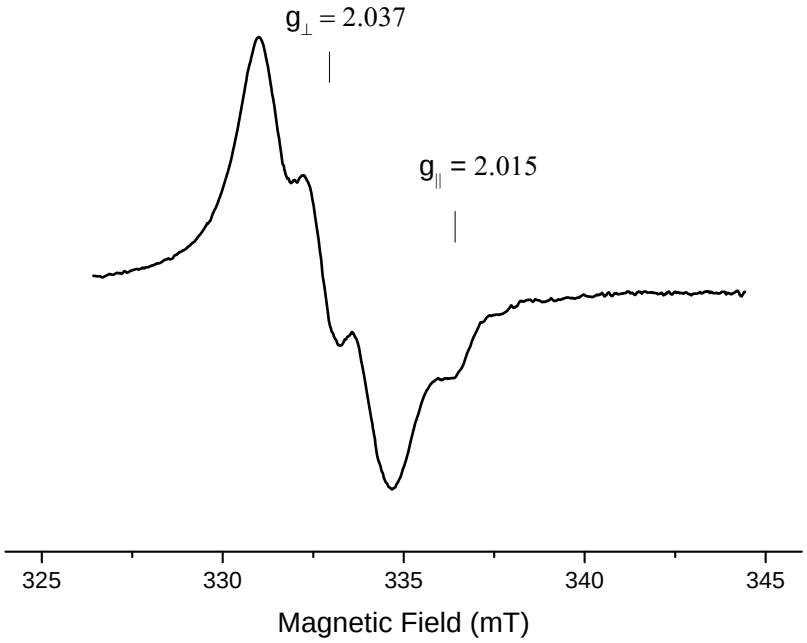

Figure 32
Characteristic ESR spectrum at 77 K of $NO^{\bullet}$-Fe(II)$(DETC)_2$ complex formed in T98G cells supplemented with ~1.8 mM $NO^{\bullet}$-donor DEANO and incubated with 0.2 mM colloidal Fe(II)$(DETC)_2$ spin trap (1 h, 37°C). $g_{\perp}$ = 2.037, $a \approx 1.25$ mT. $g_{\parallel} \approx 2.015$.
ESR settings: P=5 mW, MA=0.5 mT, #scans=1, TC= 327.68 ms, CT= 81.92 ms.

5.3.2 Standard Samples

Standard samples prepared as described in section 5.2.1 were made using T-47D and T-47D –P cells and T98G and T98G-P cells. Figure 33 below shows acquired spectra for the T-47D and –P samples. Corresponding spectra for T98G and –P are shown in Figure 34 (bottom panels).

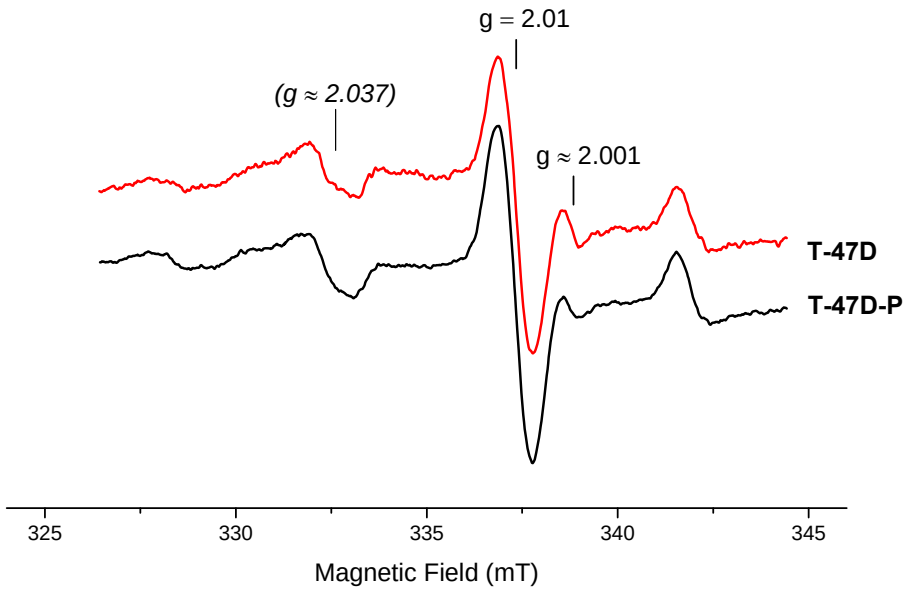

Figure 33
Representative spectra for standard samples of T-47D (red) and T-47D-P (black) cells incubated (1h, 37°C) with 0.2 mM colloidal spin trap Fe(II)(DETC)$_2$.The g-value where the NO$^{\bullet}$-Fe(II)(DETC)$_2$ signal should appear is marked in italic.
ESR settings: P=10 mW, MA=0.5 mT, #scans=1, TC= 327.68 ms, CT= 81.92 ms.

The spectra obtained show an intense line at g ≈ 2.01 with what appears to be hyperfine structure with a ≈ 5 mT. This was later identified as part of the spectrum due to a Cu-DETC complex, Cu(II)(DETC)$_2$.

Sample pellets were of different sizes (mainly due to breakage), which accounts for the differences in intensity of the spectra.

5.3.3 $Fe(II)(DETC)_2$ vs DETC Samples

Samples incubated with DETC only were made to investigate the background spectrum due to chelation by DETC of intracellular transition metals. Standard samples with $Fe(II)(DETC)_2$ were prepared for comparison.

Figure 34 compares representative spectra for T98G (left) and T98G-P (right) samples incubated with colloidal spin trap $Fe(II)(DETC)_2$ (bottom panels) and with chelator DETC only (top panels).

The T98G and T98G-P samples were prepared with spin trap contemporaneously before storage at -80°C, but spectra were recorded at two separate occasions. The T98G sample spectra were recorded as three added scans compared with nine added scans for the T98G-P spectra, explaining the comparatively lower signal-to-noise ratio for the former.

The T98G and T98G-P samples incubated with DETC only feature a more prominent $Cu(II)(DETC)_2$ signal. All four spectra feature an additional relatively intense line at $B \approx 340$ mT ($g \approx 2.001$). This is not seen to nearly the same the extent in the corresponding standard samples of T-47D and T47D-P cells (see Figure 33).

Compared with the standard sample T-47D spectra shown in Figure 33, the T98G spectra feature a more concave baseline. With a view to finding the origin of this concavity, spectra were recorded in sample-free Dewar flask with and without supporting glass tube. These yielded no particular signal (not shown). The curvature in the spectra was thus not due to background contamination of the Dewar flask or cavity, but originated in the samples themselves. That is not saying that some contaminant did not unintentionally make it into this batch of samples.

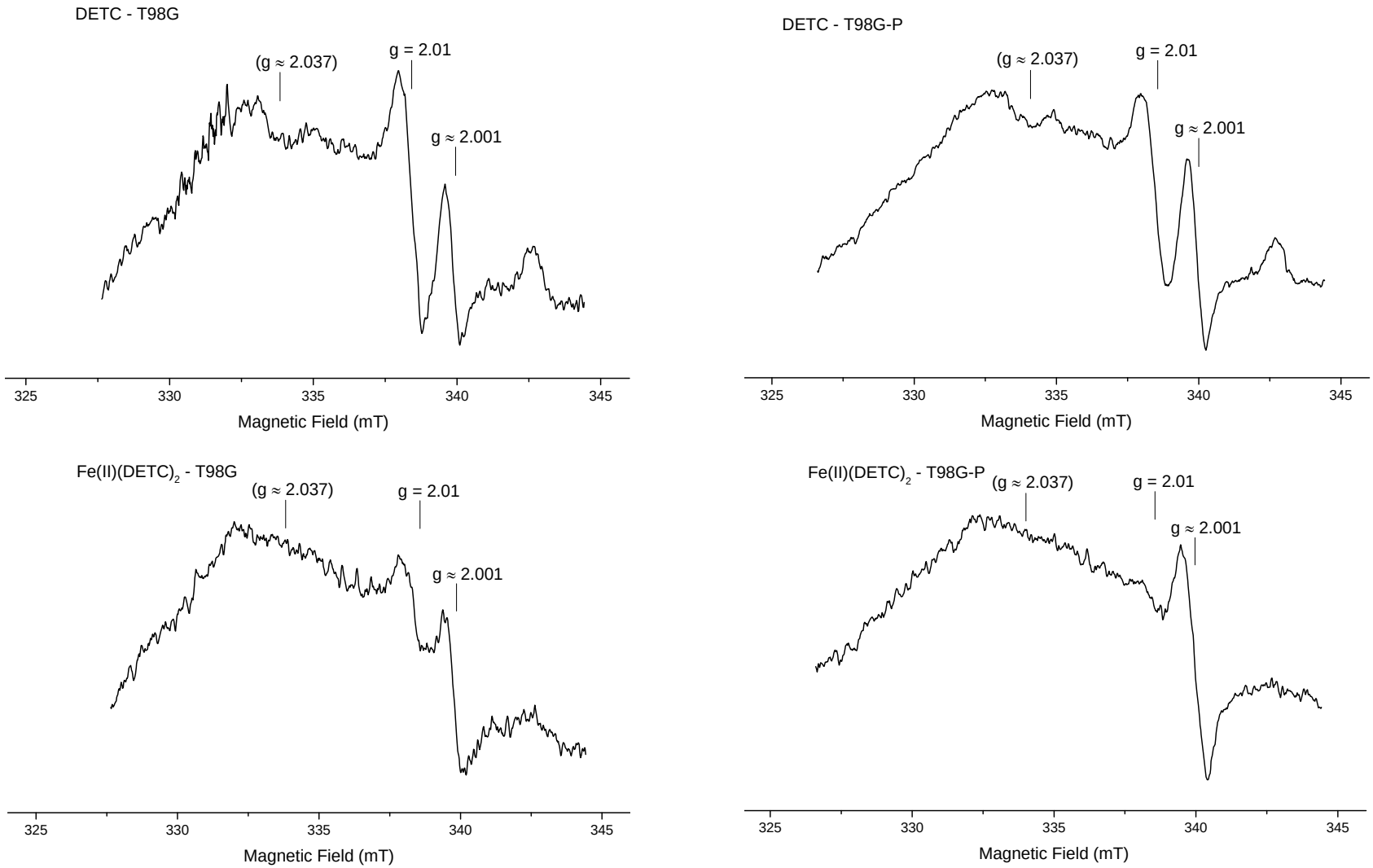

Figure 34

Samples incubated with DETC only (topmost panels) and colloidal Fe(II)(DETC)$_2$ (bottom panels). The panels to the left show spectra for T98G cells (3 added scans), whilst the ones to the right show corresponding ones for T98G-P cells (9 added scans). All four spectra feature a line at roughly g = 2.001 (B ≈ 340 mT.
ESR settings: P=10 mW, MA=0.5 mT, #scans=3 (T98G)/9 (T98G-P), TC= 327.68 ms, CT= 81.92 ms.

5.3.4 [^{60}Co]-γ Irradiated Samples

The apparent lack of any signal due to $NO^{\bullet}$-Fe(II)$(DETC)_2$ in the foregoing samples prepared with the standard method was attempted to be mediated by incubation of cells with spin trap present during LDR priming irradiation for one hour at 37°C. The idea was that increased activity of iNOS induced by protracted irradiation would generate higher quantities of $NO^{\bullet}$ which could be directly trapped by the spin trap complex. Extracellular SOD was supplemented before addition of spin trap in order to counteract to some extent the high levels of radicals generated during irradiation. The cells were given a LDR priming dose of ~0.18 Gy over one hour, and incubated with the spin trap for a total of two hours and 15 minutes.

Representative spectra are shown in Figure 35.

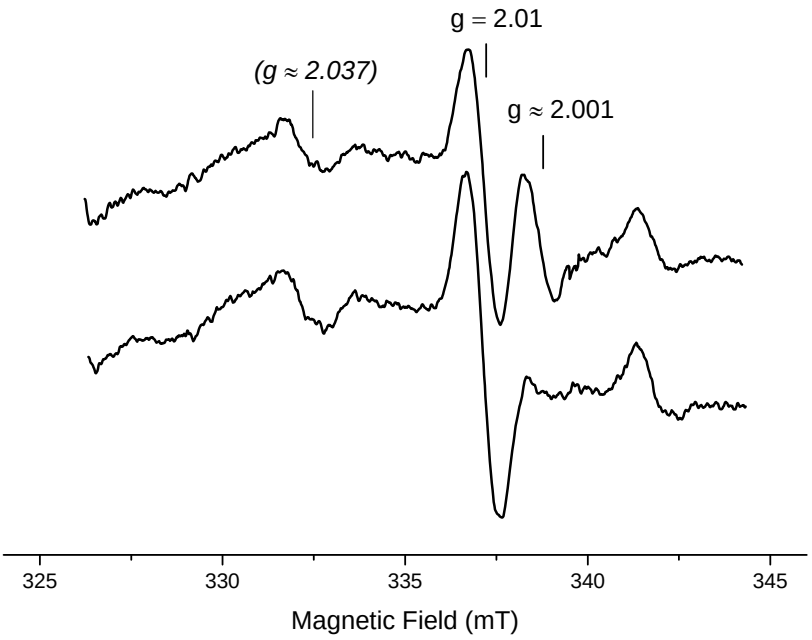

Figure 35
Representative spectra for identically treated samples of T98G cells incubated with 0.2 mM colloidal spin trap Fe(II)$(DETC)_2$ during irradiation with a ^{60}Co-source. Samples were pre-treated with SOD (100 U/ml) immediately before addition of spin trap.
ESR settings: P=10 mW, MA=0.5 mT, #scans=3, TC= 327.68 ms, CT= 81.92 ms.

These spectra display a prominent Cu(II)$(DETC)_2$ contribution, with a slight concavity of the baseline. Although ideally given identical treatment, the two samples yield slightly differing spectra in that one features a significant signal at B ≈ 338 mT, whilst the other does not.

5.4 Discussion

5.4.1 Establishment of Method

Colloidal spin trap Fe(II)$(DETC)_2$ was used to trap nitric oxide generated by $NO^{\bullet}$-donor DEANO in a system of T98G cells, with the standard method described in section 5.2.1. ESR-spectra obtained at 77 K agreed with the reported ESR-signal for the $NO^{\bullet}$-Fe(II)$(DETC)_2$ complex as shown in Figure 32. The $g_{\perp}$-value of 2.037 differs only slightly from that of $g_{\perp}$= 2.035 reported in the literature. The observed $g_{\parallel}$-value of 2.015 agreed with the less accurate reported value of $g_{\parallel}$ = 2.02.

These samples thus demonstrate that the standard method does indeed work for measuring large quantities of nitric oxide in cultured cells *in vitro*.

The DEANO samples also demonstrate that there is an abundance of spin trap complex available to trap nitric oxide.

Samples of Fe(II)$(DETC)_2$ with DEANO in cell-free system of KHB at room temperature did also yield spectra at the reported g-value of 2.04, as shown in Figure 31. These signals were relatively weak, reflecting the fact that the samples were not allowed to incubate after addition of spin trap prior to sampling. The signal-to-noise ratio is small even with four added scans. Dilution of the spin probe concentration added yielded progressively weaker signals. The signal from the 0.4 mM Fe(II)$(DETC)_2$ sample is roughly four times as high as that of the 0.2 mM sample. With the same concentration of $NO^{\bullet}$-donor present, the higher concentration used will naturally have a greater capacity to trap $NO^{\bullet}$, as well as trap $NO^{\bullet}$ at a greater rate. The lowest concentration of 0.05 mM Fe(II)$(DETC)_2$ yielded very little signal.

The lack of resolved triplet structure could be due to a number of reasons. The hypothesised Heisenberg spin exchange mechanism was investigated by diluting the spin trap concentration, but this approach did not improve matters.

An obvious concern for these spectra are the ESR spectrometer settings used. Due to inexperience these were not properly explored and fine structure may have been lost due to inappropriate settings. The power of 20 mW may have been too high, resulting in broadening

of lines. The time constant may also have been set too high (655.36 ms), leading to loss of fine structure, obscuring narrow lines. No definite conclusions can be drawn.

Kleschyov et al (2000) incubated 0.25 mM colloidal Fe(II)$(DETC)_2$ with $NO^{\bullet}$-donor spermine NO NOate (SPER/NO) in KHB for 30 min and recorded spectra at 77 K and 293 K. They reported the presence of a broad one-line signal of roughly 3.5 mT at 77 K, which agrees with that of Figure 31, but interestingly this signal was not detected 293 K. This may have had something to do with the extremely high microwave power of 50 mW used for recordings at ambient temperature. After dispersion with dimethyl sulfoxide (DMSO), the triplet structure was recovered at 77 K. This indicates that the unresolved triplet structure seen at 295 K in Figure 31 is indeed due to the hydrophobic nature of the spin trap complex.

5.4.2 Measurement of Basal $NO^{\bullet}$

When trying to measure basal nitric oxide in cellular samples, these yielded very different spectra to those seen in samples supplemented with an $NO^{\bullet}$-donor. A common feature for all basal samples was what appeared to be a signal at roughly g = 2.01, with apparent hyperfine structure with a ≈ 5 mT. Additionally, another line at g ≈ 2.001 appeared with varying intensity in most of the spectra for the basal samples. On more careful inspection of the spectrum from the DEANO-supplemented sample seen in Figure 32, the line at roughly g = 2.01 is also (barely) visible as an indent at B ≈ 337.5 mT.

The former signal with apparent g-value of 2.01 is commonly encountered as an interfering and overlapping spectrum when measuring nitric oxide with Fe(II)$(DETC)_2$. It has been attributed to a Cu(II)$(DETC)_2$ complex, which may arise in cells through scavenging by DETC of intracellular copper ions. A study by Suzuki et al. confirmed that this signal did indeed arise from Cu(II)$(DETC)_2$ and identified the entire spectrum (Suzuki et al 1997). The part of the spectrum typically encountered in the context of $NO^{\bullet}$-measurement with Fe(II)$(DETC)_2$ is that due to the normal component at $g_{\perp} = 2.025$, which is shown in Figure 36 below. This is the signal which appeared to have a g-value of 2.01 observed in most all of the recorded spectra for measurements of basal $NO^{\bullet}$ (see Figure 33, 34 and 35).

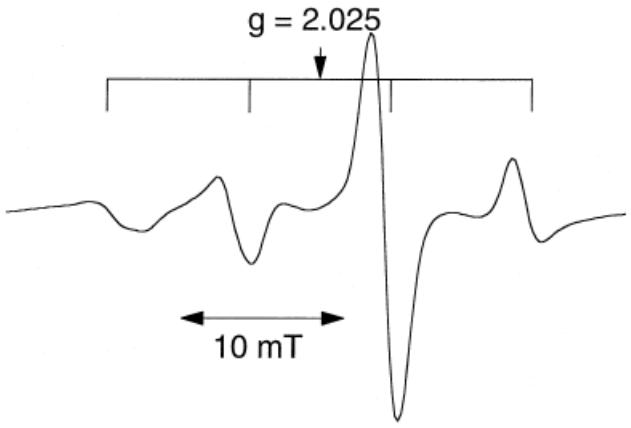

Figure 36
Part of the Cu(II)(DETC)$_2$ spectrum. This represents the $g_\perp$component of the spectrum, with $g_\perp$=2.025, $a_\perp$=4.8 mT. "Background signal" observed in DETC-injected rat brain at 77 K. From Suzuki et al (1997).

This Cu(II)(DETC)$_2$ signal is mostly reported as a major interference in studies where one uses the separate addition of iron and chelator DETC to the system in which one wishes to detect nitric oxide. This method of separate addition has been extensively used, particularly *in vivo*, since the hydrophobic property of the spin trap was regarded as an issue for delivery into cells or tissue (Vanin et al 2002). Formation of the spin trap would then take place inside the cells or tissue. DETC is a potent chelator, and will bind with not only free iron, but other metal ions, free or weakly bound. Particularly the chelation of Cu from Cu,Zn-SOD, resulting in inactivation, is a major problem with this method.

Kleschyov et al (2000) suggested the use of colloidal Fe(II)(DETC)$_2$, which is the basic method utilised in this project. Using this method, all DETC would be bonded to iron before addition to cells, thus hindering the inhibition of Cu,Zn-SOD and to a large extent avoiding the formation of interfering Cu(II)(DETC)$_2$ complex (due to ligand-exchange reactions, there is always a small Cu-DETC signal present). Kleschyov and Munzel (2002) do indeed report negligible Cu(II)(DETC)$_2$ signal in studies of vascular endothelial tissue using this method.

The spectra from samples prepared with colloidal spin trap in this project seen in Figure 33, 34 and 35 do however feature significant, if not entirely dominant Cu(II)(DETC)$_2$ signals. This is upon first consideration rather puzzling. However, when considering the effects of an oxidative environment on the spin trap complex, potential explanations arise. Shown below in Figure 37 are the different possible constellations of iron with DETC.

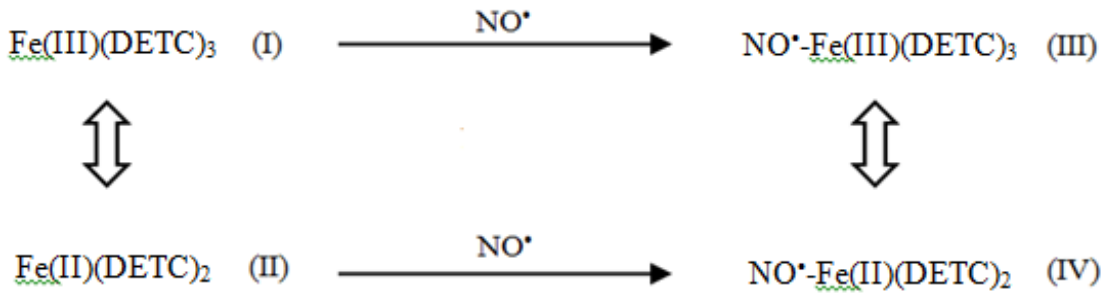

Figure 37
The four possible Fe-DETC complexes. Both the ferric (I) and ferrous (II) forms of iron-dithiocarbamate complex may trap NO•, yielding diamagnetic (III) or paramagnetic (IV) MNICs. Adapted, from Vanin and Poltorakov (2009).

Either forms of iron-DETC complex, ferrous or ferric, may bind nitric oxide. The oxidised, ferric form of iron, Fe(III), will bind with three molecules of DETC. This complex may bind NO•, yielding the ESR-silent diamagnetic complex NO•-Fe(III)$(DETC)_3$. Intracellular antioxidants, such as glutathione and ascorbate (see section 2.1.6, p. 15) may reduce this complex to the paramagnetic complex NO•-Fe(II)$(DETC)_2$, releasing one molecule of DETC. Alternatively, Fe(III)$(DETC)_3$ may be reduced to Fe(II)$(DETC)_2$, again releasing DETC. These freed DETC molecules may go on to chelate intracellular metal ions, notably copper. Thus, poorly controlled oxygenation of the sample may give a more pronounced background signal due to increased formation of Cu(II)$(DETC)_2$.

Another possible explanation for the prominent Cu(II)$(DETC)_2$ signal, which does not exclude the former scenario, is low availability of NO•. If there is very little NO• available to trap, the signals due to chelation of intracellular transition metal ions by freed DETC will naturally dominate.

The samples supplemented with DETC only do display a more prominent Cu(II)$(DETC)_2$ signal than do the samples incubated with colloidal spin trap. This is as one might expect, since DETC in this case is free to chelate any metal ions present in the cells.

There is a slight incline present in the region running up to where the ESR signal due to NO•-Fe(II)$(DETC)_2$ should appear (g = 2.037) in the spectra from samples irradiated with γ-radiation from a ^{60}Co-source (Figure 35), as compared with those from samples prepared with the standard method (Figure 33). It is however difficult to say whether this is due to nitric oxide or simply a subtle background signal.

5.4.3 Presence of a Signal of Unknown Origin

The other major feature evident in most of the spectra is the single line at g ≈ 2.001, which is close to that for free electrons. This line appears with highly varying intensity, from being almost not present (see Figure 33, bottom – T-47-P) to largely dominating the spectrum (see Figure 34, bottom right – T98G-P). This line is not part of the NO•-Fe(II)$(DETC)_2$ spectrum, nor of that for Cu(II)$(DETC)_2$, and is of unknown origin.

The signal may arise due to scavenging by DETC of some other intracellular transition metal ion, such as manganese, molybdenum, cobalt or zinc. The low g-value does not immediately suggest a transition metal, but the single line observed may potentially be part of a larger structure.

Another possible explanation is contamination of the samples with some paramagnetic species. One possibility is traces originating in the cell culture medium, such as serum and phenol red, which are known to yield ESR signals. If cell flasks were not rinsed properly to flush out all remnants of medium before addition of KHB and spin trap solution, this could give rise to a background signal. The varying intensity could be a result of varying success when rinsing the flasks. In order to explore this hypothesis, the signal from a sample of cell culture medium should be examined. If phenol red is found to be the culprit, cells for use in measurements with Fe(II)$(DETC)_2$ should be cultured in phenol red free medium.

5.4.4 Formation of Insoluble Complex Between Fe(II) and KHB

There was one minor difference between the protocol used in Munich and the standard method applied in this project, in that the spin trap parent solutions in Munich were dissolved in 0.9% NaCl, whereas here they were dissolved in KHB. The dissolution of parent compounds in KHB is used by several authors and was adopted from Deschacht et al (2010).

The reason for the use of NaCl instead of KHB, as later realised, is the potential formation of insoluble complex between Fe(II) and KHB, specifically the HEPES-component thereof. If this problem is encountered, Kleschyov and Munzel (2002) suggest that $FeSO_4$ is dissolved in pure milli-Q water and DETC is dissolved in a two times concentrated KHB solution. This problem was in fact only encountered once, with a batch of spin trap solution used for DEANO-supplemented samples. The $FeSO_4$ parent solution turned cloudy and the texture of

slightly curdled milk, but the complex was satisfyingly redispersed by careful inversion of the phial. No adverse effects were seen in the recorded spectra (not shown).

5.4.5 Overall Issues with Oxygen Contamination

As mentioned above, oxygen contamination is likely to reduce NO•-Fe(II)$(DETC)_2$ signal due to oxidation of some complexes to the diamagnetic ESR-silent state, as well as increase the Cu(II)$(DETC)_2$ background due to release of DETC molecules.

Oxygen may be introduced at several points during sample preparation. An obvious source is inadequate purging of oxygen in the buffer when bubbling with nitrogen gas.

Also when mixing the spin trap parent solutions, care must be taken not to introduce oxygen. Cell flasks are incubated with spin trap with closed caps after preparation in ambient atmosphere. This allows some diffusion of oxygen from the flask atmosphere into the buffer solution. Flasks should therefore be flushed with nitrogen gas before closing the caps to minimise oxygen contamination.

It is worth noting that for the T98G sample incubated with DEANO seen in Figure 32, the KHB used was *not* bubbled with N_2, neither that used to mix the spin trap nor that used for buffer solution. Upon mixing of the parent solutions, the resulting colloidal trap did precipitate to some extent and form blackish aggregates, indicating oxidation. One should then expect a more intense Cu-DETC signal and a relatively poorer $NO^{\bullet}$-Fe(II)$(DETC)_2$ signal, but the highly intense triplet signal characteristic of $NO^{\bullet}$-Fe(II)$(DETC)_2$ recorded shows no evident features of the Cu-DETC spectrum, indicating that very high concentrations of $NO^{\bullet}$ allows $NO^{\bullet}$-Fe(II)$(DETC)_2$ to outcompete Cu(II)$(DETC)_2$ even in the presence of high levels of molecular oxygen.

In order to avoid oxidation of the spin trap and to improve the sensitivity of the method, some authors recommend the use of reducing agents (Tsuchiya et al 1996). Under well-controlled conditions however, the colloidal preparation of Fe(II)$(DETC)_2$ should not yield a significant number of ESR-silent $NO^{\bullet}$-Fe(III)$(DETC)_3$ complexes. Kleschyov et al (2007) demonstrated this in intact blood vessels by post-incubation treatment with reducing agent sodium dithionite, which did not improve the signal compared with the untreated samples. They go as

far as claiming that the use of reducing agents does not improve the extraction of $NO^{\bullet}$, but in fact decreases it (Kleschyov & Munzel 2002).

5.4.6 Implications of Dysfunctional SOD

Some samples were supplemented with extracellular superoxide dismutase, in particular the LDR irradiated samples. SOD was added to medium at 50 – 100 U/ml ~30 min before cells were incubated with KHB and spin trap. SOD was also added to the buffer during incubation. Due to the very high rate constant of SOD, this was assumed to be sufficient for dismutase activity to take effect. Most of the papers regarding superoxide and nitric oxide measurement referenced in this thesis do not specify their protocols for SOD, beyond mentioning that it was used.

The few references which were found for the supplementation of SOD report widely disparate incubation times. Bolaños and Medina (1996) incubate cultured rat astrocytes with Cu,Zn-SOD for 18 h before commencing measurements, whereas Fabian et al (2004) supplement rats with PEG-SOD in vivo 50 min before measurements begin.

It is uncertain whether the SOD protocol of 30 minutes in culture medium and then for an hour during incubation with spin trap used for $NO^{\bullet}$-samples in this study did in fact have any effect.

If SOD was not functional in the samples, this could potentially have led to decreased levels of $NO^{\bullet}$ available for trapping by $Fe(II)(DETC)_2$ due to scavenging of $NO^{\bullet}$ by ambient levels of $O_2^{\bullet-}$. Vanin and Poltorakov (2009) however claim that the rate of $NO^{\bullet}$ binding to $Fe(II)(DETC)_2$ used at milli molar concentrations exceeds the rate of oxidation of nitric oxide by superoxide by orders of magnitude. Kleschyov et al (2007) agree with this assertion and claim that the assay is resistant to both intra- and extracellular oxidants, with concentrations of 50 – 200 μM of $Fe(II)(DETC)_2$ being able to compete even under conditions of oxidative stress (moderate, not severe). Indeed, the use of SOD is not mentioned in the majority of studies concerning quantification of nitric oxide with colloidal spin trap $Fe(II)(DETC)_2$.

For the samples incubated with spin trap under LDR irradiation however, the induced ROS levels are expected to be high giving rise to conditions which could certainly be termed severely oxidative, likely resulting in increased scavenging of $NO^{\bullet}$.

Assuming a cell diameter of 21 μm for T98G cells (Aspmodal 2011) and a cell density of ρ = 10^3 kg/m^3, one finds an estimated mass per cell of 5×10^{-12} kg. The absorbed energy per cell after exposure to 0.18 Gy is then approximately 9×10^{-13} J, or ~5.5×10^6 eV, which gives 55,000 units of 100 eV of radiation energy absorbed per cell. The yield for hydroxyl radical and hydrated electrons, i.e. the number of $^{\bullet}$OH molecules or e^-_{aq} formed per 100 eV absorbed energy, is G = 2.3 (Pettersen 2011), giving an estimated 125,000 $^{\bullet}$OH / e^-_{aq} radicals formed per cell over an hour.

Although irradiation induces a range of ROS which do not originate downstream from the generation of initial superoxide, the use of functional SOD would possibly increase the yield of NO$^{\bullet}$-trapping by Fe(II)(DETC)$_2$ by dismutating formed superoxide radical. The severely oxidative environment created during irradiation however, is highly likely to have lowered the detectable signal from the MNICs formed due to oxidation of iron in complexes to the diamagnetic ferric form.

The lack of any observed signal from the NO$^{\bullet}$-Fe(II)(DETC)$_2$ complex in the basal samples generally could very well be due to preferential scavenging of nitric oxide by elevated levels of superoxide.

5.4.7 Results Obtained in Munich

Reger (unpublished work) utilised the standard method as described in section 5.2.1, p. 81, to measure nitric oxide in primed and unprimed cells. Nitric oxide was allegedly measured in T98G and T-47D cells and the signal intensities were then normalised to protein content with the Bradford assay (unpublished work). The results are shown in Figure 38.

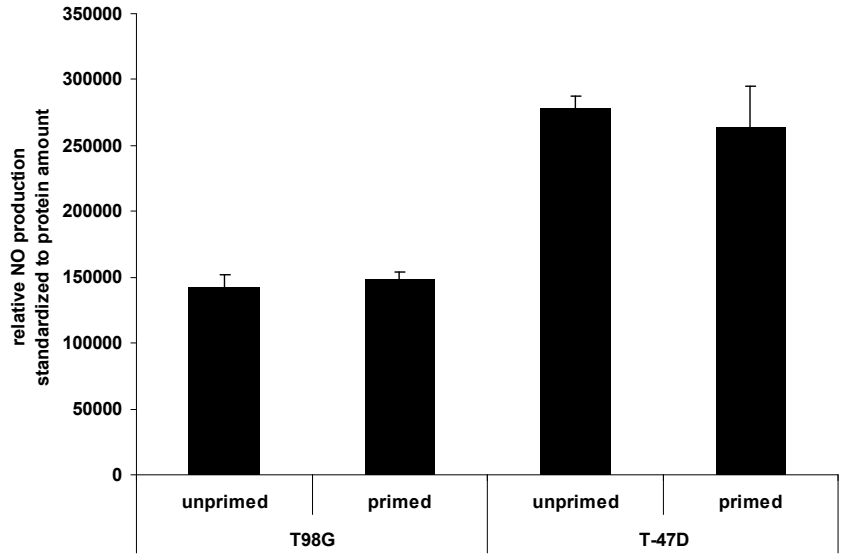

Figure 38
Relative nitric oxide levels in primed and unprimed T98G and T-47D cells measured with colloidal spin trap Fe(II)(DETC)$_2$ (0.2 mM) during 1 h incubation, 37°C. Signal is normalised to protein content. The number of experiments and sample size is unknown. From Reger (unpublished work).

No significant difference in nitric oxide levels between primed and unprimed cells was found.

No SOD was used in these measurements, and so the potentially signal enhancing effect of superoxide scavenging would not have been of benefit here.

It is questionable whether Reger actually did measure signals due to NO$^{\bullet}$-Fe(II)(DETC)$_2$ and not that of Cu(II)(DETC)$_2$. When prompted for representative spectra, none were forthcoming except for one which was clearly from a sample supplemented with an NO$^{\bullet}$-donor.

5.4.8 Alternative Methods for Attempts at NO$^{\bullet}$-detection by Others

Other methods of detection have been employed by others at our group in the process of attempting to measure NO$^{\bullet}$ in cultured cells, with the ultimate goal of comparing measured levels in primed and unprimed control cells.

Marzioch (personal communication) used two different types of sensors to measure nitric oxide; an NO$^{\bullet}$ microsensor (Unisense AS, Denmark), and a novel microchip sensor currently under testing, developed at the University of Freiburg. Nitric oxide in solution supplemented with NO$^{\bullet}$-donor N-(acetyloxy)-3-nitrosothiovaline (SNAP) and basal levels in cell culture medium and cells was examined. Nitric oxide was detected in solution with NO$^{\bullet}$-donor. However, nitric oxide was not conclusively measured in cells/medium and certainly no

significant difference between supposed $NO^{\bullet}$-levels measured in primed and unprimed cells/medium was found.

Edin approached the problem from a slightly different angle. T-47D cells were supplemented with radiolabelled L-arginine before LDR priming for one hour. L-arginine was then removed with a resin filter and radioactive citrulline was measured by liquid scintillation counting. Results were variable and the initial results confirming the proposed hypothesis of heightened $NO^{\bullet}$-production by primed cells compared with unprimed controls could not be reproduced.

These studies suggest that nitric oxide generation in the cells examined occurs at, or below, the limit of detection. ESR spin trapping is generally considered to be the most sensitive method available for nitric oxide measurement, which is why a spin trapping method was chosen for this thesis in order to explore the relation between $NO^{\bullet}$-levels with the sustained elimination of HRS in cells.

In order to test the hypothesised mechanism in which peroxynitrite scavenges freed LAP-3, thereby stabilising TGF-β3 (see section 2.3.3, p.28), Edin treated T-47D-P cells with peroxynitrite scavenger uric acid (13.05.13, unpublished work). The cells treated with uric acid were found to regain their HRS response, which provides a strong indication for the validity of the hypothesis. See Figure 39 for survival curves. The peroxynitrite would be a product of nitric oxide and superoxide produced in cells, indicating that there is indeed nitric oxide being generated.

The fact that there is scavenging of nitric oxide by superoxide going on does not necessarily suggest that experiments performed without SOD are doomed to fail. The important point is whether the spin trap is able to compete with superoxide for $NO^{\bullet}$ to a sufficient degree.

Supplementation of colloidal spin trap to LDR primed P-cells while in culture with subsequent evaluation of cell survival response could yield an insight into whether $NO^{\bullet}$ is preferentially scavenged by superoxide to form peroxynitrite or if the spin trap is able to compete, thus reinstating the HRS response.

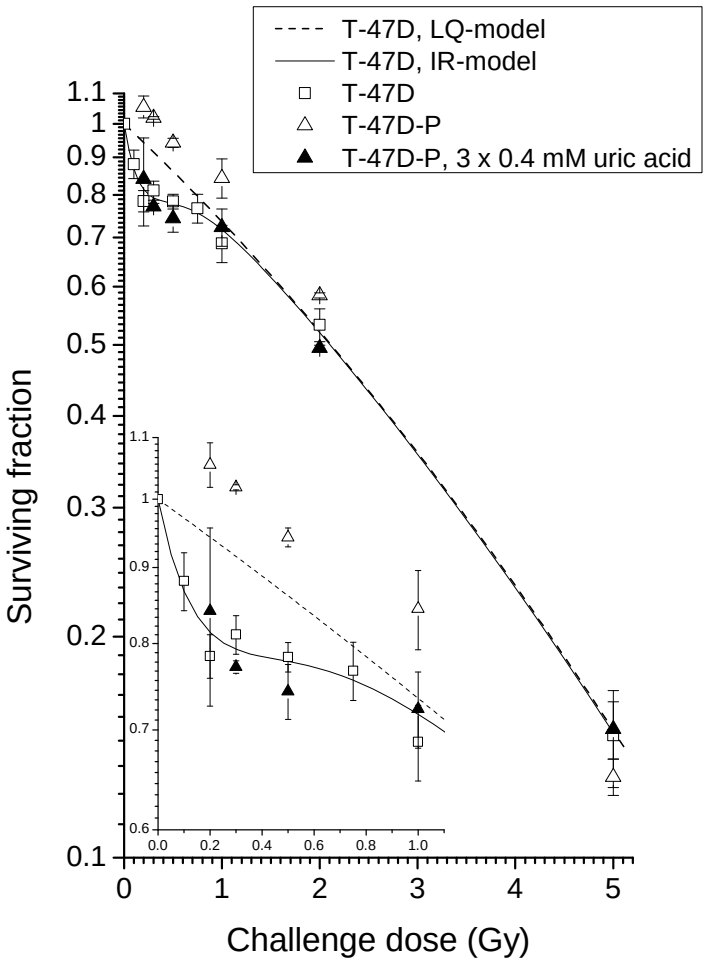

Figure 39
Shown are survival curves for different cell populations. T-47D cells display HRS (□), whilst T-47D-P cells do not (△). T-47D-P cells treated with peroxynitrite scavenger uric acid (0.4 mM) for three consecutive days have regained their HRS response (▲). From Edin (unpublished data).

Another issue raised by this result is the fact that peroxynitrite seems to be preferentially formed. As mentioned in section 2.1.4, Beckman and Koppenol (1996) claim that this is only the case if the concentration of nitric oxide approaches that of SOD, which is typically micro molar. The results obtained for $NO^{\bullet}$-measurements in P-cells (or any of the cells) do not divulge any definite presence of nitric oxide, certainly not at micro molar concentrations. One may then speculate about the levels of endogenous SOD in these cells. As described in section 2.1.6, tumour cells typically display lowered SOD-activity. This is likely the case for the cells studied in this project.

It is however not known how large concentrations of peroxynitrite are required to keep up the permanent elimination of HRS, it may be relatively little.

5.4.9 Concluding Remarks

One cannot necessarily expect to find $NO^{\bullet}$-levels as those reported in the literature. Many, if not most, of these studies are conducted with cardiovascular endothelial cells, which are specialised $NO^{\bullet}$-generators through eNOS. Additionally, these are typically examined in the form of tissue samples, which are of higher cell density, therefore yielding a stronger signal.

It is however worth noting that iNOS is generally high-output, and so cells expressing iNOS could potentially yield more $NO^{\bullet}$ measured by such means. One could so in part expect to see higher levels of nitric oxide production in LDR primed cells compared with cardiovascular endothelial cells.

Due to the fact that no signal conclusively originating from $NO^{\bullet}$-$Fe(II)(DETC)_2$ was observed in any of the basal samples, recorded signals were not normalised to protein content. In retrospect it would have been interesting to qualitatively compare for instance the normalised signals ($Cu(II)(DETC)_2$) for T98G and T-47D cells with those obtained in Munich, shown in Figure 38.

5.4.10 Suggestions for further work

Oxygen contamination seems to be an issue for NO-measurement by this method. In order to alleviate this problem, and investigate whether it in fact does make a difference, cell flasks could be prepared, incubated with spin trap and scraped in syringes in a hypoxic atmosphere.

In conjunction with testing of the proposed mechanisms for removal of HRS, Edin carried out survival experiments with the HRS negative mammary ductal carcinoma cell line NHIK 3025. These were from a fresh batch of thawed cells which acted rather oddly in that they would not attach to the cell flasks, making cell culture difficult. These cells were treated with iNOS-inhibitor 1400W in order to probe the proposed mechanism in which HRS is removed by action of $NO^{\bullet}$ (with superoxide), see section 2.3.3. Interestingly, the cells treated with 1400W reverted to their normal behaviour, attaching readily to cell flask bottoms.

There is a strong link between the development of atherosclerosis and endothelial dysfunction, in which, amongst other things, normal $NO^{\bullet}$-production by endothelial cells is deteriorated. The lack of nitric oxide promotes the adhesion of leucocytes with subsequent

inflammatory response (Chhabra 2009Chhabra 2009). Some of the adhesion molecules responsible, such as integrins, are widespread in most cells, including epithelial cells. It thus seems fair to conclude that treatment of the NHIK 3025 cells with 1400W removed the excessive $NO^{\bullet}$ generated and thus allowed cells to adhere to the flask bottom surface. It is unknown how the NHIK 3025 batch came to develop what seems to be an excessive production of nitric oxide.

It would be interesting to try and measure nitric oxide in these cells which appear to produce rather large amounts of $NO^{\bullet}$, to see if they yield any appreciable signal with the standard method of section 5.2.1.

6 Conclusion

Both ESR spin trapping protocols used in Munich for superoxide/ROS measurement with cyclic hydroxylamine spin probe CMH and nitric oxide measurement with colloidal iron-ditihiocarbamate spin trap $Fe(II)(DETC)_2$ were successfully established at our lab.

Reoxygenation of hypoxic cells (0.1% pericellular oxygenation) was seen to yield an increase in ESR signal detected in samples with time after reoxygenation . While the levels of ROS detected upon reoxygenation of hypoxic cells was found to be similar to that obtained for reoxygenation of cells cultured at ambient oxygenation, the reoxygenation of hypoxic cells (0.1% pericellular oxygenation) was reached after an initial increase in ESR signal which plateaued after 5 – 8 minutes and subsequently decreased. This may reflect the burst of ROS speculated to be responsible for the transient, and in conjunction with an $NO^{\bullet}$-donor, the sustained elimination of HRS in reoxygenated cells.

Since nitric oxide was not conclusively detected in basal samples of T98G and –P nor T-47D or –P cells, no conclusions regarding the mechanism for removal of HRS could be drawn. However, the failure to measure $NO^{\bullet}$ indicated that peroxynitrite and not $NO^{\bullet}$ might be the key mediator for HRS-elimination and recent experimental evidence obtained by Edin strongly suggests the validity of the hypothesis.

The use of a more sensitive ESR spectrometer did overall not resolve the lack of statistically significant results regarding the difference between measurements of superoxide and nitric oxide in primed and unprimed cells obtained in Munich. In the case of superoxide measurements, the method of measurements on supernatant largely chosen to examine this relationship was perhaps unfortunate, since mitochondrial ROS is indicated to be undetectable by this method. In the case of nitric oxide measurements, the lack of any definite ESR signal attributable to NO•-production in cells was at odds with the results obtained in Munich. One may speculate that the ESR signals measured in Munich were in fact due to the $Cu(II)(DETC)_2$ complex invariably seen in the NO•-samples in this work. The fact that no ESR signal due to nitric oxide was conclusively seen indicates that the amounts present are at or below the limit of detection.

7 References

Abramov AY, Scorziello A, Duchen MR. 2007. Three distinct mechanisms generate oxygen free radicals in neurons and contribute to cell death during anoxia and reoxygenation. *The Journal of neuroscience* 27: 1129-38

Alberts B. 2008. *Molecular biology of the cell*. New York: Garland Science

Amellem O, Sandvik JA, Stokke T, Pettersen EO. 1998. The retinoblastoma protein-associated cell cycle arrest in S-phase under moderate hypoxia is disrupted in cells expressing HPV18 E7 oncoprotein. *Br J Cancer* 77: 862-72

Aspmodal I. 2011. *Effekt av lavdoserate beta-bestråling på T98G humane kreftceller i kultur*. University of Oslo

Atherton NM. 1993. *Principles of electron spin resonance*: Ellis Horwood Ltd

Attix FH. 1986. *Introduction to radiological physics and radiation dosimetry*. New York: Wiley. xxi, 607 p. pp.

Beckman JS, Koppenol WH. 1996. Nitric oxide, superoxide, and peroxynitrite: the good, the bad, and ugly. *American Journal of Physiology-Cell Physiology* 271: C1424-C37

Bolaños JP, Medina JM. 1996. Induction of nitric oxide synthase inhibits gap junction permeability in cultured rat astrocytes. *Journal of neurochemistry* 66: 2091-9

Bonner WM. 2004. Phenomena leading to cell survival values which deviate from linear-quadratic models. *Mutat Res* 568: 33-9

Böttinger EP, Factor VM, Tsang M, Weatherbee JA, Kopp JB, et al. 1996. The recombinant proregion of transforming growth factor beta1 (latency-associated peptide) inhibits active transforming growth factor beta1 in transgenic mice. *Proceedings of the National Academy of Sciences* 93: 5877-82

Cadenas E, Packer L. 2005. *Nitric Oxide, Part E*: Gulf Professional Publishing. 664 pp.

Casey G, Lo-Hsueh M, Lopez ME, Vogelstein B, Stanbridge EJ. 1991. Growth suppression of human breast cancer cells by the introduction of a wild-type p53 gene. *Oncogene* 6: 1791-7

Chadwick K, Leenhouts H. 1973. A molecular theory of cell survival. *Physics in Medicine and Biology* 18: 78

Chhabra N. 2009. Endothelial dysfunction–a predictor of atherosclerosis. *Internet J Med Update* 4: 33-41

Davies KJ. 1995. *Oxidative stress: the paradox of aerobic life*. Presented at Biochemical Society Symposia

Denekamp J, Dasu A. 1999. Inducible repair and the two forms of tumour hypoxia-time for a paradigm shift. *Acta Oncologica* 38: 903-18

Deschacht M, Horemans T, Martinet W, Bult H, Maes L, Cos P. 2010. Comparative EPR study of different macrophage types stimulated for superoxide and nitric oxide production. *Free Radic Res* 44: 763-72

Dikalov S, Griendling KK, Harrison DG. 2007a. Measurement of reactive oxygen species in cardiovascular studies. *Hypertension* 49: 717-27

Dikalov SI, Dikalova AE, Mason RP. 2002. Noninvasive diagnostic tool for inflammation-induced oxidative stress using electron spin resonance spectroscopy and an extracellular cyclic hydroxylamine. *Archives of biochemistry and biophysics* 402: 218-26

Dikalov SI, Kirilyuk IA, Voinov M, Grigor'ev IA. 2011. EPR detection of cellular and mitochondrial superoxide using cyclic hydroxylamines. *Free radical research* 45: 417-30

Dikalov SI, Li W, Mehranpour P, Wang SS, Zafari AM. 2007b. Production of extracellular superoxide by human lymphoblast cell lines: Comparison of electron spin resonance techniques and cytochrome< i> C</i> reduction assay. *Biochemical pharmacology* 73: 972-80

Edin NF, Sandvik JA, Vollan HS, Reger K, Görlach A, Pettersen EO. 2013. The role of nitric oxide radicals in removal of hyper-radiosensitivity by priming irradiation. *Journal of Radiation Research*

Edin NJ, Olsen DR, Sandvik JA, Malinen E, Pettersen EO. 2012. Low dose hyper-radiosensitivity is eliminated during exposure to cycling hypoxia but returns after reoxygenation. *Int J Radiat Biol* 88: 311-9

Edin NJ, Olsen DR, Stokke T, Pettersen EO. 2007. Recovery of low-dose hyper-radiosensitivity following a small priming dose depends on priming dose-rate. *International journal of low radiation* 4: 69-86

Edin NJ, Olsen DR, Stokke T, Sandvik JA, Ebbesen P, Pettersen EO. 2009. Mechanisms of the elimination of low dose hyper-radiosensitivity in T-47D cells by low dose-rate priming. *Int J Radiat Biol* 85: 1157-65

Fabian RH, Perez-Polo JR, Kent TA. 2004. Extracellular superoxide concentration increases following cerebral hypoxia but does not affect cerebral blood flow. *International journal of developmental neuroscience* 22: 225-30

Farr SB, D'Ari R, Touati D. 1986. Oxygen-dependent mutagenesis in Escherichia coli lacking superoxide dismutase. *Proceedings of the National Academy of Sciences* 83: 8268-72

Förstermann U, Kleinert H. 1995. Nitric oxide synthase: expression and expressional control of the three isoforms. *Naunyn-Schmiedeberg's archives of pharmacology* 352: 351-64

Hall EJ, Giaccia AJ. 2006. *Radiobiology for the radiologist*. Philadelphia: Lippincott Williams & Wilkins. ix, 546 p. pp.

Hall EJ, Giaccia AJ. 2012. *Radiobiology for the Radiologist*: LWW

Halliwell B. 2005. *Free radicals and other reactive species in disease*: Wiley Online Library

Hancock J, Desikan R, Neill S. 2001. Role of reactive oxygen species in cell signalling pathways. *Biochemical Society Transactions* 29: 345-50

Hyytiainen M, Penttinen C, Keski-Oja J. 2004. Latent TGF-beta binding proteins: extracellular matrix association and roles in TGF-beta activation. *Crit Rev Clin Lab Sci* 41: 233-64

Imlay J, Fridovich I. 1991. Assay of metabolic superoxide production in Escherichia coli. *Journal of Biological Chemistry* 266: 6957-65

Jensen MM. 2013. *Biomasse*

Jiang F, Zhang Y, Dusting GJ. 2011. NADPH oxidase-mediated redox signaling: roles in cellular stress response, stress tolerance, and tissue repair. *Pharmacological reviews* 63: 218-42

Joiner M, Johns H. 1988. Renal damage in the mouse: The response to very small doses per fraction. *Radiation research* 114: 385-98

Joiner MC, Marples B, Lambin P, Short SC, Turesson I. 2001. Low-dose hypersensitivity: current status and possible mechanisms. *Int J Radiat Oncol Biol Phys* 49: 379-89

Keydar I, Chen L, Karby S, Weiss F, Delarea J, et al. 1979. Establishment and characterization of a cell line of human breast carcinoma origin. *European Journal of Cancer (1965)* 15: 659-70

Kleschyov AL, Mollnau H, Oelze M, Meinertz T, Huang Y, et al. 2000. Spin trapping of vascular nitric oxide using colloid Fe (II)-diethyldithiocarbamate. *Biochemical and Biophysical Research Communications* 275: 672-7

Kleschyov AL, Munzel T. 2002. Advanced spin trapping of vascular nitric oxide using colloid iron diethyldithiocarbamate. *Methods Enzymol* 359: 42-51

Kleschyov AL, Wenzel P, Munzel T. 2007. Electron paramagnetic resonance (EPR) spin trapping of biological nitric oxide. *Journal of Chromatography B* 851: 12-20

Koli K, Saharinen J, Hyytiäinen M, Penttinen C, Keski‐Oja J. 2001. Latency, activation, and binding proteins of TGF‐β. *Microscopy research and technique* 52: 354-62

Krueger S, Joiner M, Weinfeld M, Piasentin E, Marples B. 2007. Role of apoptosis in low-dose hyper-radiosensitivity. *Radiation research* 167: 260-7

Li C, Jackson RM. 2002. Reactive species mechanisms of cellular hypoxia-reoxygenation injury. *Am J Physiol Cell Physiol* 282: C227-41

Li J-M, Shah AM. 2004. Endothelial cell superoxide generation: regulation and relevance for cardiovascular pathophysiology. *American Journal of Physiology-Regulatory, Integrative and Comparative Physiology* 287: R1014-R30

Lund A, Shiotani M, Shimada S. 2011. *Principles and applications of ESR spectroscopy*: Springer

Marples B, Joiner M. 1993. The response of Chinese hamster V79 cells to low radiation doses: Evidence of enhanced sensitivity of the whole cell population. *Radiation research* 133: 41-51

Marples B, Joiner M. 1995. The elimination of low-dose hypersensitivity in Chinese hamster V79-379A cells by pretreatment with X rays or hydrogen peroxide. *Radiation research* 141: 160-9

Marples B, Wouters B, Joiner M. 2003. An association between the radiation-induced arrest of G2-phase cells and low-dose hyper-radiosensitivity: A plausible underlying mechanism? *Radiation research* 160: 38-45

Millar TM, Phan V, Tibbles LA. 2007. ROS generation in endothelial hypoxia and reoxygenation stimulates MAP kinase signaling and kinase-dependent neutrophil recruitment. *Free Radic Biol Med* 42: 1165-77

Mitchell CR, Folkard M, Joiner MC. 2002. Effects of exposure to low-dose-rate 60Co gamma rays on human tumor cells in vitro. *Radiation research* 158: 311-8

Moncada S, Higgs EA. 2006. Nitric oxide and the vascular endothelium. *Handb Exp Pharmacol*: 213-54

Moore DS, McCabe GP, Craig BA. 2012. *Introduction to the practice of statistics*

Oberley LW, Buettner GR. 1979. Role of superoxide dismutase in cancer: a review. *Cancer Research* 39: 1141-9

Olivieri G, Bodycote J, Wolff S. 1984. Adaptive response of human lymphocytes to low concentrations of radioactive thymidine. *Science (New York, NY)* 223: 594

Pettersen EO. 2011. *FYS4720: Cellulær Radiobiologi*

Pettersen EO, Larsen LH, Ramsing NB, Ebbesen P. 2005. Pericellular oxygen depletion during ordinary tissue culturing, measured with oxygen microsensors. *Cell proliferation* 38: 257-67

Reger K. 2012a. NO Bioavailability.

Reger K. 2012b. Superoxide Production.

Rehman A, Whiteman M, Halliwell B. 1997. Scavenging of hydroxyl radicals but not of peroxynitrite by inhibitors and substrates of nitric oxide synthases. *British journal of pharmacology* 122: 1702-6

Rhee SG. 2006. H2O2, a necessary evil for cell signaling. *Science* 312: 1882-3

Sheu S-S, Nauduri D, Anders M. 2006. Targeting antioxidants to mitochondria: a new therapeutic direction. *Biochimica et biophysica acta* 1762: 256

Short S, Woodcock M, Marples B, Joiner M. 2003. Effects of cell cycle phase on low-dose hyper-radiosensitivity. *International journal of radiation biology* 79: 99-105

Short SC, Kelly J, Mayes CR, Woodcock M, Joiner MC. 2001. Low-dose hypersensitivity after fractionated low-dose irradiation in vitro. *International journal of radiation biology* 77: 655-64

Sinclair WK. 1968. Cyclic x-ray responses in mammalian cells in vitro. *Radiation research* 33: 620-43

Stein GH. 1979. T98G: An anchorage‐independent human tumor cell line that exhibits stationary phase G1 arrest in vitro. *Journal of cellular physiology* 99: 43-54

Suzuki Y, Fujii S, Tominaga T, Yoshimoto T, Yoshimura T, Kamada H. 1997. The origin of an EPR signal observed in dithiocarbamate-loaded tissues: copper (II)-dithiocarbamate complexes account for the narrow hyperfine lines. *Biochimica et Biophysica Acta (BBA)-General Subjects* 1335: 242-5

Takizawa T, Yoshikawa H, Yamada M, Morita H. 2002. Expression of nitric oxide synthase isoforms and detection of nitric oxide in rat placenta. *Am J Physiol Cell Physiol* 282: C762-7

Tsuchiya K, Takasugi M, Minakuchi K, Fukuzawa K. 1996. Sensitive quantitation of nitric oxide by EPR spectroscopy. *Free Radical Biology and Medicine* 21: 733-7

Turrens JF. 1997. Superoxide production by the mitochondrial respiratory chain. *Bioscience reports* 17: 3-8

Vanin A, Poltorakov A. 2009. NO spin trapping in biological systems. *Front Biosci* 14: 4427-35

Vanin AF, Huisman A, Van Faassen EE. 2002. Iron dithiocarbamate as spin trap for nitric oxide detection: pitfalls and successes. *Methods in enzymology* 359: 27-42

Verhaar M, Westerweel P, Van Zonneveld A, Rabelink T. 2004. Free radical production by dysfunctional eNOS. *Heart* 90: 494-5

Vestad TA. 1999. *ESR Spin Trapping, ELECTRON SPIN RESONANCE APPLIED TO THE STUDY OF FREE-RADICAL PRODUCTION IN BIOLOGICAL SYSTEMS EXPOSED TO OZONE AND ORGANIC SOLVENTS*, UiO

Weil JA, Bolton JR. 2007. *Electron paramagnetic resonance: elementary theory and practical applications*: Wiley-Interscience

Xu B, Kim S-T, Lim D-S, Kastan MB. 2002. Two molecularly distinct G2/M checkpoints are induced by ionizing irradiation. *Molecular and cellular biology* 22: 1049-59

Zhang H, Bosch-Marce M, Shimoda LA, Tan YS, Baek JH, et al. 2008. Mitochondrial autophagy is an HIF-1-dependent adaptive metabolic response to hypoxia. *Journal of Biological Chemistry* 283: 10892-903

Appendix A - List of Chemicals

Chemical	Source
Bradford dye reagent	Bio-Rad, USA
BSA	Merck, Germany
Calibration buffer, pH 10	Radiometer Analytical, Denmark
Calibration buffer, pH 4	Radiometer Analytical, Denmark
$CaCl_2$ ($2\times H_20$)	Merck, Germany
CMH	Enzo Lifesciences, USA
Cu,Zn-SOD	Sigma, USA
DEANO	Sigma, USA
DES	Sigma, USA
D-glucose	Sigma, USA
DETC	Sigma, USA
Ethanol, 96%	Arcus AS, Norway
$FeSO_4$	Sigma, USA
Foetal calf serum	Gibco, UK
Glucose	Sigma, USA
HCl	Sigma, USA
Insulin	Sigma, USA
KH_2PO_4	Sigma, USA
L-glutamine	Sigma, USA
L-NAME	Sigma, USA
$MgSO_4$ ($7\times H_20$)	Sigma, USA
Milli-Q water	Millipore, USA
N_2	AGA,
Na_2SO_3	Sigma, USA
NaCl	Sigma, USA
$NaHCO_3$	Sigma, USA
Na-HEPES	Sigma, USA
NaOH	Sigma, USA
PBS	Euroclone, UK
PEG-SOD	Sigma, USA
RPMI	JRH Biosciences, Kansas, USA
Streptomycine	Euroclone, UK
TCA	Sigma, USA
Trypsin w/EDTA	Lonza, Belgium

Appendix B – Equipment and Instruments

Equipment	Source
Cell flasks (Nunc)	Thermo Fisher Scientific, USA / Greiner Bio-one, Germany
Hypodermic needles	Sterican, Braun Melsungen, Germany
Pipettes	BD Biosciences, USA
Filtropur filters	Sarstedt, Germany
Plastipak syringes	BD Biosciences, USA
Bürker chamber	Hycor, USA
Test tubes	Sarstedt, Germany
96 well plates (Nunc)	Thermo Fisher Scientific, USA
ESR quartz tube	Wilmad Labglass, USA
Capillary tubes	Hirschmann Laborgeräte, Germany
Putty	Phywe Systeme GmbH & Co. KG, Germany
Sugru curable rubber	Sugru, UK
Dewar flask	

Instruments	Source
Theratron 780-C (^{60}Co source)	MDS Nordion, Canada
OAS LAF VB 2040 (LAF bench)	Odd A. Simonsen AS, Norway
IN VIVO2 hypoxia glovebox	Ruskinn, UK
Mettler Toledo AG 245 (Analytical balance)	Bergman AS, Norway
Argus pH meter	Sentron, Switzerland
LEDETECT 96 micro plate reader	Labexim Products, Austria
EleXsyS 560 Super X (ESR spectrometer)	Bruker, Germany
Nikon TMS (Microscope)	Nikon, USA
Beckman CS-15 (Centrifuge)	Beckman, USA
Accuri C6 Flow cytometer	Accuri Cytometers Inc., USA
O_2 microsensor	Unisense, Denmark

Appendix C- Recipes

Krebs HEPES Buffer (KHB) – pH 7.35

Ingredients	MW (g/mol)	Content mM	Content mOsm	g/l	g/200 ml
NaCl	58.44	99	198.01	5.786	1.097
KCl	74.55	4.69	9.38	0.350	0.070
KH_2PO_4	136.10	1.03	3.09	0.142	0.029
$CaCl_2$ (x2H_2O)	147.02	2.5	7.5	0.368	0.074
$MgSO_4$ (x7H_2O)	246.48	1.2	2.4	0.296	0.059
$NaHCO_3$	84.01	25	50	2.1	0.420
D-Glucose	180.20	5.6	5.6	1.009	0.202
Na-HEPES	260.30	20	40	5.206	1.041

Prepare 10x of **bold components** in the above and store at 4ºC, then make 1:10 dilution and add $NaHCO_3$, glucose and HEPES. Adjust pH and filter using 0.22 µl Millipore filter. The buffer is good up to 3 days in 4ºC, for longer storage; keep at -20ºC.

Colloidal Fe(II)$(DETC)_2$ Spin Trap Solution

$FeSO_4$	4.50 mg / 10 ml KHB (deoxygenated)
DETC	7.2 mg / 10 ml KHB (deoxygenated)

Mix 1:1 without introducing air. Use immediately.

CMH Spin Probe Solution

DES (25 mM)	656 g/mol	16.4 mg/ml milli-Q water
DETC (5 mM)	225 g/mol	11.25 mg/10 ml milli-Q water

Add to KHB at final concentration of 25 µM (DES) and 5 µM (DETC) and bubble with N_2 > 10 min.

CMH (10 mM)	238 g/mol	2.38 mg/ml KHB with DES and DETC (deoxygenated)

L-NAME (18.5 mM)

L-NAME	269.7 g/mol	5mg/ml milli-Q water

Cu,Zn-SOD (15 kU/ml)

Cu,Zn-SOD (75 kU)	The entire vial was diluted in 5 ml milli-Q water and pipetted in aliquots of 3750 U per tube and stored at -20°C.

NaOH 0.2 N (1000 ml)

NaOH	8.0 g
Milli-Q water	1000 ml

BSA in 0.2 N NaOH (50 μg/ml)

BSA in milli-Q water	2 mg/ml milli-Q water
0.2 N NaOH	

Stock solution of BSA in milli-Q is kept at 4°C and diluted 1:40 with 0.2 N NaOH before use for protein measurement.

RPMI 1640 Medium

Stem Solution	
RPMI 1640 powder	10.43 g
$NaHCO_3$	2.00 g
Milli-Q water	1000 ml
RPMI Medium with Serum (1000 ml)	
RPMI 1640 stem solution	880 ml
Foetal calf serum	100 ml
Penicillin streptomycin	10 ml
Insulin (200 units/l)	2 ml
L-glutamine	10 ml

L-glutamine (35 ml)

L-glutamine	1.0227 g
RPMI stem solution	35 ml

PBS (1000 ml)

NaCl	8.000 g
KCl	0.201 g
KH_2PO_4	0.204 g
Na2HPO4 (x12 H_2O)	2.858 g
Milli-Q water	1000 ml

Appendix D – Experimental Data

D.1 Comparison of superoxide/ROS levels in primed and unprimed cells

T-47D_1
Date: 26.11.2012

Class	Sample #	Tot. protein (ug/ml)	ESR Signal	ESR/#scan	Average ESR	Norm. signal	Average norm	SEM ESR	SEM norm
T-47D	1	475,96	11830	3943,33	3632,8	8,28	5,34	166,2	0,78
	2	772,44	9700	3233,33		4,19			
	3	870,19	12110	4036,67		4,64			
	4	905,45	11040	3680		4,06			
	5	589,74	9812	3270,67		5,55			
T-47D-P	6	772,44	9650	3216,67	3449,4	4,16	5,1	105,5	0,34
	7	700,32	10619	3539,67		5,05			
	8	642,15	9910	3303,33		5,14			
	9	620,19	11214	3738		6,03			

T-47D_suspension
Date: 01.04.2013

Class	Sample #	Tot. protein (ug/ml)	ESR Signal	ESR/#scan	Average ESR	Norm. signal	Average norm	SEM ESR	SEM norm
T47D U	2	6,67	1206	402	644,47	60,3	34,05	162,13	12,45
	3	25	1238	412,67		16,51			
	4	6,67	1359	453		67,95			
	9	40	2097	699		17,48			
	18	156,67	3767	1255,7		8,01			
T47D L	10	471,67	3491	1163,7	825,27	2,47	4,46	129,97	1,96
	11	343,33	2601	867		2,53			
	16	123,33	3100	1033,3		8,38			
T47D-P U	5	8,33	1439	479,67	771,47	57,56	14,71	129,79	10,73
	6	130	1748	582,67		4,48			
	7	373,33	1972	657,33		1,76			
	8	175	2863	954,33		5,45			
	17	275	3550	1183,3		4,3			
T47D-P L	12	301,67	2857	952,33	982,75	3,16	16,03	16,09	10,74
	13	85	2880	960		11,29			
	14	488,33	2960	986,67		2,02			
	15	21,67	3096	1032		47,63			

T-47D_2
Date: 13.04.2013

Class	Sample #	Tot. protein (ug/ml)	ESR Signal	ESR/#scan	Average ESR	Norm. signal	Average norm	SEM ESR	SEM norm
T-47D U	3	681,63	5708	1902,56	2090	2,79	2,97	110,64	0,13
	6	706,95	6857	2285,64		3,23			
	10	720,45	6245	2081,79		2,89			
T-47D L	4	843,65	7046	2348,72	2264,4	2,78	3,04	154,72	0,24
	7	703,57	7440	2480		3,52			
	11	696,82	5894	1964,62		2,82			
T-47D-P U	1	784,58	5584	1861,33	2056,6	2,37	2,97	130,17	0,31
	2	742,39	6910	2303,33		3,1			
	9	583,74	6015	2005		3,43			
T-47D-P L	5	636,06	8315	2771,79	2446,6	4,36	3,59	163,14	0,42
	8	651,25	6784	2261,28		3,47			
	12	787,96	6920	2306,67		2,93			

T98G
Date: 26.05.2013

Class	Sample #	Tot. protein (ug/ml)	ESR Signal	ESR/#scan	Average ESR	Norm. signal	Average norm	SEM ESR	SEM norm
T98G U	1	130	7206	3603	3768,5	27,72	44,52	83,7	3,04
	3	44,67	7659	3829,5		30,39			
	5	192,67	7746	3873		20,1			
T98G L	7	112,67	9320	4660	4236,3	41,36	33,73	276,02	9,73
	9	258	7436	3718		14,41			
	11	95,33	8662	4331		45,43			
T98G-P U	2	119,33	6939	3469,5	3255,2	29,07	30,77	206,88	8,83
	4	60,67	5683	2841,5		46,84			
	6	210,67	6909	3454,5		16,4			
T98G-P L	8	168,67	6441	3220,5	3218,8	19,09	28,66	6,98	6,00
	10	81,33	6460	3230		39,71			
	12	118	6412	3206		27,17			

D.2 Reoxygenation Experiments

Reox #1
Date:
13.12.12

Reox Time (min)	Sample #	Tot. protein (ug/ml)	ESR Signal	ESR/#scan	Average ESR	Norm. signal	Average norm	SEM ESR	SEM norm
0	1	838,89	19610	6536,67	8083,33	7,79	9,89	1546,67	2,10
	2	802,78	28890	9630,00		12,00			
2	3	844,44	25100	8366,67	8366,67	9,91	9,91	NA	NA
4	4	952,78	26610	8870,00	9513,33	9,31	10,73	643,33	1,42
	5	836,11	30470	10156,67		12,15			

8	6	872,22	40530	13510,00	17780,00	15,49	18,44	4270,00	2,95
	7	1030,56	66150	22050,00		21,40			
15	8	938,89	33780	11260,00	11260,00	11,99	11,99	NA	NA

Reox #2

Date: 07.01.13

Reox Time (min)	Sample #	Tot. protein (ug/ml)	ESR Signal	ESR/#scan	Average ESR	Norm. signal	Average norm	SEM ESR	SEM norm
0	1	286,95	38580	12860,00	11038,89	44,82	37,66	2095,18	7,15
	2	298,95	40190	13396,67		44,81			
	3	293,61	20580	6860,00		23,36			
1	4	502,95	26420	8806,67	8040,00	17,51	23,25	766,67	5,74
	6	250,95	21820	7273,33		28,98			
2	7	276,28	20960	6986,67	8060,00	25,29	24,61	1073,33	0,68
	8	381,61	27400	9133,33		23,93			
3	11	348,28	33210	11070,00	9313,33	31,78	46,62	1756,67	14,84
	13	122,95	22670	7556,67		61,46			
5	14	148,28	37740	12580,00	11951,67	84,84	73,59	628,33	11,25
	15	181,61	33970	11323,33		62,35			
7	16	384,28	44540	14846,67	12451,67	38,64	33,70	2395,00	4,93
	17	349,61	30170	10056,67		28,77			
9	5	276,28	17570	5856,67	6788,33	21,20	74,63	931,67	NA
	9	*60,28*	23160	7720,00		128,07			
12	10	252,28	9672	3224,00	6972,00	12,78	29,73	3748,00	16,95
	12	229,61	32160	10720,00		46,69			
		109,61	32510	10836,67	10836,67	98,86	98,86		

Reox #3

Date: 13.01.13

Reox Time (min)	Sample #	Tot. protein (ug/ml)	ESR Signal	ESR/#scan	Average ESR	Norm. signal	Average norm	SEM ESR	SEM norm
0	12	605,56	18700	6233,33	6855,00	10,29	10,11	621,67	0,18
	13	752,78	22430	7476,67		9,93			
1	15	969,44	9696	3232,00	3549,33	3,33	3,78	317,33	0,45
	18	913,89	11600	3866,67		4,23			
3	1	841,67	8582	2860,67	3648,67	3,40	4,10	788,00	0,70
	2	925,00	13310	4436,67		4,80			
5	4	919,44	28300	9433,33	6738,33	10,26	8,16	2695,00	2,10
	6	666,67	12130	4043,33		6,07			
7	7	827,78	27830	9276,67	6751,67	11,21	7,52	2525,00	3,68
	10	1100,00	12680	4226,67		3,84			
8	19	905,56	14860	4953,33	3687,17	5,47	4,16	1266,17	1,31

	20	850,00	7263	2421,00		2,85			
9	3	930,56	17070	5690,00	5551,67	6,11	5,80	138,33	0,31
	11	986,11	16240	5413,33		5,49			
10	16	905,56	7324	2441,33	2441,33	2,70	2,70	NA	NA
11	5	638,89	13190	4396,67	4396,67	6,88	6,88	NA	NA
60	9	827,78	14950	4983,33	3595,83	6,02	4,22	1387,50	1,80
	14	911,11	6625	2208,33		2,42			
120	8	930,56	4848	1616,00	3006,33	1,74	5,75	1390,33	4,02
	17	450,00	13190	4396,67		9,77			

Reox #4
Date: 02.02.13

Reox Time (min)	Sample #	Tot. protein (ug/ml)	ESR Signal	ESR/#scan	Average ESR	Norm. signal	Average norm	SEM ESR	SEM norm
0	8	802,52	5883	2941,50	3,67	3,94	3150,75	209,25	0,28
	9	796,00	6720	3360,00	4,22				
2	1	784,85	4410	2205,00	2,81	3,02	2354,67	147,17	0,15
	3	800,00	5298	2649,00	3,31				
	12	751,52	4420	2210,00	2,94				
3	5	806,06	5492	2746,00	3,41	3,86	3252,50	506,50	0,46
	6	869,70	7518	3759,00	4,32				
5	7	684,85	6708	3354,00	4,90	4,56	3542,00	188,00	0,34
	10	884,85	7460	3730,00	4,22				
6	2	809,09	5457	2728,50	3,37	4,43	3674,67	747,42	0,78
	4	866,67	10300	5150,00	5,94				
	11	790,91	6291	3145,50	3,98				

Reox #5
Date: 03.02.13

Reox Time (min)	Sample #	Tot. protein (ug/ml)	ESR Signal	ESR/#scan	Average ESR	Norm. signal	Average norm	SEM ESR	SEM norm
4	2	288,89	8965	4482,50	3556,63	15,52	8,37	325,86	1,63
	4	575,31	6701	3350,50		5,82			
	18	624,69	5913	2956,50		4,73			
	20	464,20	6874	3437,00		7,40			
5	6	451,85	8219	4109,50	4364,75	9,09	9,47	255,25	0,25
	16	469,14	9240	4620,00		9,85			
7	8	503,70	10400	5200,00	4894,00	10,32	9,72	306,00	0,41
	21	503,70	9176	4588,00		9,11			
8	11	340,74	11400	5700,00	5400,00	16,73	12,54	300,00	2,79
	14	611,11	10200	5100,00		8,35			
9	1	585,19	7693	3846,50	3602,50	6,57	6,62	244,00	0,03
	19	503,70	6717	3358,50		6,67			
10	3	343,21	6993	3496,50	3292,25	10,19	10,53	204,25	0,23
	5	283,95	6176	3088,00		10,88			

11	7	441,98	7816	3908,00	5582,00	8,84	9,69	1303,01	1,08
	9	488,89	10200	5100,00		10,43			
	13	671,60	7840	3920,00		5,84			
	17	688,89	18800	9400,00		13,65			
20	10	503,70	9910	4955,00	4353,67	9,84	7,94	587,29	0,93
	12	390,12	6812	3406,00		8,73			
	15	893,83	9400	4700,00		5,26			

Reox #20%
Date: 18.01.13

Reox Time (min)	Sample #	Tot. protein (ug/ml)	ESR Signal	ESR/#scan	Average ESR	Norm. signal	Average norm	SEM ESR	SEM norm
1	1	1018,52	5110	2555,00	2718,50	2,51	3,02	238,33	0,42
	2	825,93	6376	3188,00		3,86			
	3	900,00	4825	2412,50		2,68			
3	6	485,19	7498	3749,00	2744,63	7,73	4,19	385,45	1,22
	8	614,81	4297	2148,50		3,49			
	16	877,78	5900	2950,00		3,36			
	24	977,78	4262	2131,00		2,18			
4	12	1062,96	7000	3500,00	2963,50	3,29	3,16	399,49	0,49
	14	966,67	4365	2182,50		2,26			
	18	814,81	6416	3208,00		3,94			
5	10	855,56	8329	4164,50	3458,00	4,87	4,06	356,78	0,43
	20	774,07	6036	3018,00		3,90			
	22	937,04	6383	3191,50		3,41			
6	4	1014,81	5630	2815,00	2984,88	2,77	3,11	269,74	0,43
	25	1085,19	4796	2398,00		2,21			
	26	940,74	6073	3036,50		3,23			
	28	874,07	7380	3690,00		4,22			
7	15	696,30	6374	3187,00	3406,50	4,58	4,72	120,05	0,58
	29	951,85	7201	3600,50		3,78			
	23	592,59	6864	3432,00		5,79			
8	7	966,67	7400	3700,00	3263,63	3,83	3,49	209,37	0,12
	9	900,00	6102	3051,00		3,39			
	17	848,15	5575	2787,50		3,29			
	27	1022,22	7032	3516,00		3,44			
9	11	916,67	10000	5000,00	4369,67	5,45	5,12	444,13	0,43
	13	823,33	7025	3512,50		4,27			
	19	813,33	9193	4596,50		5,65			
11	5	716,67	6297	3148,50	3939,00	4,39	4,59	428,41	0,16
	21	906,67	8096	4048,00		4,46			
	23	943,33	9241	4620,50		4,90			

D.3 Protein Measurement Test

Total # of cells	Average #	SEM #cells	ESR Signal	ESR/scan	Average ESR	SEM ESR
173751,667	147056,67	26695	13000	4333,33	4013,33	960
120361,667			11080	3693,33		
300108	279314,00	20794	10520	3506,67	3481,67	75
258520			10370	3456,67		
496808	484444,00	12364	11260	3753,33	3901,67	445
472080			12150	4050,00		
599935	599935,00	0	13660	4553,33	4346,67	620
599935			12420	4140,00		
814197,5	795932,50	18265	15400	5133,33	4955,00	535
777667,5			14330	4776,67		

Total protein (ug)	Average protein (ug)	SEM Protein	Normalised signal	Av. Norm. signal	SEM Norm signal
61,62	66,90	5,28	210,96	182,23	28,73
72,18			153,50		
104,06	104,70	0,63	101,09	99,77	1,32
105,33			98,45		
162,15	130,88	31,27	69,44	95,71	26,27
99,61			121,98		
220,23	219,69	0,54	62,03	59,35	2,68
219,15			56,67		
148,39	161,30	12,91	103,78	93,02	10,76
174,20	--		82,26		

D.4 Sampling in Hypoxic Atmosphere

	ESR	ESR/scan	Average ESR	SEM ESR	Total protein (ug)	Normalised signal	Average norm signal	SEM norm signal
hyp	3700	1233,33	2055,56	756,54	1090,91	1,13	1,91	0,62
	4100	1366,67			923,23	1,48		
	10700	3566,67			1139,39	3,13		
reox	7100	2366,67	2511,11	144,44	1096,97	2,16	2,17	0,05
	7100	2366,67			1133,33	2,09		
	8400	2800,00			1236,36	2,26		

Appendix E – R Code and Output – t-tests

R Code

```
# m1, m2: the sample means
# s1, s2: the sample standard deviations
# n1, n2: the same sizes
# m0: the null value for the difference in means to be tested for. Default is 0.
# equal.variance: whether or not to assume equal variance. Default is FALSE.
t.test2 <- function(m1,m2,s1,s2,n1,n2,m0=0,equal.variance=FALSE)
{
   if( equal.variance==FALSE )
   {
      se <- sqrt( (s1^2/n1) + (s2^2/n2) )
      # welch-satterthwaite df
      df <- ( (s1^2/n1 + s2^2/n2)^2 )/( (s1^2/n1)^2/(n1-1) + (s2^2/n2)^2/(n2-1) )
   } else
   {
      # pooled standard deviation, scaled by the sample sizes
      se <- sqrt( (1/n1 + 1/n2) * ((n1-1)*s1^2 + (n2-1)*s2^2)/(n1+n2-2) )
      df <- n1+n2-2
   }
   t <- (m1-m2-m0)/se
   dat <- c(m1-m2, se, t, 2*pt(-abs(t),df))
   names(dat) <- c("Difference of means", "Std Error", "t", "p-value")
   return(dat)
}
```

R Output

- T98G:

```
## T98G p vs not-p, no LN, ESR:
 t.test2(m1=3768.5, m2=3255.17, s1=83.70, s2=206,88, n1=3, n2=3, equal.variance=TRUE)
Difference of means          Std Error                  t            p-value
      513.33000000       128.37664637         3.31314154         0.02956743


 ## T98G p vs not-p, no LN, norm:
 t.test2(m1=26.07, m2=20.88, s1=3.04, s2=8.83, n1=3, n2=3, equal.variance=TRUE)
Difference of means          Std Error                  t            p-value
        5.1900000          5.3916757          0.9625950          0.3902617


 ## T98G p vs not-p, with LN, ESR:
 t.test2(m1=4236, m2=3255, s1=276.02, s2=6.98, n1=3, n2=3, equal.variance=TRUE)
Difference of means          Std Error                  t            p-value
      9.810000e+02       1.594112e+02       6.153898e+00       3.537683e-03
```

T98G p vs not-p, with LN, norm:
t.test2(m1=33.73, m2=29.66, s1=9.73, s2=6.00, n1=3, n2=3, equal.variance=TRUE)

Difference of means	Std Error	t	p-value
4.0700000	6.5998207	0.6166834	0.5708119

T98G LN vs no LN not-p
t.test2(m1=3768.5, m2=4236, s1=83.70, s2=276.02, n1=3, n2=3, equal.variance=TRUE)

Difference of means	Std Error	t	p-value
-467.50000000	166.52600438	-2.80736935	0.04844649

- T-47D_2:

T-47D_2 p vs not-p, no LN, ESR:
t.test2(m1=2090.00, m2=2056, s1=110.64, s2=130.17, n1=3, n2=3, equal.variance=TRUE)

Difference of means	Std Error	t	p-value
34.0000000	98.6330548	0.3447120	0.7476726

T-47D_2 p vs not-p, no LN, norm:
t.test2(m1=2.97, m2=2.97, s1=0.13, s2=0.31, n1=3, n2=3, equal.variance=TRUE)

Difference of means	Std Error	t	p-value
0.000000	0.194079	0.000000	1.000000

T-47D_2 p vs not-p, with LN, ESR:
t.test2(m1=2264.44, m2=2446.58, s1=154.72, s2=163.14, n1=3, n2=3, equal.variance=TRUE)

Difference of means	Std Error	t	p-value
-182.1400000	129.8113221	-1.4031134	0.2332406

T-47D_2 p vs not-p, with LN, norm:
t.test2(m1=3.04, m2=3.59, s1=0.24, s2=0.42, n1=3, n2=3, equal.variance=TRUE)

Difference of means	Std Error	t	p-value
-0.5500000	0.2792848	-1.9693159	0.1202637

- T-47D_suspension:

T-47D_suspension p vs not-p, no LN, ESR:
t.test2(m1=644.47, m2=771.47, s1=162.13, s2=129.79, n1=3, n2=3, equal.variance=TRUE)

Difference of means	Std Error	t	p-value
-127.0000000	119.9049360	-1.0591724	0.3492421

T-47D_suspension p vs not-p, no LN, norm:
t.test2(m1=34.05, m2=14.71, s1=12.45, s2=10.73, n1=3, n2=3, equal.variance=TRUE)

Difference of means	Std Error	t	p-value
19.340000	9.489211	2.038104	0.111183

T-47D_suspension p vs not-p, with LN, ESR:
t.test2(m1=1021.33, m2=982.75, s1=85.85, s2=18.00, n1=3, n2=3, equal.variance=TRUE)

Difference of means	Std Error	t	p-value
38.5800000	50.6432704	0.7617991	0.4886216

T-47D_suspension p vs not-p, with LN, norm:
t.test2(m1=4.46, m2=16.03, s1=1.96, s2=10.74, n1=3, n2=3, equal.variance=TRUE)

Difference of means	Std Error	t	p-value
-11.5700000	6.3031527	-1.8355894	0.1403145

T-47D_suspension LN vs no LN, not-p norm:
t.test2(m1=34.05, m2=4.46, s1=12.45, s2=1.96, n1=3, n2=3, equal.variance=TRUE)

Difference of means	Std Error	t	p-value
29.59000000	7.27653993	4.06649318	0.01526691

T-47D_suspension LN vs no LN, p norm:
t.test2(m1=14.71, m2=16.03, s1=10.73, s2=10.74, n1=3, n2=3, equal.variance=TRUE)

Difference of means	Std Error	t	p-value
-1.3200000	8.7650917	-0.1505974	0.8875825

- T-47D_1:

T-47D_1 p vs not-p, ESR
t.test2(m1=3632.8, m2=3449.42, s1=166.20, s2=105.50, n1=3, n2=3, equal.variance=TRUE)

Difference of means	Std Error	t	p-value
183.3800000	113.6554589	1.6134729	0.1819395

T-47D_1 p vs not-p, norm
t.test2(m1=5.34, m2=5.10, s1=0.78, s2=0.34, n1=3, n2=3, equal.variance=TRUE)

Difference of means	Std Error	t	p-value
0.2400000	0.4912569	0.4885428	0.6507392